

Advanced Numerical Modeling of Vibrations Induced by Railway Traffic

A dissertation submitted to the:

Lille 1 University Science and Technology – ED SPI

Laboratory of Civil Engineering and geo-Environment (LGCgE)

&

Lebanese University – Doctoral School of Science and Technology

Research Laboratory “Modeling Center”

for the degree of Doctor of Philosophy in Civil Engineering

by

Reda MEZEH

11 July 2017

Supervisors : Marwan SADEK – Fadi HAGE CHEHADE

Members of the Jury :

M. Daniel Dias, Professor, Polytech’ Grenoble

Reviewer

M. Sébastien Burlon, HDR, IFSTTAR Paris

Reviewer

M. Isam Shahrour, Professor, Director LGCgE, Lille 1 University

Examiner

M. Fadi Geara, Dean, Saint-Joseph University - ESIB

Examiner

Mrs. Marlène BRAX, CNRS-L, Director of Geophysics Center

Examiner

This page is intentionally left blank

*Parfois notre lumière s'éteint, puis elle est rallumée par
un autre être humain. Chacun de nous doit de sincères
remerciements à ceux qui ont ravivé leur flamme.*

Albert Schweitzer

Je dois terminer ce travail en disant un grand merci aux personnes qui ont cru en moi et qui m'ont donné la chance d'arriver au bout de cette thèse. Mais par où commencer ? par quel ordre ? C'est la décision la plus difficile, mais quand même je me lance!

Je tiens tout d'abord à remercier mon directeur de thèse, Mr Marwan Sadek, pour m'avoir accordé sa confiance et permis d'effectuer cette thèse en collaboration entre l'université de Lille 1 Sciences et Technologies et l'université Libanaise. C'est à lui que je dois toute ma reconnaissance pour mon entrée dans le monde de la recherche. J'aimerais également lui dire à quel point, j'ai été sensible à ses qualités humaines d'écoute et de compréhension tout au long de ce travail doctoral.

Je remercie également Mr Fadi Hage Chehade, professeur à l'Université Libanaise, qui m'a encadré tout au long de cette thèse et qui m'a fait partager ses brillantes intuitions. Qu'il soit aussi remercié pour sa gentillesse, sa disponibilité permanente et pour les nombreux encouragements qu'il m'a prodigués.

Je remercie Mr Isam Shahrour pour avoir accepté de présider mon jury de thèse et pour sa participation scientifique ainsi que le temps qu'il a consacré à ma recherche. J'adresse tous mes remerciements également à Mr Daniel Dias, Professeur à Polytech' Grenoble, ainsi qu'à Mr Sébastien Burlon, HDR à l'IFSTTAR Paris, de l'honneur qu'ils m'ont fait en acceptant d'être rapporteurs de cette thèse. Leurs remarques m'ont permis d'envisager mon travail sous un autre angle. J'exprime ma gratitude aussi à Madame Marlène Brax membre au CNRS-Liban et à Monsieur Fadi Geara, doyen de l'université Saint-Joseph - ESIB, qui ont bien voulu être examinateurs.

Un grand merci à tous les membres du département génie civil de Polytech Lille et en particulier à, Mr Hussein Mroueh. Je remercie aussi toutes les personnes formidables que j'ai rencontrées au LGCgE pour la bonne ambiance de travail mais également pour les nombreux moments passés ensemble (Christelle, Sana, Mohannad, Rami, Shaker, Oras, Faten, Amar, Ahmad, Fayez, Elias, Fatima, Sheyar et Lyes).

Je voudrais remercier mes amis avec qui j'ai passé la plupart des moments inoubliables (les nouveaux mariés Marie-Joe et Naim, Marc, Ghaith et Rim, Salman et Karima, Steve, Salim, Nicolas, Elio, Anthony, Céline).

Je remercie mes parents et mes frères Ali et Achraf de m'avoir soutenu de loin. Ils ont tous cru en moi et ouf ! Maintenant j'y suis !

Mes derniers remerciements vont à ma chérie Dima qui a tout fait pour m'aider, qui m'a soutenu et surtout supporté dans tout ce que j'ai entrepris.

Encore un grand merci à tous pour m'avoir conduit à ce jour mémorable.

ABSTRACT

Over the last decade, the development of high-speed lines (HSL) has grown considerably. Although it has been the subject of continuous theoretical and experimental studies that lead to major technological innovation, the HSL are still considered as an important source of environmental disturbance that are less and less tolerated by inhabitants. In order to understand the dynamics of these systems, it is important to develop numerical models to simulate the vibration problems vehicle/track and understand the interactions of the track and vehicle components. Hence, the main purpose of this dissertation is to provide reliable predictive tools in the time domain that aim to correctly simulate the track/ground interaction problems.

A new approach based on periodic configuration update “PCU method” is firstly proposed for the assessment of the dynamic response of continuously supported infinite beams under high speed moving loads. The PCU method retains the principle of the spatial follow of loads while zeroing the relative velocity with the traversed beam via a step-by-step adaptive integration of the equation of structural dynamics. It is then used to assess the dynamic response of a simplified track/ground system in which the rail foundation is replaced by a continuous viscoelastic layer. The model show a high efficiency in the dynamic analysis of the high speed trains problems.

On the other hand, a 3D numerical modeling that considers the complex mutual dynamic coupling between the track components and the subgrade layer is developed. An adaptive meshing scheme is applied to simulate the moving loads effect; it is represented by the creation of load-attached moving nodes on the rail-beam. The spatiotemporal mesh parameters are investigated within the frame of adaptive meshing and appropriate recommendations are drawn. This modeling is successfully applied in the sub-Rayleigh and super-Rayleigh velocity range.

In the last part, the 3D numerical modeling is used to calibrate the dynamic impedances of the simplified beam model proposed in the first chapter. An iterative curve fitting procedure is carried out using the genetic algorithm. Constitutive laws that govern the dynamic behavior of the discrete elements are proposed at different load frequency and velocity range. The numerical experiments show an important capacity to achieve satisfactory results with significant reduction in computational cost. The obtained results emphasize the major impact of the excitation characteristics on the parameters of the discrete models that are widely used in the literature.

Keywords: track/ground interaction, 3D numerical modeling, rail response, high-speed trains, adaptive meshing

Modélisation numérique avancée des vibrations induites par le trafic ferroviaire

RESUME

Les lignes à grande vitesse sont considérées comme une source importante de perturbations environnementales qui sont de moins en moins tolérées par les habitants. Afin de comprendre la dynamique de ces systèmes, il est important de développer des modèles numériques pour simuler les problèmes de vibration véhicule/voie ferrée et comprendre les interactions de la voie ferrée et des composants du véhicule. Par conséquent, le but principal de cette thèse est de fournir des outils prédictifs fiables dans le domaine temporel qui visent à simuler correctement les problèmes d'interaction voie ferrée/sol. Une nouvelle approche basée sur la mise à jour périodique de la configuration « Méthode PCU » est d'abord proposée pour l'évaluation de la réponse dynamique des poutres infinies continuellement supportées sous charges mobiles à grande vitesse. La méthode PCU est utilisée pour évaluer la réponse dynamique d'un système simplifié voie ferrée/sol dans lequel la fondation du rail est remplacée par une couche viscoélastique continue. D'autre part, une modélisation numérique 3D considérant le couplage dynamique mutuel complexe entre les composantes de la voie ferrée et la couche du sol est développée. Un schéma de maillage adaptatif est appliqué pour simuler l'effet des charges mobiles ; il est représenté par la création des nœuds mobiles attachés aux charges. Cette modélisation est appliquée avec succès dans la gamme de vitesses sub-Rayleigh et super-Rayleigh. Dans la dernière partie, la modélisation numérique 3D est utilisée pour calibrer les impédances dynamiques du modèle simplifié proposé dans le premier chapitre. Une procédure itérative d'ajustement de courbe est réalisée à l'aide d'un algorithme génétique. Des lois constitutives qui régissent le comportement dynamique des éléments discrets sont proposées aux différentes fréquences de chargement et gamme de vitesses. Les expériences numériques montrent une capacité importante à obtenir des résultats satisfaisants avec une réduction significative du coût de calcul.

Keywords: interaction voie ferrée /sol, modélisation numérique 3D, réponse du rail, trains à grande vitesse, maillage adaptatif

Table of Contents

Introduction	1
Chapter 1:	
Adaptive Analysis of Infinite Beams Dynamics Problems Using the Periodic Configuration Update Method in the Time Domain	3
1. Introduction	4
2. Mathematical Formulation	6
2.1. Dynamic Equation of the Beam	7
2.2. Numerical Algorithm- Adaptive Procedure in the Time Domain	8
3. Validation of the PCU Method	12
3.1. Statement of the problem	13
3.2. Convergence of the PCU method	16
3.2.1. Non-convergence zone	16
3.2.2. Stability of the numerical method	17
3.2.3. Consistency of the numerical method	19
4. Numerical Study	20
4.1. Effect of interpolation parameters	20
4.2. Effect of progressive mesh	23
4.3. Execution time	25
5. Conclusions	25
References	27
Chapter 2:	
Adaptive Meshing Scheme for Prediction of High-Speed Moving Loads Induced Ground Vibrations ..	31
1. Introduction	32
2. Description of the Reference Case	35
2.1. Geo-mechanical properties	35
2.2. Three-Dimensional computational grid	36
3. Adaptive Meshing Scheme: L-AMN Approach	38
3.1. Mathematical formulation	39
3.2. Numerical parameters of the L-AMN approach	40
3.2.1. Track foundation spatial mesh	41
3.2.2. Rail-beam spatiotemporal mesh	44
3.2.3. Computation of stable time step	46

3.2.4.	Execution time	47
4.	Validation of the L-AMN Approach	48
4.1.	Sub-Rayleigh range	48
4.1.1.	Harmonic excitation	49
4.1.2.	Multi-frequency domain	52
4.2.	Super-Rayleigh range.....	55
5.	Conclusions.....	56
	References.....	58
Chapter 3:		
	Frequency and Velocity Dependent Simplified Model for Rail/Foundation Dynamics	61
1.	Introduction	62
2.	Reference Case- 3D Modeling	64
3.	TTI Predictive Tool for Rail Vibrations	66
3.1.	Preliminary study.....	68
3.2.	TTI Model- Dynamic impedances	71
4.	Conclusions.....	76
	References.....	77
Conclusions and Further Work		
		79
1.	Conclusions.....	79
2.	Recommendations for Further Work	80
Appendix A:		
	Matlab Code of the Periodic Configuration Update Method: Formulation in the Time Domain.....	83
Appendix B:		
	Matlab Code of the L-AMN Adaptive Meshing Scheme: 3D Finite Difference Modeling	105

List of Figures

Figure 1-1: General view of the considered problem

Figure 1-2: Interpolation polynomial of Hermite with set of β points

Figure 1-3: Interpolation process applied to meshed beam at time t

Figure 1-4: Investigation of boundary effects: the influence of beam length on the accuracy of the PCU method; case of $V=0.5V_0$

Figure 1-5: The temporal limit of the non-convergence zone according to the mesh size (a) $\omega=0.5\omega_0$ (b) $\omega=1.0\omega_0$ (c) $\omega=2.0\omega_0$

Figure 1-6: Evolution of the error at the center of the beam according to the number of loading periods for different mesh size (a) $\omega=0.5\omega_0$ (b) $\omega=1.0\omega_0$ (c) $\omega=2.0\omega_0$

Figure 1-7: Influence of coupled mesh size-time step on the accuracy of the PCU-method

Figure 1-8: Influence of interpolation parameters on the accuracy of the PCU-method; case of $e=0.2$ m (a) $\beta=3$ (b) $\beta=5$

Figure 1-9: Influence of interpolation parameters on the accuracy of the PCU-method; case of $e=0.4$ m (a) $\beta=3$ (b) $\beta=5$

Figure 1-10: Influence of progressive mesh on the accuracy of the PCU method; case of $V=V_0$ (a) $\omega=0.5\omega_0$ (b) $\omega=1.0\omega_0$ (c) $\omega=2.0\omega_0$

Figure 2-1: Cross section of the studied railway track; the dimensions are measured in mm

Figure 2-2: Computational mesh grid: 275028 zones and 292020 grid points

Figure 2-3: Internal attachment conditions between the model components

Figure 2-4: Load attached moving node L-AMN algorithm for moving load problems

Figure 2-5: Effect of soil mesh on the dynamic response of the rail; $V=0$ and $f=50$ Hz

Figure 2-6: Effect of soil mesh on the dynamic response of the rail; $V=50$ Km/h and $f=50$ Hz

Figure 2-7: Effect of soil mesh on the dynamic response of the rail; $V=300$ Km/h and $f=10$ Hz

Figure 2-8: Effect of soil mesh on the dynamic response of the rail; $V=300 \text{ Km/h}$ and $f=50 \text{ Hz}$

Figure 2-9: Effect of the adaptive meshing scheme on the dynamic response of the rail; $V=50 \text{ Km/h}$ and $f=50 \text{ Hz}$

Figure 2-10: Stable time step of the L-AMN adaptive scheme depending on the progression of the loading process of a finite element; (a) $f=5 \text{ Hz}$ (b) $f=50 \text{ Hz}$

Figure 2-11: Calculation time of the L-AMN scheme; $V=50 \text{ Km/h}$ and $f=50 \text{ Hz}$

Figure 2-12: Response of the track/ground interaction model ($70 \times 30 \times 5 \text{ m}^3$) after three-period harmonic loading; $V=50 \text{ Km/h}$ and $f=10 \text{ Hz}$

Figure 2-13: Response of the track/ground interaction model ($60 \times 20 \times 5 \text{ m}^3$) after three-period harmonic loading; $V=50 \text{ Km/h}$ and $f=20 \text{ Hz}$

Figure 2-14: Response of the track/ground interaction model ($45 \times 20 \times 5 \text{ m}^3$) after three-period harmonic loading; $V=50 \text{ Km/h}$ and $f=30 \text{ Hz}$

Figure 2-15: Response of the track/ground interaction model ($45 \times 20 \times 5 \text{ m}^3$) after three-period harmonic loading; $V=50 \text{ Km/h}$ and $f=40 \text{ Hz}$

Figure 2-16: Response of the track/ground interaction model ($45 \times 20 \times 5 \text{ m}^3$) after three-period harmonic loading; $V=50 \text{ Km/h}$ and $f=50 \text{ Hz}$

Figure 2-17: Dynamic response of the rail ($X_r=-4 \text{ m}$) in the multi-frequency domain: first scenario $V=200 \text{ Km/h}$; (a) case 1 (b) case 2

Figure 2-18: Dynamic response of the rail in the multi-frequency domain: Second scenario $V=200 \text{ Km/h}$; (a) $X_r=0$ (b) $X_r=-4 \text{ m}$

Figure 2-19: Mobilized velocity [mm/sec] at the soil surface after three-period harmonic loading; $V=300 \text{ Km/h}$

Figure 2-20: Soil response ($E_{\text{soil}}=0.2E_s$) in the super-Rayleigh range after three-period harmonic loading; $V=350 \text{ Km/h}$ and $f=20 \text{ Hz}$

Figure 3-1: Components of the ballasted track structure

Figure 3-2: Computational finite difference grid: 194972 zones and 207972 grid points

Figure 3-3: Dynamic response of the track/ground interaction model due to single moving load

Figure 3-4: Sub-structuring approach for the assessment of ground vibrations

Figure 3-5: Calibration process of the simplified rail vibrations predictive tool

Figure 3-6: Flowchart of the Genetic Algorithm

Figure 3-7: Dynamic components of the rail viscoelastic foundation

Figure 3-8: Optimal capacity of the viscoelastic foundation to represent the dynamic behavior of the track foundation

Figure 3-9: Dynamic response of the rail at $X_r=0$; case of harmonic load moving at $V=50$ *Km/h*. Solid line: 3D numerical system, dotted line: TTI model

Figure 3-10: Dynamic response of the rail at $X_r=0$; case of harmonic load moving at $V=100$ *Km/h*. Solid line: 3D numerical system, dotted line: TTI model

Figure 3-11: Dynamic response of the rail at $X_r=0$; case of harmonic load moving at $V=200$ *Km/h*. Solid line: 3D numerical system, dotted line: TTI model

Figure 3-12: Dynamic response of the rail at $X_r=0$; case of harmonic load moving at $V=300$ *Km/h*. Solid line: 3D numerical system, dotted line: TTI model

List of Tables

Table 1-1: Parameters for track-foundation model

Table 1-2: Required time for numerical algorithm execution; case of $V=V_0$ and $\omega=2\omega_0$

Table 2-1: Mechanical properties of railway track foundation materials (elastic)

Table 2-2: Mechanical properties of the rail

Table 2-3: Peaks of the rail response at $t=3T$; $V=50 \text{ Km/h}$

Table 2-4: Frequency content of the deterministic multi-frequency moving loads

Table 2-5: Characteristics of the simultaneous harmonic moving loads

Introduction

In today's urban development, transport is one of the keys to the organization of our cities. Among the existing modes of transport, rail transport provides reliable and regular networks. The rapid growth of this popular mode of transport is mainly due to economic and social benefits. Unfortunately this mode of transport uses machines that generate significant vibrations in the ground. Generally, the generated vibrations do not pose a threat to the structure itself, but they can be sufficiently high in buildings to annoy the inhabitants, and cause personal distress in communities residing close to the lines. Therefore it is important to predict vibration levels before the line is constructed.

As a matter of fact, these vibrations are generated at the wheel/rail interface and arise mainly from the train weight and from irregularities in the wheel/rail geometry, wheel defects and variation of stiffness due to the discrete supporting of rail. Add that, the Vibration amplitude becomes significant if the train speed increases and becomes close to the natural Rayleigh wave speed of the surrounding soil and for a loading frequency comparable to the track natural frequency.

With the continuous progress in the informatics field, the numerical modeling techniques become a classical way for high accuracy simulation of soil/structure interaction problems. The study of ground-borne vibration due to railways traffic using numerical models requires a balance of model accuracy and efficiency to produce in a reasonable time frame. Many of these models are developed in the frequency domain. However, they are restricted to linear steady-state problems. To take into account the geometrical and/or mechanical nonlinearities in the track or soil subsystems, or to simulate a transient problem, the time domain approach still the more appropriate, but require a high computational effort especially when dealing with high speed and frequency loading domain.

The present work aims to provide a comprehensive numerical model that correctly reproduces the mutual dynamic interactions between the system components. The model is capable of predicting the distribution of the dynamic responses at the wheel-rail interface in the downward direction to the track subgrade and in the upward direction to the car body.

Chapter 1 presents an innovative approach the “Periodic Configuration Update” or PCU method to assess the dynamic response of an infinite Euler-Bernoulli beam posed at the top of continuous foundation. In this approach the foundation material moves relative to the FE mesh after a certain number of time steps so that the moving loads do not need to move relative to the mesh. To compensate the distance lag, a periodic injection of a new initial condition into the numerical system is performed at the end of each step. This gives a better efficiency and smaller demand of model size.

Chapter 2 proposes an advanced three dimensional finite difference modeling for the prediction of track/soil induced vibrations due to passage of high speed moving loads. Each moving load is simulated using an adaptive meshing scheme the “L-AMN” based upon the creation of a load-attached moving node on the rail rolling surface. The novel feature of the formulation is the use of mesh superposition to produce spatial refinement in the transient problem. The analysis is performed within the frame of a reference case consisting of a classical straight ballasted track supported by a homogeneous soil layer underlain by a rigid substratum. Numerical experiments are carried out in the sub-Rayleigh and super-Rayleigh velocity range show an important capacity of the proposed scheme to model the impact of moving loads on ground response.

Chapter 3 investigates the reliability of a simplified model which is the infinite Euler-Bernoulli beam resting on continuous viscoelastic foundation. Firstly, numerical simulations are conducted using the sophisticated 3D finite difference model for a wide range of selected loading frequency. The results of the 3D modeling is used to calibrate the dynamic impedances of the simplified beam model where an iterative curve fitting procedure based on the Genetic Algorithm (GA) is applied in order to obtain the convergence between the output signals of the two models. This process leads to a frequency and velocity dependent prismatic beam model with constant material density.

Chapter 1

Adaptive Analysis of Infinite Beams Dynamics Problems Using the Periodic Configuration Update Method in the Time Domain

ABSTRACT

This chapter proposes a new approach for the assessment of the dynamic response of continuously supported infinite beams under high speed moving loads. A change in the representation of equations of motion in the dynamics of discrete structures is proposed in order to obtain an improved accuracy of the numerical integration in the time domain. The proposed numerical method called “The Periodic Configuration Update” or “PCU Method” is applied to solve the problem of a vertical moving harmonic load on an infinite classical Euler-Bernoulli beam resting on a continuous viscoelastic foundation. This study shows the superiority of the proposed method in comparison with other methods presented in the literature which suffer from the material time derivative, i.e. convective terms; that arises from the Galilean transformation. To overcome this numerical problem, the PCU method retains the principle of the spatial follow of loads while zeroing the relative velocity with the traversed beam via a step-by-step adaptive integration of the equation of structural dynamics. The dynamic load is modeled with high theoretical velocities that can reach the critical velocity of the studied beam with different angular frequencies belonging to moderate frequency range. A parametric study is carried out in order to analyze the influence of key parameters on the convergence. The obtained results show a high efficiency of the PCU method for solving these types of problems relative to the dynamics of high speed trains-tracks.

Keywords: infinite beams, periodic configuration update, moving load, high speed, time domain

1. Introduction

The problem of infinite beams resting on equivalent foundation and subjected to high speed time-variant moving loads has represented a challenge in structural dynamics domain due to the complex spatiotemporal coupling. Usually these models are encountered when solving the train/track interaction problems. By virtue of the relevance in the analysis and design of railway tracks, the dynamic response of beams resting on elastic foundation and subjected to moving loads has been extensively investigated [1–3]. With the increasing train speed, the problem of interactions between wheel and rail becomes more complicated as a result of the emergence of several numerical barriers. In dealing with moving load problems, the classical Finite Element Method (FEM) encounters difficulty when the moving load approaches the boundary of the truncated domain. The effect of this problem will be amplified when the load travels with high velocity. These difficulties can sometimes be overcome by employing a large enough-refined domain but at the expense of significant increase in computational time. This has encouraged many researchers to propose numerical algorithms to overcome these complications [4–7].

Koro et al. [4] attempted to address the problem of moving loads. They have pointed out the dynamic response of the train-track interaction problem considering the rail as a Timoshenko beam. The method proposed by these investigators is based on the idea of creating a node which moves with the location of the concentrated load. This method experiences some difficulties in formulation, such as restructuring of system matrices at every time step. Krenk et al. [5] proposed the use of the FEM in a load-attached coordinates system to obtain the response of an elastic half space subject to a moving load. Koh et al. [6] adopted the idea of moving coordinates system to solve the train-track interaction problems, and called the numerical algorithm as the Moving Element Method (MEM). It has since been used by many other researchers. Ang and Dai [8] and Ang et al. [9] applied the MEM to investigate the “jumping wheel” phenomenon in high-speed train motion at constant velocity over a transition region where there is a sudden change of foundation stiffness. Tran et al [10] proposed a reformulation of the MEM to find the vertical dynamic response of high speed rail systems involving accelerating/decelerating trains.

However, the key disadvantage of these approaches appears through the material time derivative (convective terms) that arises from the Galilean transformation. It has been noticed that when the load velocity increases the induced negative impact of the convective terms

increases especially on the stiffness matrix which is likely to become ill-conditioned [11]. According to Leonard [12] the possible error mechanisms that can be associated with a differencing process of convection problems are the unphysical oscillatory behavior in an implicit solution, the disastrous non-convergence in an explicit convection computation and the truncation error. In this context, Wu et al. [13] have analyzed the stability of an explicit numerical scheme the “Central Difference Method” which showed a tendency to deteriorate with higher damping ratio of the structure. This fact is due to the proportional relationship between the physical damping of the structure and the induced numerical damping which comprises the numerically induced energy dissipation and the distorted frequency of the numerical solution.

When linear elements are used in the FEM discretization of wave propagation with convection, a numerical instability occurs due to negative numerical damping [14]. This implies a significant limitation of the MEM. However, to achieve accurate results a special treatment of the numerical disturbance should be taken into account. Lately, Nguyen and Duhamel [7] have managed to reduce this undesirable factor that appears during the discrete resolution of the dynamic equation. They have proposed a procedure that consists of the split of the displacement field into two parts in which the first depends on the instantaneous position of the load whereas the second is a pure function of time. Next, a Galilean transformation is applied to the time-discretized expression (developed based on the Generalized- α Method [15]) of the first component of beam response. In addition to the important residual influence of the convective terms, there is another shortcoming that appears when elaborating the elementary matrices of the system in the nonlinear domain. Instead of explicit expressions, numerical quadrature by Gauss points should be used. Moreover, its intrinsic parameters have been proposed by assuming that the element sizes are identical.

Hence, the aim of this research work is to present an innovative approach to assess the steady-state response of an infinite Euler-Bernoulli beam posed at the top of continuous foundation. Herein the case of viscoelastic layer that formed from infinite series of spring-damper unites is taken into account. The proposed method called the “Periodic Configuration Update” or PCU method retains the principle of the spatial follow of loads while zeroing the relative velocity with the traversed beam. The convective terms are omitted via a step-by-step adaptive integration of the equation of structural dynamics in which the beam is considered to be subjected to time-variant stationary loads during each calculation step. To compensate the

distance lag, a periodic injection of a new initial condition into the numerical system is performed at the end of each step.

The PCU method is tested in the case of a problem involving theoretical moving loads traveling with high velocity that can reach the critical velocity of the foundation model. For a case of undamped vibration, a load moving at this velocity produces unbounded amplitude of traveling waves [16]. In order to investigate the convergence of the proposed method, a parametric study is carried out on the main influential parameters comprising the period of a single step, the degree of the interpolation polynomial and the spatial mesh effect. The validity of the PCU method is demonstrated by comparing its results with those of analytical existing study [14].

This chapter is organized as follows: In section two, the mathematical modeling of the PCU method is presented; in section three we demonstrate the numerical convergence of the proposed method by means of error propagation analysis and consistency verification. In section four we investigate numerically the influence of various spatiotemporal parameters which govern the accuracy of the PCU method. And finally in section five we discuss and critically evaluate the obtained results.

2. Mathematical Formulation

The main idea of the proposed method is to numerically solve the dynamic equation of infinite beams that posed on a continuous foundation under high-speed moving loads via consecutive steps of stationary state loading. To compensate the induced spatial delay at the end of each step, the geometric configuration of the computational grid is periodically changed using the generalized form of the Hermitian polynomial. The proposed solution is none other than a periodic adaptation of a truncated part of the infinite structure. This is equivalent to an inverse mechanism to those formulated in moving spatial reference [4–7], in which the moving loads are attached to a deterministic position while the beam seems like a “moving beam” at the same velocity V of loads. Consequently the relative speed, i.e., convection velocity, vanishes.

In this study, the PCU method is applied to find the dynamic response of infinite Euler-Bernoulli beam resting on a continuous viscoelastic foundation subjected to a single moving harmonic load. The effect of shear deformation and rotational inertia of the cross-section of the beam is neglected (Euler-Bernoulli Theory). The Winkler hypothesis is taken into account which postulates that a foundation behaves like an infinite series of closely spaced,

independent, linearly elastic, vertical springs k . The damping of the material forming the foundation is assessed through linear viscous dampers η continuously distributed beneath the Euler-Bernoulli beam. Figure 1-1 presents a general view of the considered problem, where the spatial reference system (x,y) is attached to the load/structure system. Its origin is arbitrarily located along the beam. However, for convenience, it is taken at the center of the truncated part used in the simulation. This reference system is localized at every calculation step with respect to a fixed Galilean reference (X,Y) .

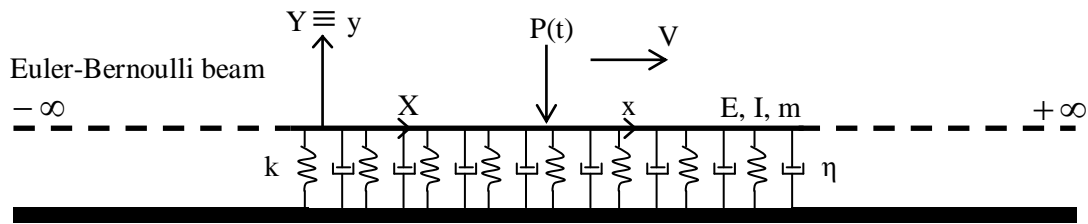


Figure 1-1: General view of the considered problem

Obviously, in numerical simulations just a finite domain is modeled, where its length is selected to minimize the boundary effect that can induce disturbances in the dynamic response. Consequently a large-enough mesh size is adopted to prevent the reflection of non-dissipated waves. Nevertheless, appropriate infinite elements can be easily integrated in the numerical system.

2.1. Dynamic Equation of the Beam

The FEM is employed to establish the equation of motion, by adopting Galerkin's approach and procedure of writing the weak form in terms of the displacement field [10]. After spatial discretization of the dynamic system with one-dimensional beam elements, the global equation of motion providing the bending deformation expressed in the time domain can be written in the own reference system of the structure as follows:

$$M\ddot{U} + C\dot{U} + KU = F \quad (1.1)$$

Where:

$$M = \sum \left(m \int_0^{L_e} Q^T Q dr_e \right) \quad (1.2a)$$

$$C = \sum \left(\eta \int_0^{L_e} Q^T Q dr_e \right) \quad (1.2b)$$

$$K = \sum \left(EI \int_0^{L_e} Q''^T Q'' dr_e + k \int_0^{L_e} Q^T Q dr_e \right) \quad (1.2c)$$

Where U and F denote the global displacement and external forces vectors respectively, and superposed dots and primes indicate the order of time and space differentiation respectively. E , I and m are Young's modulus, second moment of inertia, and mass per unit length of the beam, respectively. For beam element of length L_e , it is common to use the shape functions matrix Q based on Hermitian cubic polynomials expressed in the elementary spatial reference r_e [10].

In Eq. 1.2, these are the global mass M , damping C and stiffness K matrices for the dynamic system, which can be assembled by matrices of element mass, damping and stiffness respectively. It can be seen that the presented element matrices are identical to the matrices derived by Koh et al. [17] by setting the convection velocity equal to zero. This fact shows clearly the difference with the upper mentioned methods which include convective terms.

2.2.Numerical Algorithm- Adaptive Procedure in the Time Domain

In order to simulate the motion of the loads along the beam, it is proposed to solve the global equation of motion (Eq. 1.1) in the moving beam-attached coordinates system (x,y) by injecting after a time interval $\Delta t = \alpha \times dt$ (where α is a nonzero integer and dt is an infinitesimal time step) a new initial condition based on the generalized Hermite's interpolating polynomial. A change in the configuration of the beam in terms of displacement, rotation and their first and second derivatives with respect to time is proposed. This process serves to compensate the relative distance delay at time t (denoted in the following by δx) between the studied structure and the applied load that arises from the stationary- loading state calculation during the interval $[t-\Delta t, t]$. The updated configuration will be considered to be the starting point of the following calculation step during the interval $[t, t+\Delta t]$; and so on. Thus, this numerical algorithm simulates an equivalent motion mechanism of the structure to ensure zero convection velocity.

The interpolating polynomial of Hermite Ψ_h of order $2\beta-1$ expressed in Eq. 1.3 and presented in Figure 1-2 is considered in this work. It is used to represent a function Ψ on the r -axis (whose origin coincides with the position of central node) by using its known values at a discrete set of β points which is taken as odd integer to ensure the symmetry condition.

$$\Psi_h(r) = \sum_{j=1}^{j=\beta} [N_{2j-1}(r)\Psi(r_j) + N_{2j}(r)\Psi'(r_j)] \text{ such that } r_1 \leq r \leq r_\beta \quad (1.3)$$

Note that, the polynomials N_{2j-1} and N_{2j} are constructed in such a way to enforce the following set of β conditions:

$$\Psi_h(r_j) = \Psi(r_j) \quad (1.4a)$$

$$\Psi_h'(r_j) = \Psi'(r_j) \quad (1.4b)$$

This leads to the following expressions:

$$N_{2j-1}(r) = \frac{q_j(r)}{q_j(r_j)} \left[1 - (r - r_j) \frac{q_j'(r_j)}{q_j(r_j)} \right] \quad (1.5a)$$

$$N_{2j}(r) = \frac{q_j(r)}{q_j(r_j)} (r - r_j) \quad (1.5b)$$

In which q_j is the square of the Lagrange polynomial associated to the node j :

$$q_j(r) = \prod_{a=1, a \neq j}^{a=\beta} \left(\frac{r - r_a}{r_j - r_a} \right)^2 \quad (1.6)$$

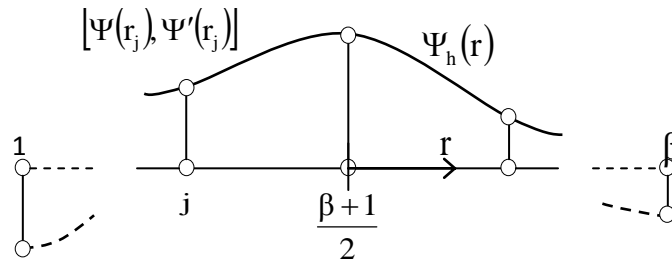


Figure 1-2: Interpolation polynomial of Hermite with set of β points

In order to repair the configuration of the beam at the end of each calculation step, the polynomial Ψ_h is used (Eq. 1.3). Considering an arbitrary node n (global numbering) located

on the computational grid of the structure, the following equation represents the interpolation relationship of the displacement field at time t :

$$\tilde{u}_n = \sum_{j=j_l}^{j=j_u} [u_j N_{2l(j)-1}^n(\delta x) + \theta_j N_{2l(j)}^n(\delta x)] \quad (1.7)$$

Where \tilde{u}_n is the updated displacement on the central node n in which it is proposed to equalize that of the neighbor point located at $r=+\delta x$; u_j and θ_j are the displacement and the bending rotation on node j before the configuration change of the truncated beam. Note that the lower and upper bounds of the summation operator are determined according to the number of nodes integrated in the interpolation process. They are given as follows:

$$j_l = n - \frac{\beta - 1}{2} \quad (1.8a)$$

$$j_u = n + \frac{\beta - 1}{2} \quad (1.8b)$$

In equation 1.7, the set of β constitutive polynomials ($N_{2l(j)-1}^n, N_{2l(j)}^n$) are distinguished by the index n to highlight the target node; $I(j)$ is a bijective function used to switch from global (ranging from 1 to the total number of the nodes, N_t) to local (ranging from 1 to β) system of numbering and it is expressed as follows:

$$j \rightarrow I(j) = j - \left[n - \frac{\beta - 1}{2} \right] + 1 \quad (1.9)$$

For clarity and convenience we consider the following auxiliary relationships:

$$A_j^n = \frac{\partial N_{2l(j)-1}^n}{\partial r} \quad (1.10a)$$

$$B_j^n = \frac{\partial N_{2l(j)}^n}{\partial r} \quad (1.10b)$$

By differentiating the equation 1.7 with respect to r , the interpolating polynomial of the bending rotation $\tilde{\theta}_n$ is obtained as follows:

$$\tilde{\theta}_n = \sum_{j=j_l}^{j=j_u} [u_j A_j^n(\delta x) + \theta_j B_j^n(\delta x)] \quad (1.11)$$

Figure 1-3 presents a schematic explanation of the interpolation process considered in this study.

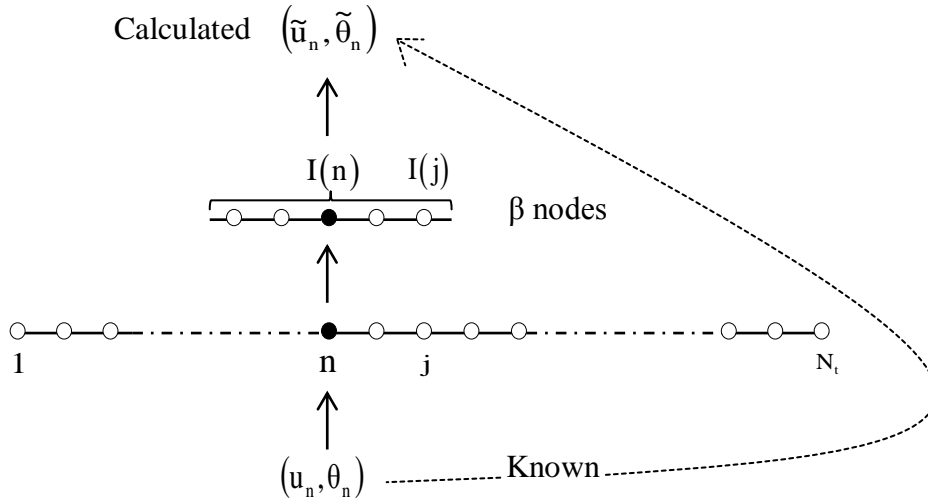


Figure 1-3: Interpolation process applied to meshed beam at time t

To avoid the recalculation of the nodal interpolation polynomials at the start of each step, the previous equations (Eq. 1.3 to 1.11) are rearranged in matrix form. Therefore considering the matrix H constructed as follows:

$$H[n, j] = \begin{cases} N_{2j-1}^n(r) & 1 \leq j \leq \beta \\ N_{2(j-\beta)}^n(r) & \beta + 1 \leq j \leq 2\beta \end{cases} \quad (1.12)$$

On the other hand, we consider the matrix G grouping the nodal displacements and rotations at time t that derived from a stationary- loading state calculation; it is expressed as follows:

$$G[j, n] = \begin{cases} u_{I^{-1}(j)} & 1 \leq j \leq \beta \\ \theta_{I^{-1}(j-\beta)} & \beta + 1 \leq j \leq 2\beta \end{cases} \quad (1.13)$$

It should be mentioned that the index n appears implicitly in the reciprocal function I^{-1} . Moreover, when calculating the elements of matrices H and G at the model boundaries, i.e. when the equation 1.14 is satisfied, the symmetry condition in the interpolation process is maintained but there is a restriction in the number of nodes (less than β). In other words, the order of the interpolating polynomial will increase by four when passing (in the load traveling direction) to the neighbor node in the left side of the beam while it will decrease by four in the right side.

$$1 \leq n \leq \frac{\beta-1}{2} \text{ or } N_t - \frac{\beta-3}{2} \leq n \leq N_t \quad (1.14)$$

Therefore the updated nodal linear displacement and rotation vectors are obtained using the matrices H (after substituting the variable r by δx) and G as follows:

$$\tilde{u}[j,1] = S_1[j, j] \quad (1.15a)$$

$$S_1 = H(\delta x).G \quad (1.15b)$$

$$\tilde{\theta}[j,1] = S_2[j, j] \quad (1.16a)$$

$$S_2 = H'(\delta x).G \quad (1.16b)$$

By assembling the above vectors, the updated global displacement vector \tilde{U} at time t can be obtained.

Similar matrix equations are used to find the updated global velocity \tilde{U} and acceleration \tilde{U} vectors, in which the matrix G in Eq. 1.15 and 1.16 is replaced by a corresponding matrix regrouping the nodal linear and angular velocities and accelerations respectively just after the stationary- loading state calculation. Hence, the obtained configuration of the beam $(\tilde{u}, \tilde{\theta}, \tilde{U})$ is injected back into the global equation of motion (Eq. 1.1) as an initial condition for the next step of calculation during the interval $[t, t+\Delta t]$. Within this interval an appropriate time integration scheme is used to linearize the system of differential equations. This process will be repeated over the entire time of calculation.

3. Validation of the PCU Method

To test the performance and accuracy of the proposed method, the dynamic response of an infinite beam resting on a viscoelastic foundation subjected to a single moving harmonic load $P(t)$, crossing the beam with a constant velocity V found analytically is compared to that provided by the numerical method. Where:

$$P(t) = P_0 e^{-i\omega t} \quad (1.17)$$

P_0 and ω denote the amplitude and the angular frequency of the load respectively, and $i = \sqrt{-1}$.

3.1.Statement of the problem

Based on the analytical solution of Andersen et al. [14] the displacement field $u_a(x, t)$ of the beam is expressed in the spatial reference (x,y) as follows:

$$u_a(x, t) = \begin{cases} A_1 e^{-\tau_1 x + i(\sigma_1 x - \omega t)} + A_2 e^{-\tau_2 x + i(\sigma_2 x - \omega t)} \\ A_3 e^{-\tau_3 x + i(\sigma_3 x - \omega t)} + A_4 e^{-\tau_4 x + i(\sigma_4 x - \omega t)} \end{cases} \quad (1.18)$$

Where A_j ($j=1, 2, 3, 4$) are the amplitude parameters to be determined using the conditions of continuity of the displacement, the bending moment and the shear force fields at the loading point; τ_j and σ_j are respectively the real and imaginary part of the j^{th} wave number. Physically τ_j represents the propagation and σ_j the attenuation of the j^{th} component of the propagated waves.

The validations are performed on linear structures for which the analytical solution can be found for all velocities and loading frequencies. In this analysis, the mechanical characteristics of an European railway traversed by high-speed trains, proposed by Nguyen and Duhamel [7] are used; values are summarized in Table 1-1.

Table 1-1: Parameters for track-foundation model (Nguyen and Duhamel [7])

Parameters	Value
Flexural rigidity	$6.12 \times 10^6 \text{ N.m}^2$
Track section	76.86 cm^2
Density of track material	7850 Kg/m^3
Stiffness of foundation	$1.6 \times 10^7 \text{ N/m}^2$
Viscous damping ratio	10%

Furthermore, for convenience and reasonable choice of load parameters; critical velocity V_0 and frequency ω_0 values are defined in Eq. 1.19 [7], which depend only on the structural characteristics of the system.

$$V_0 = \left(\frac{EI k}{m^2} \right)^{1/4} \quad (1.19a)$$

$$\omega_0 = \sqrt{\frac{k}{m}} \quad (1.19b)$$

To evaluate the order of magnitude of V_0 (≈ 1458 Km/h), it should be mentioned that the experimental maximum speed of the TGV train in France has reached 515 Km/h [18]. It represents 35% of the critical velocity of the adopted model of European railway track. Recently in Spain, the Córdoba–Antequera High Speed Train (HST) line was designed for a maximum speed of 350 Km/h [19] (24% of V_0). Thus the upper bound of the studied velocity range is considered much larger than the current HST traveling speed.

On the other hand, Adam and von Estorff [20] have been highlighted the ground vibrations that lie in the frequency range of 4-50 Hz in view of the distress to adjacent structures and annoyance to residents. However, in this study three frequencies are considered in which one of them $\omega=0.5\omega_0$ (corresponds to ≈ 41 Hz) is located in the interval cited in [20]. The two other cases $\omega=\omega_0$ and $\omega=2\omega_0$ are adopted to make the numerical problem more delicate due to the increase in the rate of temporal variation of $P(t)$.

A finite domain of length L_t is modeled; the numerical integration is performed over a time interval $T_t=\lambda \times T$ where T represents the period of the excitation load and λ is a nonzero integer. The analysis is conducted for a harmonic excitation at various combinations of load frequency and velocity of passage. Note that the analytical solutions are stationary, whereas the numerical solutions include a transition part which arises because the load also excites the Eigen modes of the numerical model and is fully removed after approximately eight load periods.

In this section, the beam is meshed non-uniformly on both end portions while the central portion of the beam called "diffusion zone" i.e. almost all of the energy is dissipated in this zone, is uniformly meshed by elements with size e . The harmonic load is considered to be the imaginary part of P (Eq. 1.17), so $U_A(x, t) = \text{imag}(u_a)$ was taken for the analytical solution.

$\xi_c(t)$ is defined in Eq. 1.20 as the instantaneous relative error on the displacement field at the point of application of the moving load, calculated as follows:

$$\xi_c(t) = \left| \frac{U_A(0,t) - \tilde{U}_N[0,t]}{U_A(0,t)} \right| \times 100 \quad (1.20)$$

Where \tilde{U}_N denotes a summary matrix regrouping the vectors \tilde{U} which are found by the PCU method (see Eq. 1.7 to 1.16) in which the time difference between two consecutive columns can reach Δt (depending on the available memory allocation). The two arguments of \tilde{U}_N are the position of the desired node and the time instead of the line and column numbers.

To test the correct diffusion of the load over the entire span at time t_s , a new parameter $\xi_{tr}(x,t_s)$ is introduced in order to describe the error committed on the displacement field at the nodes, calculated as follows:

$$\xi_{tr}(x,t_s) = \left| \frac{U_A(x,t_s) - \tilde{U}_N[x,t_s]}{\max_x |U_A(x,t_s)|} \right| \times 100 \quad (1.21)$$

Γ_1 and Γ_2 are the maximum values of ξ_c and ξ_{tr} respectively.

In order to minimize the boundary effect, a preliminary study was conducted to find the length of the domain to consider in the numerical calculation. The load is considered to cross the beam with a speed $0.5V_0$; the three cases of angular frequencies are taken into account. Figure 1-4 shows the variation of Γ_1 and Γ_2 with the change of L_t . The graphs show that the boundary effect becomes predominant when the frequency of the load increases.

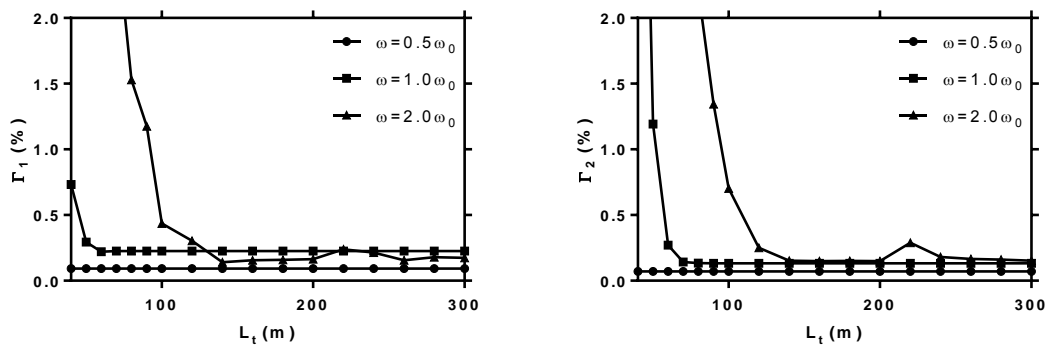


Figure 1-4: Investigation of boundary effects: the influence of beam length on the accuracy of the PCU method; case of $V=0.5V_0$

In the sequel, a total length of 220 m is taken for the beam.

3.2. Convergence of the PCU method

In the field of numerical resolution, several time integrators have been proposed with wide range of efficiency degree, among them the Runge-Kutta, the central difference, the Newmark, the Wilson- θ and the Houbolt methods [21,22] in which they are used to compute the time response of initial value problem. According to Verlinden [23] the Newmark method offers a good compromise between efficiency and reliability over a large range of multibody applications; it is rigorously established in the case of linear systems[24]. In contrast, the second order accuracy and the controllable algorithmic dissipation in the higher modes cannot exist simultaneously within this family of algorithms [25].

To perform the stationary- loading state calculations in the frame of the PCU method, the temporal solver of Newmark is adopted. Several mathematical concepts are introduced when solving ordinary differential equations through their equivalent discretized system. The three main ones are convergence, stability and consistency which are used for linking the exact solution of continuous equations to the numerically resolved solution.

3.2.1. *Non-convergence zone*

This study is intended to find the zone where the numerical scheme is inevitably divergent; the proposed solution is to carry out two sets of calculations with $V=0$ and $V=V_0$, for finding the dt values as a function of the mesh size, that lead to non-convergence of the PCU method. The three cases of angular frequencies are taken into account. The central part of the beam is meshed using elements with constant length e varying between 0.2 m and 0.4 m. Figure 1-5 shows the effect of mesh size on the time step that leads to the numerical divergence. The maximum committed error by the method when finding the displacement field at the beam center is depicted for both velocity cases and at different angular frequencies

The obtained results show that the value of dt delimiting the divergence zone which increases with the increase in the mesh size is independent on the traveling velocity of the moving load. In other words, the simulation of the moving load problem by the PCU method causes no constraint on the convergence of the dynamic equation under stationary loading (see Eq. 1.1 and 1.2). This conclusion remains valid for the three treated cases of frequency.

On the other hand, the general trend of curves expressing Γ_1 with dt is increasing in the case of critical velocity with a tendency to approach zero when dt tends to zero; Γ_1 is almost

negligible in the other case. In the following; the deduced values of dt are used to perform the numerical simulations.

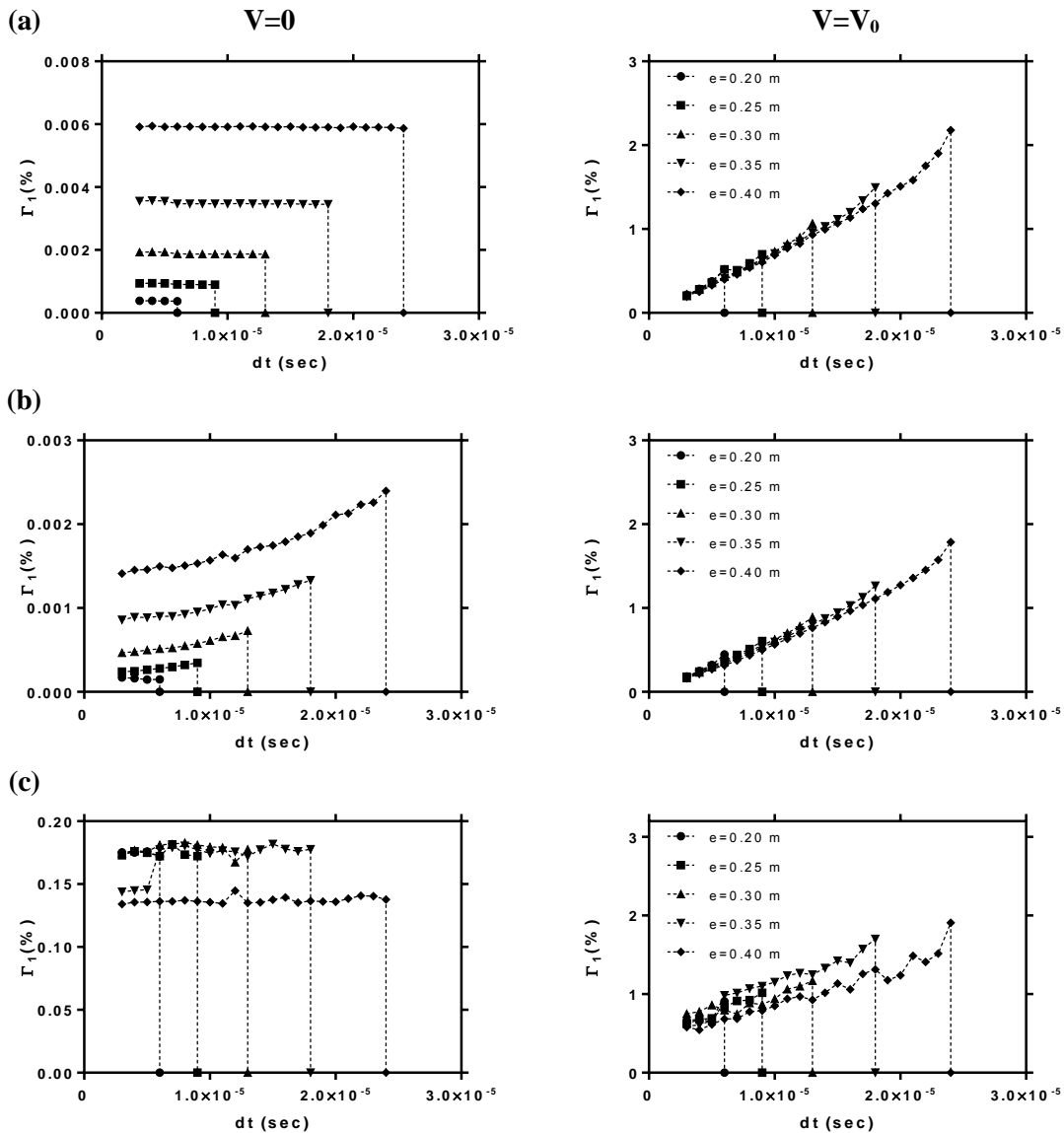


Figure 1-5: The temporal limit of the non-convergence zone according to the mesh size (a) $\omega=0.5\omega_0$ (b) $\omega=1.0\omega_0$ (c) $\omega=2.0\omega_0$

3.2.2. Stability of the numerical method

This section aims to prove that with suitable choice of discretization parameters, the numerical solutions computed by the proposed method stay within the desired state space throughout the computational domain. For this reason, the stability of the PCU method is examined when solving the problem of infinite beam on viscoelastic continuous foundation, knowing that the problem is physically stable. It is therefore ensured that the difference

between the obtained numerical solution and the exact solution of the differential equations remains bounded. Stability indicates whether or not the error increases over time.

Figure 1-6 shows the variation of the error $\xi_c(t)$ at the center of the beam according to the number of periods T of the moving load exciting the dynamic system at the two extreme values of velocity for different mesh size and for the three values of angular frequencies.

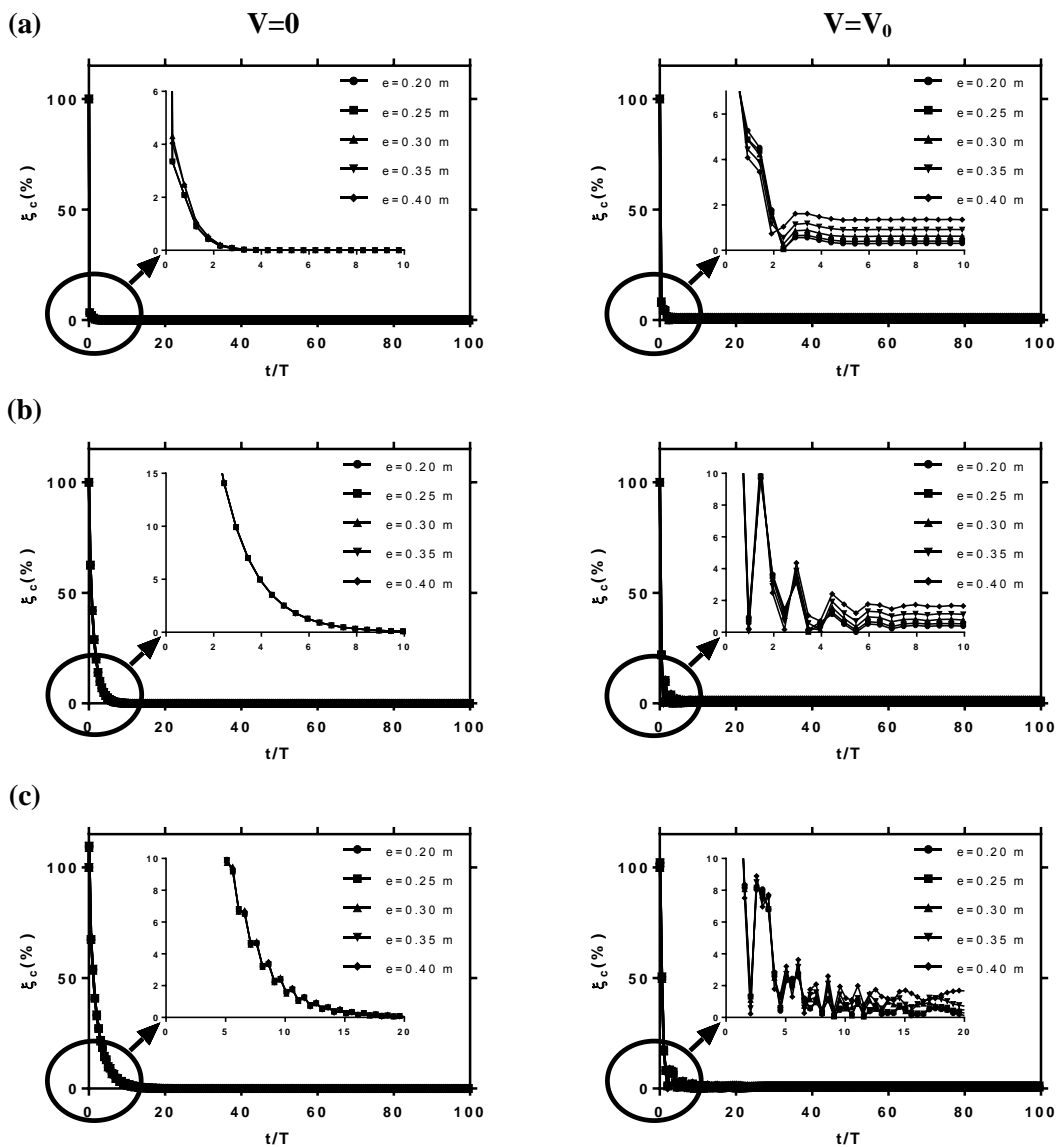


Figure 1-6: Evolution of the error at the center of the beam according to the number of loading periods for different mesh size (a) $\omega=0.5\omega_0$ (b) $\omega=1.0\omega_0$ (c) $\omega=2.0\omega_0$

The results show a strong stability of the PCU method even after $\lambda=100$ loading periods which excite the beam with its critical velocity, the numerical solution remains bounded, and the error is not amplified with the calculation progress. Moreover, the results show a minor effect of the mesh size on the stability diagram for the proposed numerical method. Add that

when the loading frequency changes, the transition part before reaching the stationary response has a constant duration with respect to the frequency ($\approx 16\pi/\omega_0$).

3.2.3. Consistency of the numerical method

Consistency is the property which ensures that the numerical solution of the discretized equation that tends to the exact solution when the mesh size e and the time step dt tend to zero. Staying within the same demonstration logic of numerical properties, Figure 1-7 shows the effect of simultaneous reduction of e and dt (according to the graphs of Fig. 1-5) on Γ_1 and Γ_2 .

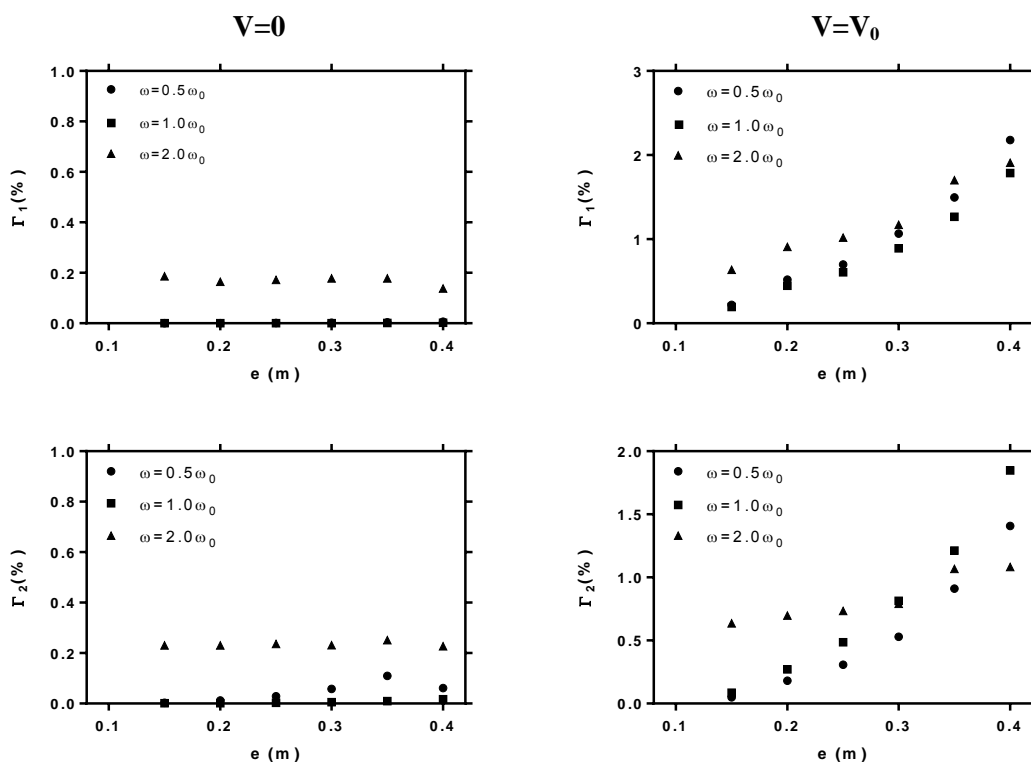


Figure 1-7: Influence of coupled mesh size-time step on the accuracy of the PCU-method

The obtained results show that the numerical solution becomes exact when the mesh size tends to zero which intersect with those presented in Fig. 1-5, i.e. the truncation error tends to zero. This trend is clear when the velocity is the critical value of the beam. In the case of stationary time variant loading, the error is almost negligible for all cases. It can be concluded that the numerical algorithm is consistent.

The theorem of Lax [26] provides that, in evolutionary problem with initial condition, using a consistent numerical scheme, the stability of this scheme is a necessary and sufficient condition for its convergence. Hence the PCU method is convergent.

4. Numerical Study

In this section, a parametric analysis is conducted on the PCU method. The influence of the interpolation parameters α and β on the accuracy and efficiency of the numerical algorithm is discussed on the entire traveling velocity axis and for the three values of the angular frequency. The analysis is carried out for different types of mesh size. Finally, the effect of a progressive mesh in the diffusion zone is studied.

A truncated segment of the beam with a length of 220 m is used. As demonstrated in section 3, this length is considered to be sufficient, to minimize the effects of erroneous artificial boundaries resulting from the use of a finite field model for the infinite domain problem of moving loads. In this study, the method of Newmark with Fox-Goodwin coefficients which lead to conditionally stable, second order accurate implicit scheme [22], is applied to linearize the system of differential equations during the stationary- loading state calculations.

4.1. Effect of interpolation parameters

To reach a good compromise between the accuracy of numerical results and the required computational effort, a parametric analysis is conducted on the effect of α and β . Knowing that it is expected a priori, in the one hand to have a major impact on the performance of the PCU method, and on the other hand to strongly affect the volume of required numerical operations which is simultaneously proportional to $1/\alpha$ and β (see Eq. 1.15 and 1.16). Thus, this analysis aims to investigate the reliability of the proposed method according to its intrinsic parameters.

Two cases of mesh size including $e=0.2$ m and $e= 0.4$ m are taken into consideration; the obtained results are plotted according to the traveling velocity of the harmonic load up to V_0 and they are presented respectively in Figures 1-8 and 1-9.

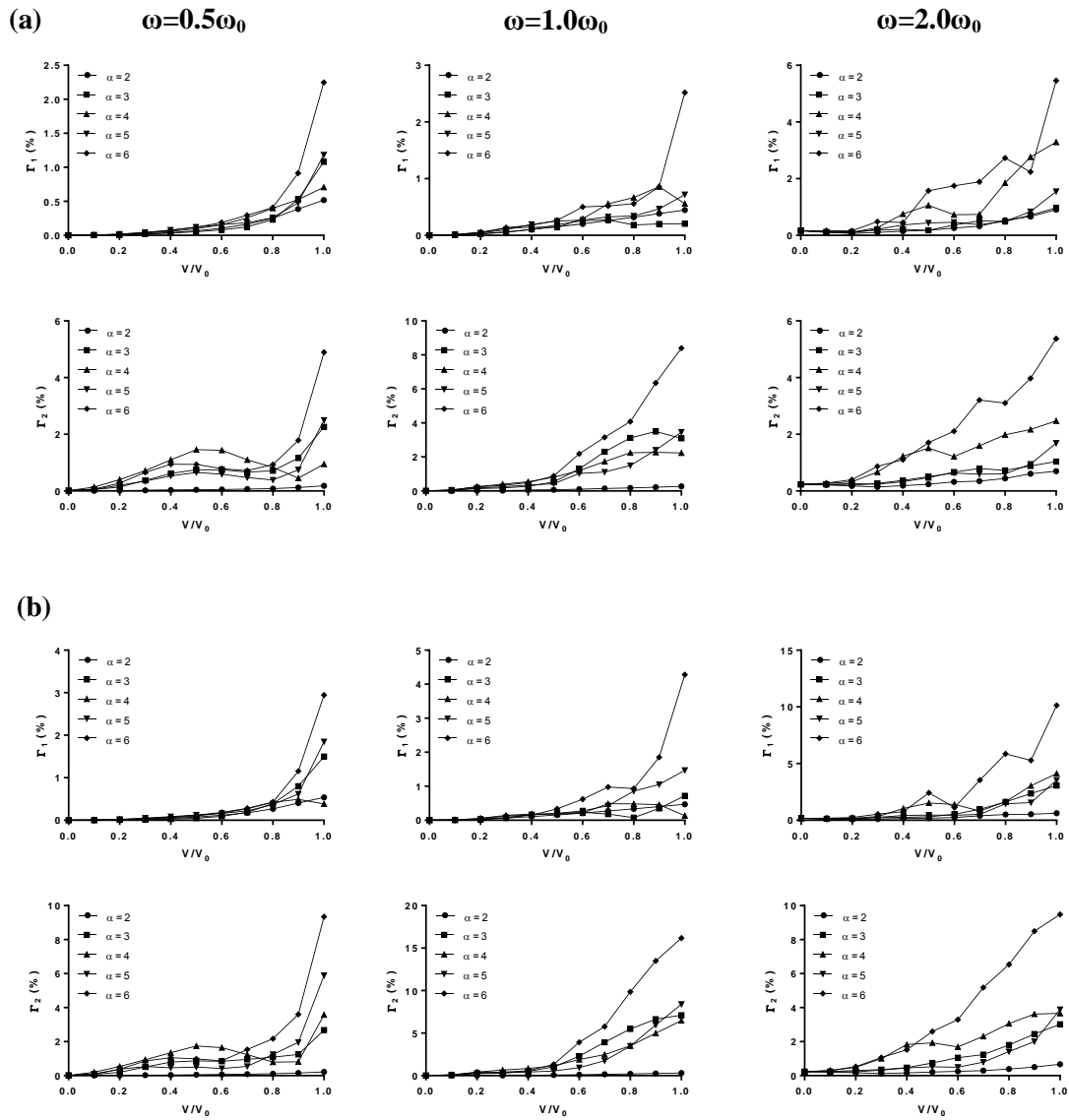


Figure 1-8: Influence of interpolation parameters on the accuracy of the PCU-method; case of $e=0.2$ m (a) $\beta=3$ (b) $\beta=5$

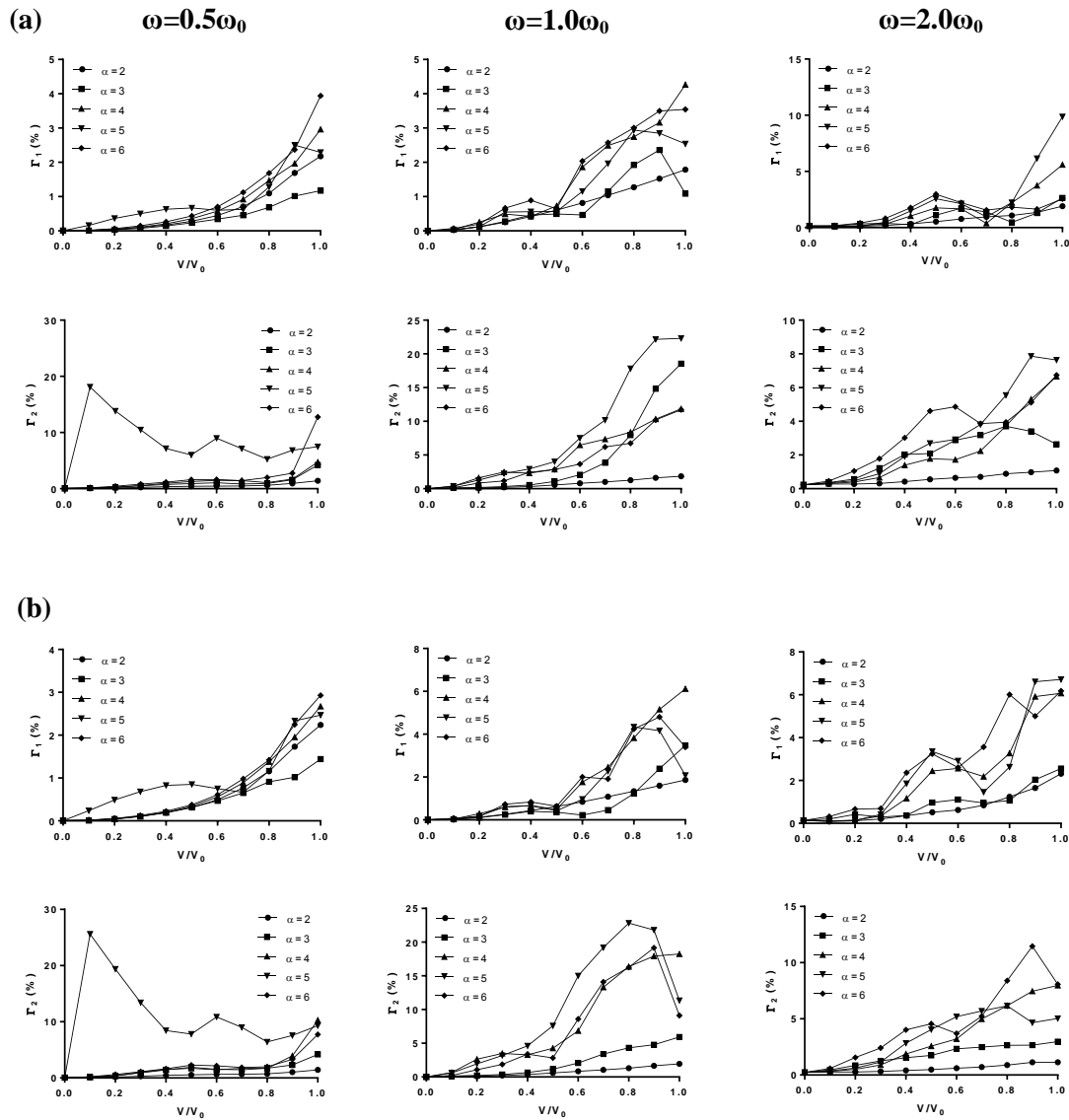


Figure 1-9: Influence of interpolation parameters on the accuracy of the PCU-method; case of $e=0.4$ m (a) $\beta=3$ (b) $\beta=5$

The numerical results show that the general trend of the graphics expressing the variation of Γ_1 and Γ_2 is almost unchanging over the entire considered velocity range when β is increased. Obviously, when V increases the accuracy of the method will decrease but still acceptable in some range of α ; therefore the trend is generally increasing. This conclusion remains valid for both mesh size adopted in this study. On the other hand, the use of a high number of nodes in the adaptive process induces an increase in the error calculated on the displacement field; which leads to an undesirable effect related to the choice of high value of β , especially in the high velocity range. To highlight this fact, for a harmonic load with angular frequency ω_0 traveling a $e=0.2$ m meshed beam at constant velocity $V=0.5V_0$, the passage from three to five points-interpolation process, leads to an increase in Γ_1 and Γ_2 of 3.98% and 15.9%

respectively. These values become 3.37% and 8.09% in the case of $e=0.4$ m; it shows an effect of β less significant when the mesh becomes coarser.

However, the number of time steps presents a significant influence on the accuracy of the PCU method especially for high velocity; the results related to $\alpha=2$ show a good behavior of the numerical method over the entire angular frequency-traveling velocity plane. When increasing α the precision of the method decreases dramatically essentially on the span. Note that, when V is less than $0.5V_0$, a very good performance is shown in all cases, with negligible errors.

The results presented in section 3 are performed with $\alpha=2$ and $\beta=3$. This choice is maintained for the following numerical investigations.

4.2. Effect of progressive mesh

In this analysis, the effect of using a progressive mesh in the diffusion zone is investigated. This zone is meshed symmetrically relative to the point of application of the load according to the following expressions:

$$L_j = L_0 \times \gamma^j \quad (1.22a)$$

$$L_d = L_0 \times \frac{1 - \gamma^{n_e}}{1 - \gamma} \quad (1.22b)$$

L_j denotes the length of the j^{th} element, γ is the constant ratio of the geometric series, and n_e is the number of the elements used to discretize each side of the diffusion zone of length L_d . Three calculation series are conducted at the critical velocity in which each of them is characterized by the size of the central element L_0 which is taken equal to 0.2, 0.3 and 0.4 m respectively. Figure 1-10 shows the influence of the largest mesh size to L_0 ratio (denoted in the following by Φ) on the accuracy of the PCU method for the three considered cases of angular frequency.

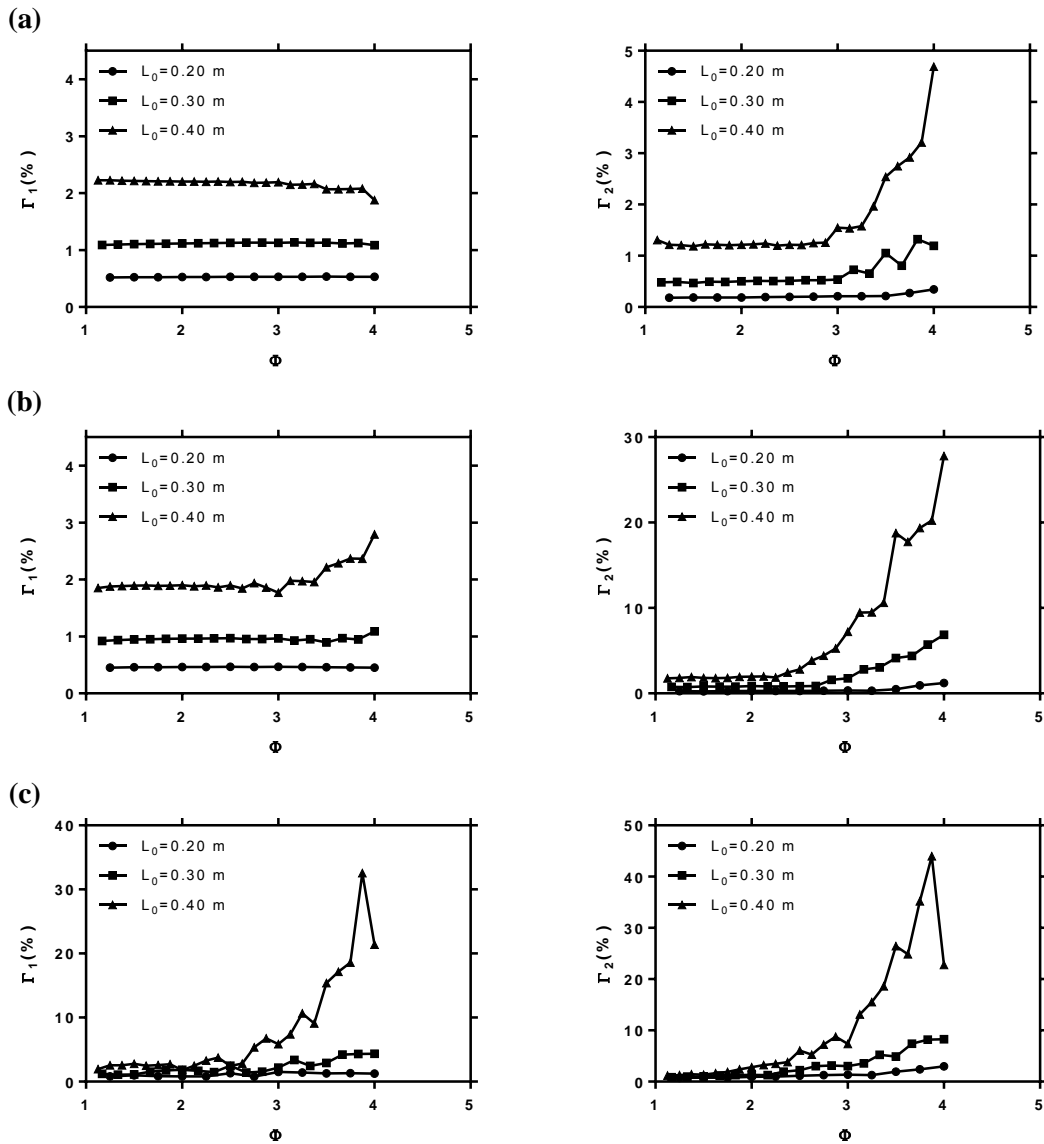


Figure 1-10: Influence of progressive mesh on the accuracy of the PCU method; case of $V=V_0$ (a) $\omega=0.5\omega_0$ (b) $\omega=1.0\omega_0$ (c) $\omega=2.0\omega_0$

The obtained results show that the accuracy of the numerical method tends to decrease with the increase in the dimensionless ratio Φ essentially on the span; this tendency appears clearly when increasing the size of the central finite element. Note that by increasing the value of Φ , the nodes discretizing the diffusion zone becomes more and more distant, that is why in those cases special precaution must be taken to prevent the divergence of the interpolation process. Moreover the curves illustrate the detrimental impact of increasing the loading frequency on a progressively meshed grid; it leads to accelerate the numerical divergence. Nevertheless, the PCU method shows an excellent performance up to $\Phi=2.5$ in the considered range of studied parameters.

On the other hand, it should be mentioned that the load velocity has a major impact on the accuracy of the numerical calculations (see Fig. 1-5); therefore for current train traveling velocity the level of committed errors on the displacement field is necessarily much smaller than that presented in Figure 1-10.

A parallel analysis shows that the central finite element on the beam mesh determines the maximum value of Δt which leads to the convergence of the numerical scheme.

4.3. Execution time

This section discuss the necessary time of execution of the numerical algorithm. The computer used to perform $\lambda=100$ loading periods is characterized by an Intel® Core™ i5-3340 CPU@3.10GHZ (4CPU). Table 1-2 summarizes the required time of the numerical simulations with different mesh sizes. It clearly shows an increase in time with decreasing the mesh size while remaining on a success completion of the numerical algorithm; it demonstrates once more the effectiveness of the PCU method to solve such problems.

Table 1-2: Required time for numerical algorithm execution; case of $V=V_0$ and $\omega=2\omega_0$

e [m]	Time [sec]
0.20	929
0.25	527
0.30	364
0.35	290
0.40	227

5. Conclusions

This chapter proposed an innovative adaptive method for the assessment of the dynamic response of infinite beams resting on continuous foundation under high speed moving loads. The key advantage of the proposed approach appears through the vanishing of the convective terms that lead to a numerical instability due to the induced negative numerical damping when linear elements are used in the FEM discretization. The case of viscoelastically damped foundation with high velocities that can reach the critical velocity of the beam is studied in the linear domain. However, any kind of behavioral nonlinearity can be easily integrated in the present temporal formulation by adopting an appropriate iterative solver.

The obtained results show the efficiency of the periodic configuration update PCU method. The numerical scheme is proven to be stable, consistent and numerically convergent. It's an efficient tool to resolve the problems relative to the dynamics of high speed trains-tracks. The accuracy of the PCU method has been studied as a function of the interpolation parameters. Two-time steps which precede the interpolation process performed using a fifth-order Hermite's interpolating polynomial (three points of interpolation) shows good numerical performance on the entire velocity axis at the studied frequency range. The use of progressive mesh doesn't present a constraint for the PCU method.

References

1. Frýba L. Infinite beam on elastic foundation. *Vibration of solids and structures under moving loads*, Springer Netherlands; 1972. DOI: 10.1007/978-94-011-9685-7_14.
2. Chen YH, Huang YH, Shih CT. Response of an infinite Timoshenko beam on a viscoelastic foundation to a harmonic moving load. *Journal of Sound and Vibration* 2001; **241**(5): 809–824. DOI: 10.1006/jsvi.2000.3333.
3. Sun L. An explicit representation of steady state response of a beam on an elastic foundation to moving harmonic line loads. *International Journal for Numerical and Analytical Methods in Geomechanics* 2003; **27**(1): 69–84. DOI: 10.1002/nag.263.
4. Koro K, Abe K, Ishida M, Suzuki T. Timoshenko beam finite element for vehicle—track vibration analysis and its application to jointed railway track. *Proceedings of the Institution of Mechanical Engineers, Part F: Journal of Rail and Rapid Transit* 2004; **218**(2): 159–172. DOI: 10.1243/0954409041319687.
5. Krenk S, Kellezi L, Nielsen SRK, Kirkegaard PH. Finite elements and transmitting boundary conditions for moving loads. *Proceedings of the 4th European Conference on Structural Dynamics, Eurodyn '99*, Balkema Publishers, A.A. / Taylor & Francis The Netherlands; 1999.
6. Koh CG, Chiew GH, Lim CC. A numerical method for moving load on continuum. *Journal of Sound and Vibration* 2007; **300**(1–2): 126–138. DOI: 10.1016/j.jsv.2006.07.038.
7. Nguyen VH, Duhamel D. Finite element procedures for nonlinear structures in moving coordinates. Part II: Infinite beam under moving harmonic loads. *Computers & Structures* 2008; **86**(21–22): 2056–2063. DOI: 10.1016/j.compstruc.2008.04.010.
8. Ang KK, Dai J. Response analysis of high-speed rail system accounting for abrupt change of foundation stiffness. *Journal of Sound and Vibration* 2013; **332**(12): 2954–2970. DOI: 10.1016/j.jsv.2013.01.005.
9. Ang KK, Dai J, Tran MT, Luong VH. Analysis of high-speed rail accounting for jumping wheel phenomenon. *International Journal of Computational Methods* 2013; **11**(03): 1343007. DOI: 10.1142/S021987621343007X.
10. Tran MT, Ang KK, Luong VH. Vertical dynamic response of non-uniform motion of high-speed rails. *Journal of Sound and Vibration* 2014; **333**(21): 5427–5442. DOI: 10.1016/j.jsv.2014.05.053.
11. Nguyen VH, Duhamel D. Finite element procedures for nonlinear structures in moving coordinates. Part 1: Infinite bar under moving axial loads. *Computers & Structures* 2006; **84**(21): 1368–1380. DOI: 10.1016/j.compstruc.2006.02.018.
12. Leonard BP. A stable and accurate convective modelling procedure based on quadratic upstream interpolation. *Computer Methods in Applied Mechanics and Engineering* 1979; **19**(1): 59–98. DOI: 10.1016/0045-7825(79)90034-3.

13. Wu B, Bao H, Ou J, Tian S. Stability and accuracy analysis of the central difference method for real-time substructure testing. *Earthquake Engineering & Structural Dynamics* 2005; **34**(7): 705–718. DOI: 10.1002/eqe.451.
14. Andersen L, Nielsen SRK, Kirkegaard PH. Finite element modelling of infinite Euler beams on Kelvin foundations exposed to moving loads in convected co-ordinates. *Journal of Sound and Vibration* 2001; **241**(4): 587–604. DOI: 10.1006/jsvi.2000.3314.
15. Hilber HM, Hughes TJR, Taylor RL. Improved numerical dissipation for time integration algorithms in structural dynamics. *Earthquake Engineering & Structural Dynamics* 1977; **5**(3): 283–292. DOI: 10.1002/eqe.4290050306.
16. Basu D, Kameswara Rao NSV. Analytical solutions for Euler–Bernoulli beam on visco-elastic foundation subjected to moving load. *International Journal for Numerical and Analytical Methods in Geomechanics* 2013; **37**(8): 945–960. DOI: 10.1002/nag.1135.
17. Koh CG, Ong JSY, Chua DKH, Feng J. Moving element method for train-track dynamics. *International Journal for Numerical Methods in Engineering* 2003; **56**(11): 1549–1567. DOI: 10.1002/nme.624.
18. Xia H, Zhang N, De Roeck G. Dynamic analysis of high speed railway bridge under articulated trains. *Computers & Structures* 2003; **81**(26–27): 2467–2478. DOI: 10.1016/S0045-7949(03)00309-2.
19. Galvín P, Domínguez J. Experimental and numerical analyses of vibrations induced by high-speed trains on the Córdoba–Málaga line. *Soil Dynamics and Earthquake Engineering* 2009; **29**(4): 641–657. DOI: 10.1016/j.soildyn.2008.07.001.
20. Adam M, von Estorff O. Reduction of train-induced building vibrations by using open and filled trenches. *Computers & Structures* 2005; **83**(1): 11–24. DOI: 10.1016/j.compstruc.2004.08.010.
21. Dokainish MA, Subbaraj K. A survey of direct time-integration methods in computational structural dynamics—I. Explicit methods. *Computers & Structures* 1989; **32**(6): 1371–1386. DOI: 10.1016/0045-7949(89)90314-3.
22. Subbaraj K, Dokainish MA. A survey of direct time-integration methods in computational structural dynamics—II. Implicit methods. *Computers & Structures* 1989; **32**(6): 1387–1401. DOI: 10.1016/0045-7949(89)90315-5.
23. Verlinden O. Simulation du comportement dynamique de systèmes multicorps flexibles comportant des membrures de forme complexe. *Ph.D. Thesis*. Faculté Polytechnique de Mons, 1994.
24. Fiset P, Vaneghem B. Numerical integration of multibody system dynamic equations using the coordinate partitioning method in an implicit Newmark scheme. *Computer Methods in Applied Mechanics and Engineering* 1996; **135**(1): 85–105. DOI: 10.1016/0045-7825(95)00926-4.
25. Hilber HM, Hughes TJR. Collocation, dissipation and [overshoot] for time integration schemes in structural dynamics. *Earthquake Engineering & Structural Dynamics* 1978; **6**(1): 99–117. DOI: 10.1002/eqe.4290060111.

26. Lax PD, Richtmyer RD. Survey of the stability of linear finite difference equations. *Communications on Pure and Applied Mathematics* 1956; **9**(2): 267–293. DOI: 10.1002/cpa.3160090206.

Chapter 2

Adaptive Meshing Scheme for Prediction of High-Speed Moving Loads Induced Ground Vibrations

ABSTRACT

This chapter aims to study the vibrations induced by high speed time-variant moving loads in the high frequency range up to 50 Hz. It proposes a three-dimensional explicit finite difference model derived for solving the transient interaction problem in the time domain. The proposed model considers the complex mutual dynamic coupling between the track components and the subgrade layer, thus a high realistic simulation of force transmission from rail interface to soil is involved. To prevent numerical disturbance that can arise at the truncated interfaces due to the parasitic reflected waves, an absorbing boundary condition ensured via infinite elements is placed. It simulates the unbounded nature of the physical domain. On the other hand, the Rayleigh viscous damping is adopted to model the energy dissipation within the model borders. An adaptive meshing scheme is proposed to simulate the moving loads effect; it consists on an automate creation of load-attached moving nodes on the rail-beam depending on the moving load position. The spatiotemporal mesh parameters are investigated within the frame of adaptive meshing and appropriate recommendations are drawn. Numerical experiments are carried out in the sub-Rayleigh and super-Rayleigh velocity range; they show an important capacity of the proposed scheme to model the impact of moving loads on the ground response.

Keywords: track-soil interaction, adaptive meshing, finite difference, sub-Rayleigh, super-Rayleigh, high frequency, 3D

1. Introduction

In recent years, the rapid development of High Speed Lines (HSL) leads to large crossing zones with urban areas; therefore they are increasingly representing one of the most important sources of nuisance for residents living in the vicinity of condensed traffic. The International Organization for Standardization ISO [1] specify the limit for human perception of vibration as 0.2 mm/s. Physically this threshold can be easily exceeded, hence the importance of studying the emission problem of noise and vibration in areas with railway traffic.

By focusing on structure borne sound and vibration from rail traffic, Heckl et al. [2] have categorized the rail excitation mechanisms; they cited firstly the quasi-static contribution due to load kinetic energy, then the dynamic contribution comprising the parametric, transient, wheel/rail roughness and track unevenness excitation mechanisms. In this context, Sheng et al. [3] found that the quasi-static excitation is dominant when the train speed is close to a critical phase velocity of the coupled track/soil system which it is found to be close to the minimum velocity of the Rayleigh waves in the subsoil. However, the contribution of the other components of load is significant for other values of train speed.

To highlight the impact of trains speed when approaches that of waves in the ground, rail deflection measurements were carried out at a railway track south of Peterborough over Stilton Fen in UK. The subgrade consists of a relatively soft material made of peat with some clay to a depth of about 7 m. Results showed that when the speed increased from 130 to 185 Km/h, the vertical rail deflections were increased from about 6 mm to 12 mm [4]. A more critical case was observed in 1998, at a location with very soft soil at Ledsgard, Sweden [5,6] during the passage of an X-2000 passenger train at 200 Km/h. The recorded level of track vibration has reached 20 mm which exceeded the limit for safety and stability.

For railway engineering, numerical tools are required to predict the pattern and to assess the amplitude of the train-induced ground vibrations in order to avoid any malfunction of the system that could lead to catastrophic damage. Numerical procedures have been presented by several authors. Paolucci et al. [7] proposed a comprehensive model to simulate the ground vibrations at the Ledsgard site through a spectral element discretization. In their study, the track motion is reproduced in the frequency range up to about 10 Hz. The soil transmissibility for vibrations induced by moving trains is studied by Yang et al. [8] in which the moving loads are calculated

using the deflection curve of an infinitely elastically supported beam and are directly applied on the soil stratum. Subsequently the soil complex response function has been computed using the finite/infinite element approach in the frequency domain. Alves Costa et al. [9] proposed an iterative two-and-a-half-dimensional (2.5D) procedure based on an equivalent linear elastic scheme in order to evaluate the relevance of the non-linear behavior of the soil on the track response. The fact that the condition of geo-material symmetry in the load-moving direction is necessary to apply the 2.5D methodology; they assumed an equivalent continuous medium to model the discrete supports of the rail.

According to Hall [10], the three-dimensional (3D) analyses are necessary to achieve a better simulation of the train-induced ground vibrations. Galvin et al. [11,12] developed a fully 3D multi-body-finite element (FE)-boundary element (BE) model to study vibrations due to train passage on ballast and non-ballast tracks and then to analyze the dynamic behavior of a transition zone. They found that the soil behavior changes significantly with track system. Connolly et al. [13] investigated the effect of embankment constituent material on ground borne vibration levels using a 3D FE-multi-body model. They noticed that embankments formed from stiff material reduce vibrations in the near and far field. Subsequently, this model was used to develop an assessment prediction tool for HSL induced vibrations based upon a synthetic records for a wide range of soil types [14]. Relationships between soil conditions, train speed and vibration levels are found using a machine learning approach. They demonstrated that, for typical soil properties, the Young's modulus has a much greater influence on vibration levels than density or Poisson's ratio.

As presented in the previous studies, the present-day models consider some simplifying assumptions at the expense of modeling accuracy. In addition to the simulation of the load transmission through a partial profile of track structure, the most disastrous is the modeling of the high speed moving loads at their contact with the rail. The problem of moving loads was addressed by many investigators. A classical algorithm for numerical resolution in the time domain using the finite difference and element techniques is to apply the equivalent nodal forces and moments on loaded beam elements by means of shape functions [15–18]. However, the performance of this approach is strongly influenced by the mesh size essentially in the case of high frequency moving loads. This shortcoming can be overcome by employing a refined domain but at the expense of significant increase in computational time.

On the other hand, special techniques were developed to resolve the dynamic problem in a moving reference system. Krenk et al. [19] was the first to use the FE method in a convected coordinate system moving with the load. They presented a FE model for convective wave propagation in a bi-dimensional (2D) continuum in order to account for an infinite medium. Since then, many researchers have investigated this approach. Andersen et al. [20] have presented a FE time domain analysis in convected coordinates with a simple upwind scheme, including a special set of boundary conditions permitting the passage of outgoing waves in the convected coordinate system. Zhai and Song [21] have proposed a 3D FE model in a convected coordinate system moving with the load used to assess the transient vibration of railway/ground model. However, this approach is complicated and difficult to embed in commercial software.

The analysis of wave propagation in structures and media with complex geometrical and material properties necessitates the use of numerical models formulated in a fixed reference system. This chapter proposes an advanced three dimensional finite difference modeling for the prediction of track/soil induced vibrations due to passage of high speed moving loads. In order to ensure a good representation of the wheel/rail interaction, the moving load is simulated by an adaptive meshing scheme based upon the creation of a load-attached moving node on the rail rolling surface. The novel feature of the formulation is the use of mesh superposition to produce spatial refinement in the transient problem. The Load-Attached Moving Node (L-AMN) scheme that is used to perform the spatial adaptation of the mesh is efficiently implemented in the $FLAC^{3D}$ software in which a Matlab subroutine has been created to allow a rapid development of the generic input files; the complete code is given in Appendix B.

For accurate representation of wave transmission through the model and to prevent numerical distortion, the spatiotemporal mesh parameters are investigated, and appropriate recommendations are provided. Numerical results for high range frequency dynamic loading as well as for velocities that exceed the Rayleigh wave speed of the subsoil layer prove the efficiency of the proposed numerical model.

The chapter is organized as follows: Section 2 presents a detailed description of the adopted reference case with the geo-mechanical and dynamic properties of the system components. Section 3 is concerned with the adaptive meshing scheme that has been developed and coupled to finite difference modeling, and the impact of this process on the modeling convergence. The

last section presents a thorough analysis of the dynamic response of the track/ground interaction model for a wide range of frequency and velocity loading.

2. Description of the Reference Case

This section presents a detailed description of the studied ballasted railway track in order to present its geo- mechanical and dynamic properties. Figure 2-1 shows the cross section of the adopted track structure with the considered dimensions (measured in mm). It consists of a flat framework made up of two parallel rails discretely supported by uniformly spaced horizontal sleepers which in turn rest on a ballast layer. The ballast bed lies on a sub-ballast layer which forms the transition layer to the subsoil. The track is located at the surface of a homogeneous clayey soil that represents a soft soil with total depth $H = 5$ m.

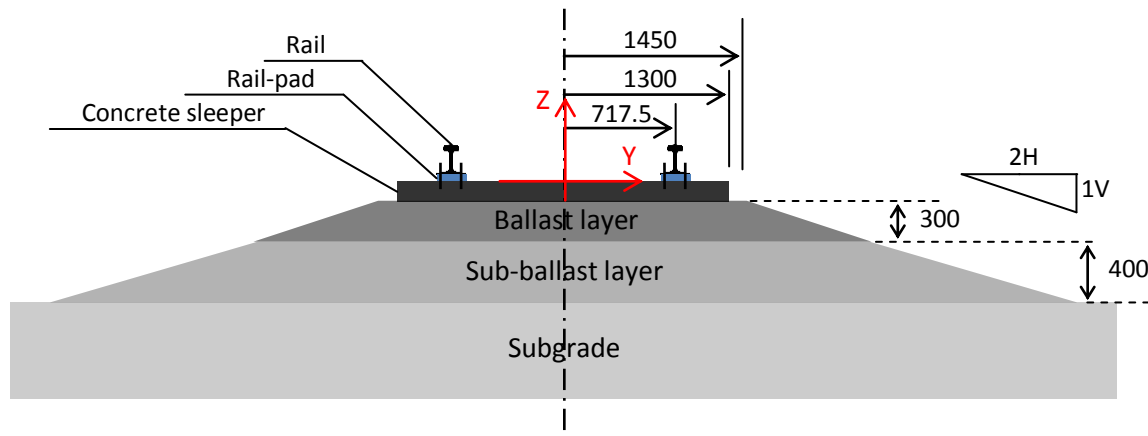


Figure 2-1: Cross section of the studied railway track; the dimensions are measured in mm

2.1. Geo-mechanical properties

The track ballast, sub-ballast and subgrade are considered to be linear and homogeneous; however mechanical nonlinearities are easily modeled in the program since it formulated in the time domain. Table 2-1 gives values of the track foundation elastic properties; where E , ν and ρ are the Young's modulus, Poisson's ratio and material density respectively. The mechanical parameters of the continuous welded rail which lay at 1.435 m gauge, are given in Table 2-2; where I_y and I_z are the second moment of inertia around y and z respectively (see Fig. 2-1) and J_x is the torsional stiffness around x axis (the loads running direction). The data presented in Tables 2-1 and 2-2 are taken from reference [22].

Table 2-1: Mechanical properties of railway track foundation materials (elastic)

Track Part	E [GPa]	ν	ρ [Kg/m ³]
Ballast	0.13	0.4	1600
Sub-ballast	0.08	0.4	1600
Clay	0.025	0.45	1800

Table 2-2: Mechanical properties of the rail

E [GPa]	ν	I_y [m ⁴]	I_z [m ⁴]	J_x [m ⁴]	Area [m ²]	ρ [Kg/m ³]
210	0.25	1.2449e-5	4.5261e-6	1.6975e-5	6.5538e-3	7897

Also note that the standard pre-stressed concrete mono-block sleeper with external dimensions 2600 (length) \times 235 (width) \times 205 (height) mm³ having a mass $m=300$ Kg is considered in the present analysis. It is distributed in regular interval $s=0.6$ m.

2.2.Three-Dimensional computational grid

A three-dimensional cuboid time domain track/ground model has been proposed in the finite difference explicit code FLAC3D. The substructure of the railway consisting of ballast, sub-ballast and subgrade is represented by eight noded brick elements. The rails and sleepers are modeled using beam structural elements (beam SELs) which are two noded, straight finite elements with six degrees of freedom per node: three translational components and three rotational components. Each beam SEL behaves as a linearly elastic material with non-failure limit. Beam SELs are rigidly connected to the grid such that forces and bending moments develop within the beam as the grid deforms. The rail-pad is implemented in the numerical model based on a linear vertical spring with constant stiffness $K_{rp}=150$ MN/m. Thus the two separate nodes at the rail-sleeper interface are connected by a node to node link, with elastically deformable attachment condition.

In view of the fact that loads acting on the track structure are assumed to be applied equally on each of the two rails; this hypothesis was used to enforce the symmetry condition on the boundary of the model. The symmetry condition along the track centerline implies that only the

half of the physical model in the transversal direction is considered. This property reduces the required resolution time and the necessary memory allocation. Indicatively, Figure 2-2 depicts an example of the 3D spatial mesh which includes 275028 zones and 292020 grid points.

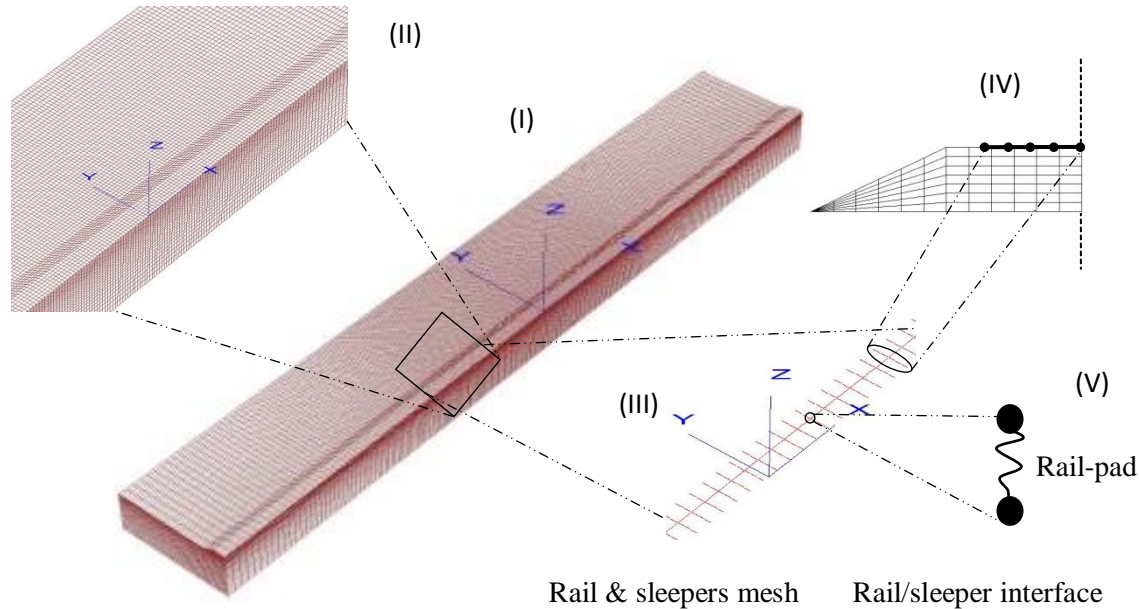


Figure 2-2: Computational mesh grid: 275028 zones and 292020 grid points

Within the frame of finite difference method, the spatial spread of induced waves is numerically evaluated by considering a truncated domain limited by an artificial boundary. Consequently the soil-track system is modeled as a multi-layered half-space with three sides truncated by an absorbing boundary condition insured by viscous elements [23] placed to prevent spurious reflections, and a fourth face where the symmetry boundary condition is applied. Therefore when an outgoing seismic wave collides with the quiet boundary layer its amplitude will undergo a progressive decaying over time, thus simulating an infinitely long domain. As the physical space is assumed to overly bedrock, a fixed base boundary condition is applied, while its top surface is free. Figure 2-3 shows a schematic view of the internal attachment conditions as well as that at model boundary.

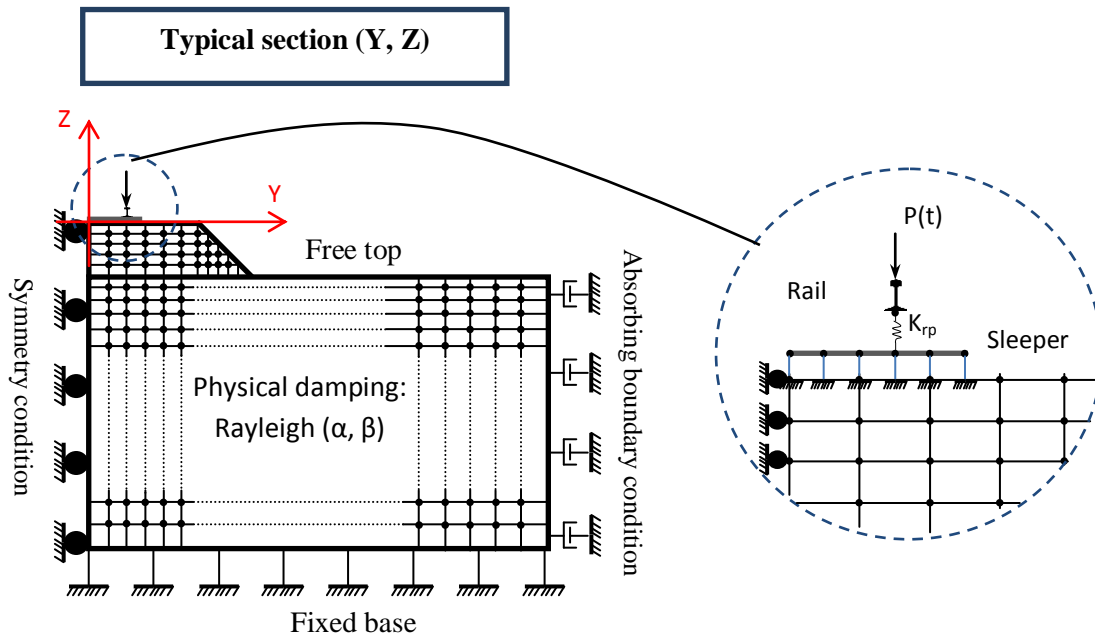


Figure 2-3: Internal attachment conditions between the model components

In addition to energy dissipation at the model boundary, material damping should be defined carefully since it governs the amplitude variation during the wave propagation process. In this context, the Rayleigh damping is considered the more representative protocol for the soil/structure interaction problems under small deformation levels. It has frequently used in the analysis of structures and elastic continua to damp their natural oscillation modes [24–26].

3. Adaptive Meshing Scheme: L-AMN Approach

This study proposes an enhanced approach aimed to accurately capture the dynamic response of the track/ground system. Instead of a global mesh refinement, the spatial-follow of loads location via the creation of moving nodes is proposed. This numerical scheme is used to simulate the loading process of the full computational model presented in section 2 in which a moving harmonic point load $p(t)$ is dedicated to excite the system through the rail-beam. The load trajectory is assumed to be symmetrical with respect to the center of the model. Figure 2-4 shows an illustration of the proposed numerical approach. For convenience it will be named subsequently as L-AMN (Load-Attached Moving Node) approach.

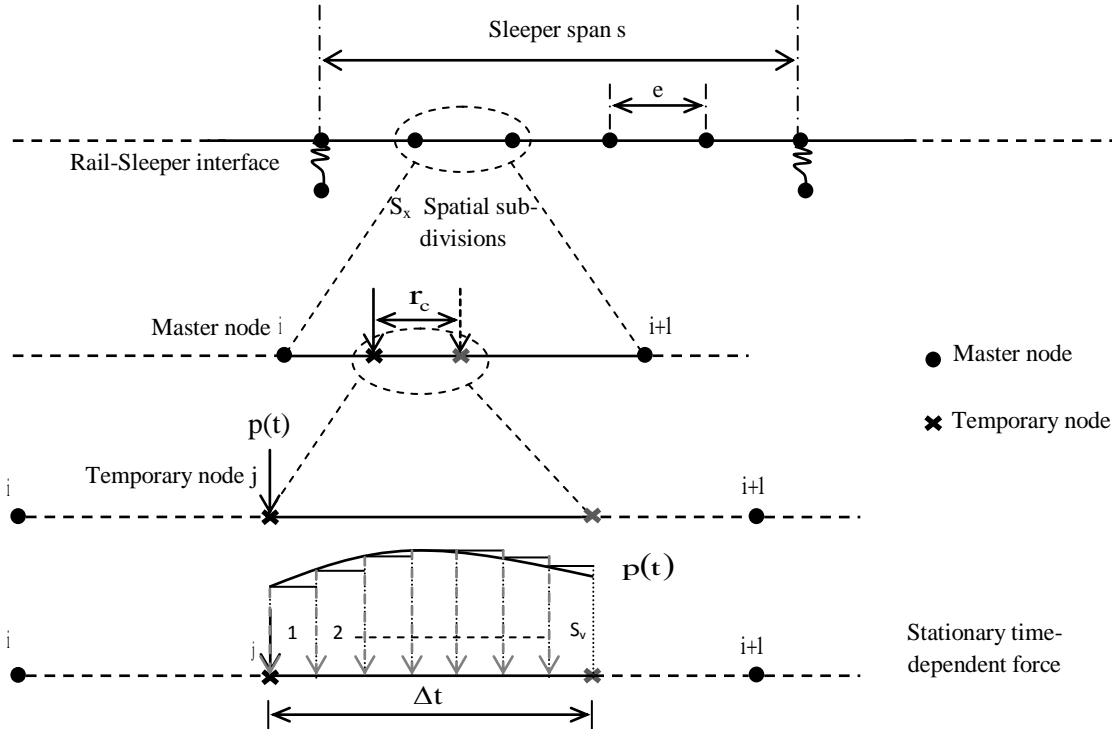


Figure 2-4: Load attached moving node L-AMN algorithm for moving load problems

3.1. Mathematical formulation

The L-AMN approach is based on a step-by-step mesh adaptation mechanism of the load/rail interface in which it is considered to be subjected to time-variant stationary loads during each calculation step. After spatial discretization of the rail with rectilinear beam elements intersecting at master nodes, the equation of structural dynamics providing the bending deformation is formulated in the time domain. Herein, the notion of “master node” is referred to a non-removable node during the adaptive meshing scheme.

Each spatial domain of length e delimited between two master nodes and forms part of the load trajectory is divided into S_x subdivisions. They determine the successive position of the moving node in which Δt represents the required time to cross each subdivision. At time $t = \alpha \times \Delta t$ (where α is a multiple of the predefined integer S_x), the moving load $p(t)$ is located at the master node i (initial numbering). Then, based on the position of the load on the finite element which is delimited between the master nodes i and $i+1$, a j^{th} (local numbering: $1 \leq j \leq S_x - 1$) temporary node is created to act in the numerical system during the interval $[t + j \times \Delta t, t + (j+1) \times \Delta t]$. It

remains loaded as long it exists, before being deleted allowing to create a neighbor temporary node $j+1$, and so on.

It should be mentioned that, by using the cubic Hermitian polynomials $N_{k/k=\{1,2,3,4\}}$ [17] as the interpolation formulas, which ensure both the deflection and slope compatibility on the adjacent elements, the vertical displacement $u_{I(j+1)}$ (Eq. 2.1) and the plane rotation $\theta_{I(j+1)}$ (Eq. 2.2) as well as their derivatives with respect to time are found at time $t=[\alpha+(j+1)] \times \Delta t$. This periodic process is used to initialize the dynamic response of the rail at the upcoming temporary node which has a global node number $I(j+1)$; where I is a bijective function used to switch from local to global system of numbering at the beginning of each step of calculation. Consequently the rail mesh changes at each time step Δt which represents a key parameter of the proposed approach, and the obtained numerical system of equations becomes non-linear because there a periodic local variation in the mass, damping and stiffness distribution. Mathematically this is reflected by the following system of equations:

$$u_{I(j+1)} = N_1(r = r_c)u_{I(j)} + N_2(r = r_c)\theta_{I(j)} + N_3(r = r_c)u_{I(i+1)} + N_4(r = r_c)\theta_{I(i+1)} \quad (2.1)$$

$$\theta_{I(j+1)} = N_1'(r = r_c)u_{I(j)} + N_2'(r = r_c)\theta_{I(j)} + N_3'(r = r_c)u_{I(i+1)} + N_4'(r = r_c)\theta_{I(i+1)} \quad (2.2)$$

Where r_c denotes the distance between two successive temporary nodes. The prime refers to the derivative with respect to the elementary reference system r .

Similar equations are used to find the linear and angular velocity and acceleration at temporary node $j+1$.

In order to improve the efficiency of the L-AMN approach, a temporal discretization of Δt is carried out using S_v sub-intervals allowing more refined representation of the time-variant moving load.

3.2. Numerical parameters of the L-AMN approach

To prevent numerical distortion of wave propagation in a dynamic analysis, the model dimensions should be determined as a function of the frequency range intended to study. In the field of track/soil dynamics, the interactions of interest fall within the frequency range of 2-50

Hz [27]. This section aims to investigate the modeling conditions of the three-dimensional finite difference model in the context of adaptive meshing. The effects of track foundation spatial mesh and L-AMN spatiotemporal parameters on the dynamic response of the system are analyzed. This analysis is performed using a harmonic load of linear frequency f traveling the rail at a constant velocity V . Its amplitude is assumed to be 100 KN. The rail displacement history is recorded at four discrete positions (including unloaded moving nodes) which are spatially detected relative to the punctual moving load-attached reference system X_r . These points are located at $X_r = 0, 1, 4$ and 5 m respectively to the left of load.

3.2.1. Track foundation spatial mesh

The early study of Kuhlemeyer and Lysmer [28] shows that for accurate representation of wave transmission through a model, the wavelength associated with the highest frequency component f_{sup} of the input wave should be represented by eighth to ten finite elements. In order to investigate the validity of this hypothesis in the context of moving loads simulation using adaptive meshing approach, four sets of numerical calculations are conducted including a reference case that of stationary harmonic loading [$V=0$; $f=50$ Hz] whereas the three other cases of dynamic loading are characterized by [$V=50$ Km/h; $f=50$ Hz], [$V=300$ Km/h; $f=10$ Hz] and [$V=300$ Km/h; $f=50$ Hz].

According to Shih et al. [29] the response of the track is mainly dominated by the elements that are close to the excitation point whereas elements further away have a smaller influence. Thus, a graded mesh is considered with a size Δl for the region close to the load path. Note that, Δl is controlled by the shear wavelength. Consequently, due to the relationship between wavelength and frequency, the following dimensionless parameter R_m can be derived to measure the refinement degree of the spatial mesh of foundation:

$$R_m = \frac{C_s}{\Delta l \times f_{sup}} \quad (2.3)$$

Where C_s is the shear wave (S-wave) speed in the subsoil layer.

Figures 2-5 to 2-8 illustrate the impact of the foundation mesh size Δl on the dynamic response of the system; they correspond respectively to the four cases of loading. The displacement

histories on four moving nodes are presented in each Figure. At time t (the axis of abscissa), the considered nodes are spatially detected relative to the moving load position in which they are located at $X_r=0$ (loaded moving node), -1 , -4 and -5 m (unloaded moving nodes) respectively.

A general conclusion can be extracted namely the major effect of the spatial mesh on the response of the system. The results presented in Figure 2-5 intersect with that found in reference [28]; $R_m=9$ is sufficient to model a stationary loading problem. On the other hand, Figures 2-6 to 2-8 show the influence of track foundation mesh on the convergence of the L-AMN scheme in which it increases with the decrease in the wavelength of the excitation signal; i.e. load velocity divided by load frequency. After comparing the obtained results with the more refined mesh analysis for each calculation series which is obviously the closest solution to the exact one, the mesh ratio $R_m=14$ can be considered suitable for reducing the mesh effect. This ratio corresponds to Δl equals to 0.1 and 0.5 m for the case where $f=50$ and 10 Hz respectively.

In the sequel 14 finite elements will be adopted to simulate the minimum wavelength problem within the frame of L-AMN scheme.

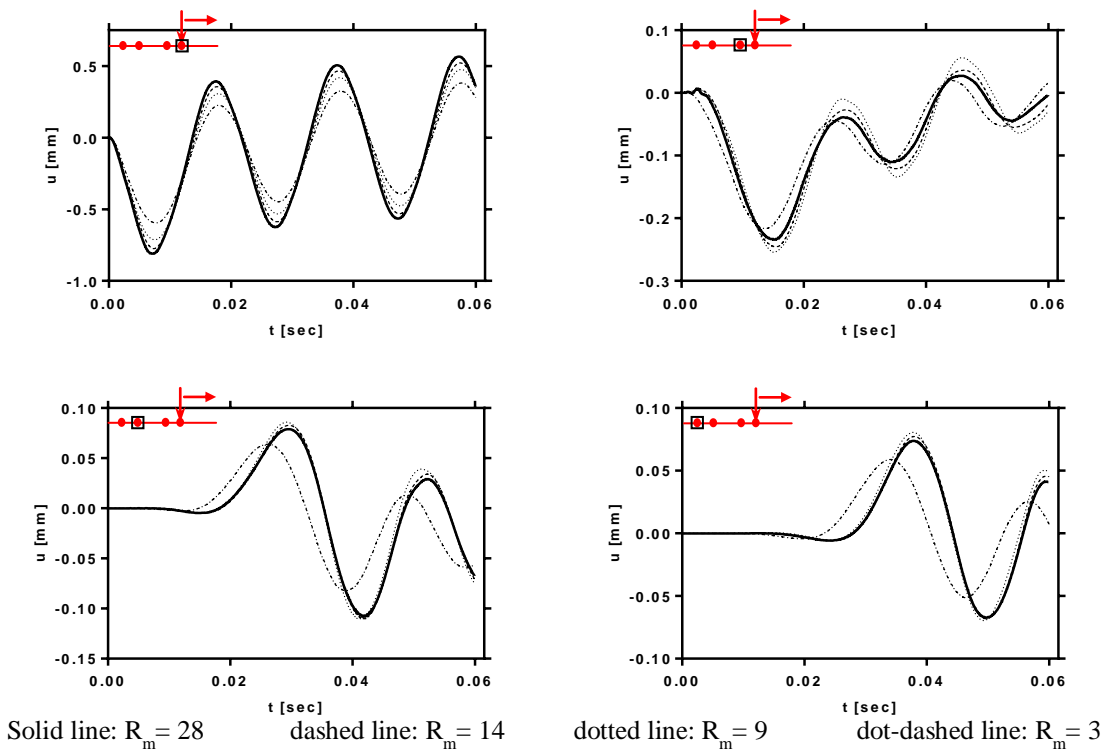


Figure 2-5: Effect of soil mesh on the dynamic response of the rail; $V=0$ and $f=50$ Hz

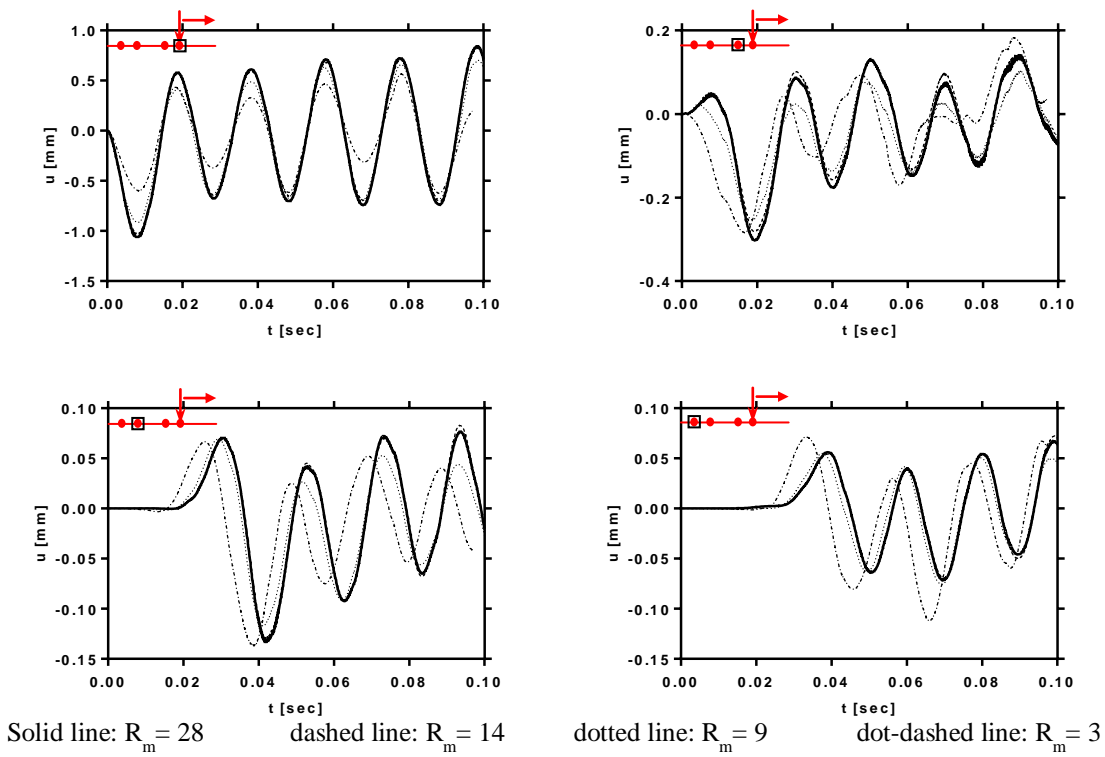


Figure 2-6: Effect of soil mesh on the dynamic response of the rail; $V=50 \text{ Km/h}$ and $f=50 \text{ Hz}$

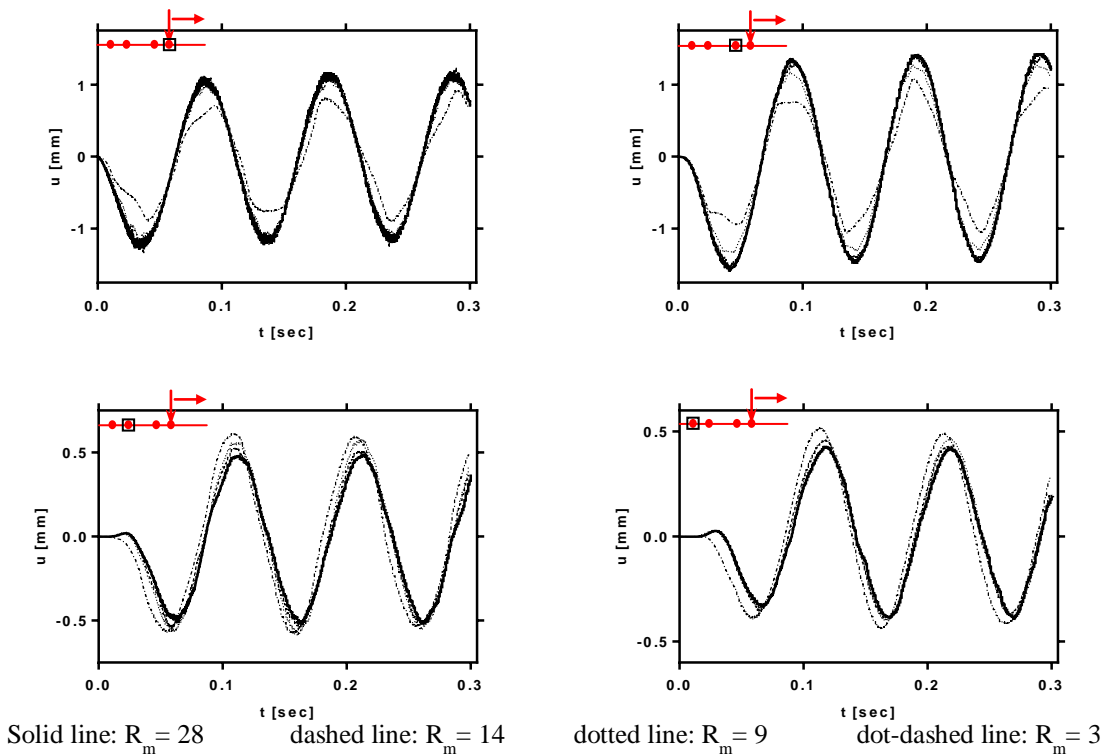


Figure 2-7: Effect of soil mesh on the dynamic response of the rail; $V=300 \text{ Km/h}$ and $f=10 \text{ Hz}$

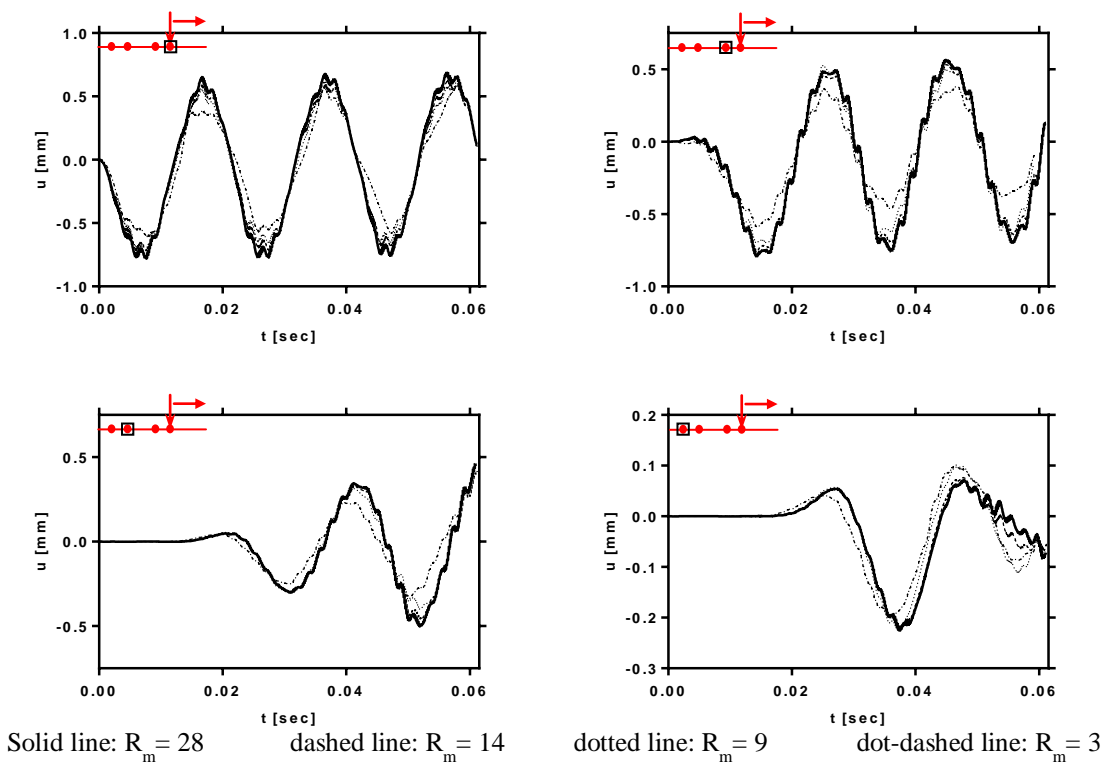


Figure 2-8: Effect of soil mesh on the dynamic response of the rail; $V=300 \text{ Km/h}$ and $f=50 \text{ Hz}$

3.2.2. Rail-beam spatiotemporal mesh

In order to study the influence of the rail-beam spatiotemporal mesh on the discrete representation of the moving load signal, a parametric study is carried out and the optimal discretization is determined function of the error committed on the returned dynamic response. In this study, the rail is uniformly meshed using 0.15 m beam elements and each half-sleeper is represented by five finite elements. The 3D solid domain which is devoted to model the infinite elastic medium is discretized according to the results found in the previous analysis. To evaluate the refinement degree of the temporary spatial mesh, a dimensionless parameter R_r is defined as the ratio between the wavelength of the dynamic excitation and the distance between two successive temporary nodes, and it is expressed as follows:

$$R_r = \frac{V \cdot S_x}{f \cdot e} \quad (2.4)$$

Where S_x is the number of spatial sub-divisions which determine the successive position of the moving node on a loaded beam element of length e (see Fig. 2-4).

Figure 2-9 illustrates a sequence of numerical solutions of the track/ground interaction problem with increasingly refined domain that correspond to $[V=50 \text{ Km/h}; f=50 \text{ Hz}]$. Also, the displacement histories are presented at the moving load position $X_r=0$ as well as on moving unloaded nodes that located at $X_r=-1, -4$ and -5 m. The various scenarios show a primordial influence of the adaptive spatial mesh of the load/rail interface on the accuracy of the numerical calculation. They prove that the truncation error tends to zero when the mesh becomes more refined; thus the developed scheme is numerically convergent. A ratio $R_r=130$ temporary nodes per wavelength of the external excitation which corresponds to $S_x=70$ leads to a satisfactory numerical convergence of the developed step-by-step procedure. Note that, this condition was respected in the previous analysis and will maintain for the following numerical investigations.

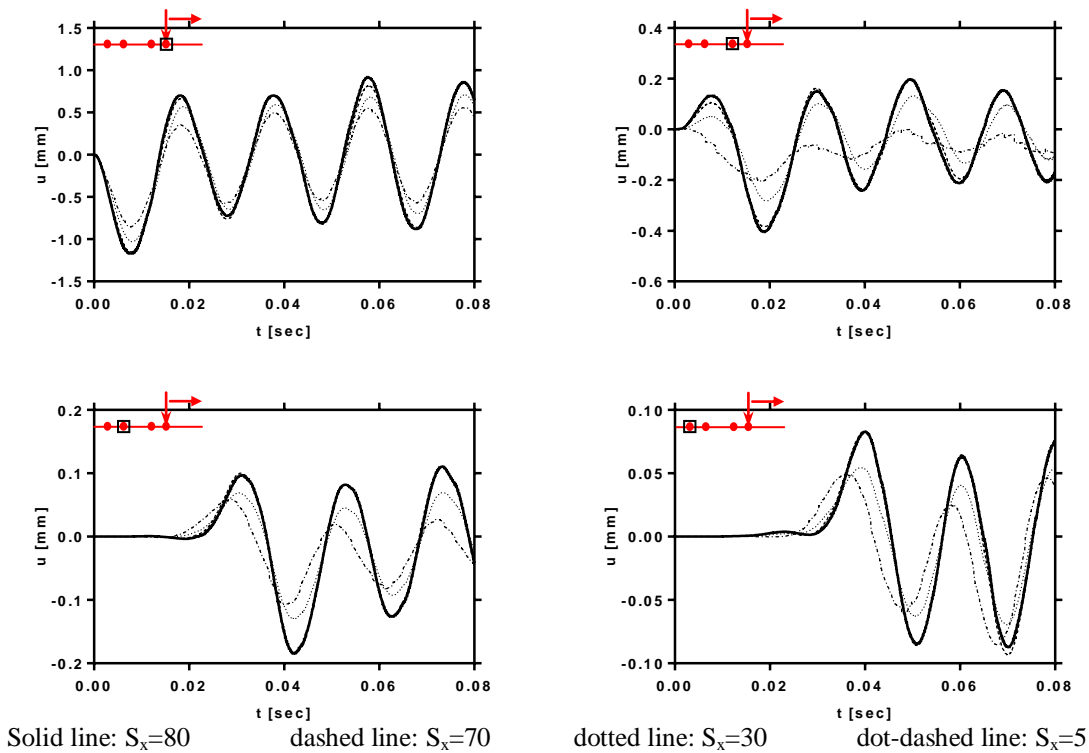


Figure 2-9: Effect of the adaptive meshing scheme on the dynamic response of the rail; $V=50 \text{ Km/h}$ and $f=50 \text{ Hz}$

A parallel study highlights the influence of the temporal meshing rate which is expressed in terms of S_v shows a minor effect of this parameter on the convergence of the L-AMN approach.

3.2.3. Computation of stable time step

The time increment must be carefully chosen to ensure stability and accuracy of numerical calculation. Numerical instability may cause the solution to diverge if the time increment is too large. Conversely, a very short time increment can cause spurious oscillations (Gibb's phenomenon) [30]. In Flac^{3D}, the time integration is carried out using the central-difference method which is a conditionally stable process. In finite element terminology, Flac^{3D} uses lumped masses and a diagonal mass matrix.

The stable time step dt_{stab} when stiffness-proportional damping is used, must be reduced for stability; it is computed according to Belytschko and Hughes [31]:

$$dt_{stab} = \frac{2}{\omega_{max}} F(\xi_{max}) \quad (2.5)$$

Where ω_{max} denotes the highest natural frequency of the discretized system and ξ_{max} is the fraction of critical damping at ω_{max} . $F(\xi)$ is expressed as follows:

$$F(\xi) = \sqrt{1 + \xi^2} - \xi \quad (2.6)$$

Figure 2-10 depicts the variation of the stable time step dt_{stab} as a function of the progression of the loading process of a finite element which is represented by the percentage of the traversed part by the moving load for two values of loading frequency and various load velocity. Note that, the obtained trend of dt_{stab} is periodic during the adaptive numerical calculation while in non-adaptive meshing case it does not change with time.

The presented curves show a sharp drop in dt_{stab} at the beginning of the adaptive meshing process due to the spatial proximity between the starting node (left master node) of the loaded beam element and the first temporary node; it appears earlier in the case of $f=50$ Hz in view of the high required number of subdivisions per finite element (according to Eq. 2.4). Then, from this point the time step increases to reach a local maximum that corresponds to a mid-length loading level before starting to decrease again when the moving node approaches the right master node. On the other hand, the effect of load velocity could be considered negligible especially when the frequency increases.

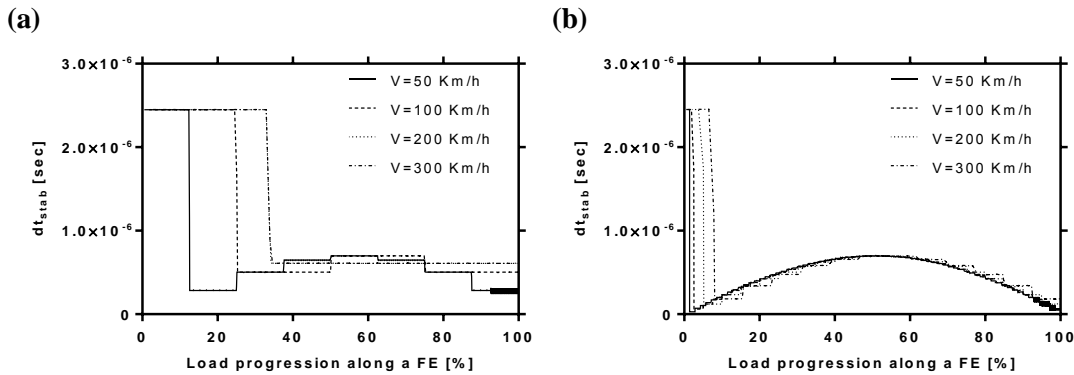


Figure 2-10: Stable time step of the L-AMN adaptive scheme depending on the progression of the loading process of a finite element; (a) $f=5$ Hz (b) $f=50$ Hz

3.2.4. Execution time

The present part aims to demonstrate the superiority of the proposed scheme over the classical aforementioned numerical techniques and to confirm its potential to solve the moving load problems. To achieve this target, the impact of the previously obtained numerical requirements for accurate simulations on the execution time T_e of the L-AMN algorithm is studied by means of comparing T_e with the time required to perform a similar calculation within the frame of a non-adaptive spatiotemporal mesh. The computer used to perform the simulations is characterized by an AMD Phenom™ II X2 B59 Processor (2CPUs), ~ 3.4 GHz.

The case of a single harmonic load having $f=50$ Hz and traveling the rail at constant velocity $V=50$ Km/h during 3 load-periods is considered in this analysis. The rail is uniformly meshed in both resolution techniques using beam elements of length e . The value of e is fixed at 0.15 m for the case of L-AMN approach while the mesh refinement is produced via the successive creation of temporary loaded nodes, i.e. a moving node. Figure 2-11 shows the obtained results which clearly prove the efficiency of the L-AMN approach; the required time ratio between the two techniques reaches 7.35 when the temporary/uniform mesh size equals to 0.03 m. This ratio decreases to 1 when the mesh size increases to $e=0.15$ m. Note that, with the adaptive scheme the temporary mesh size can reach 0.002 m ($S_x=70$) while maintaining an acceptable calculation time even less than that of a uniform spatial mesh using $e=0.03$ m beam elements.

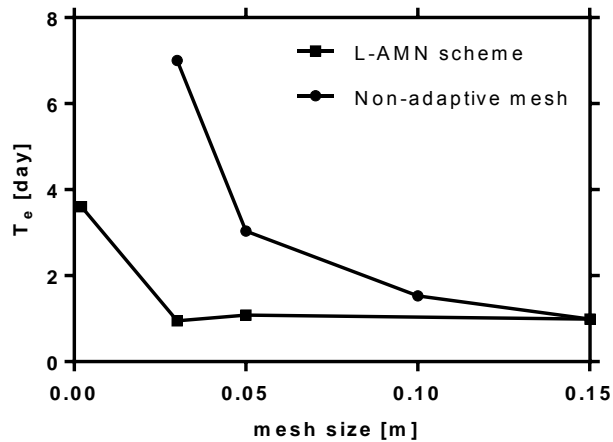


Figure 2-11: Calculation time of the L-AMN scheme; $V=50 \text{ Km/h}$ and $f=50 \text{ Hz}$

4. Validation of the L-AMN Approach

This section aims to investigate the ability of the proposed numerical scheme to capture the dynamic response of the system for different velocity range. According to Lefeuvre-Mesgouez et al. [32] two different cases for the soil vibrations induced by moving train are possible: the sub-Rayleigh case which occurs when the train speed is smaller than the velocity of Rayleigh waves propagating into the surface layer of the subsoil, in this case the major effect is essentially located beyond the train as usual, while in the second case (super-Rayleigh) some energy is radiated under the train, and possibly leading to some dynamic amplification in the track response.

In this context, the study of Paolucci and Spinelli [33] proved that the sub-Rayleigh case usually associated with a curved wave front whereas the super-Rayleigh case leads to Mach type cones similar to that obtained for supersonic flights. They are called “super-seismic” Mach cones. Consequently the validation work consists of two series of calculations; they are carried out in the sub-Rayleigh and super-Rayleigh range respectively.

4.1.Sub-Rayleigh range

In exploration seismology, the main type of surface wave of importance is the Rayleigh wave; often called ground roll. This wave travels along the surface of the ground and involves a combination of longitudinal and transverse motion with a definite phase relation to each other. The Rayleigh waves speed C_R depends upon the elastic constants near the surface and is slightly

less than the S-Wave speed C_s [34]. Based on the adopted mechanical properties for the subsoil layer (see table 2-1), C_R is approximately equal to 69 m/sec (≈ 248 Km/h).

4.1.1. Harmonic excitation

Results presented in Figures 2-12 to 2-16 show the displacement and the velocity contours of the track/ground interaction model after three periods of dynamic excitation using a single moving load traveling the infinite structure at $V=50$ Km/h; they are associated respectively to $f= 10, 20, 30, 40$ and 50 Hz.

The obtained results intersect with those found in reference [33] by virtue of curved wave front. Another conclusion can be drawn that by getting closer to the natural frequency of the subsoil layer f_s which equals to 3.5 Hz (C_s divided by 4 times the layer depth H) the dynamic response of the solid continuum becomes increasingly amplified. This clearly appears through the disturbed area at the ground surface which tends to expand when the loading frequency decreases since the propagated waves become able to travel through long distance before being attenuated. It is noteworthy to mention that these waves are considered as the major reason to the transmitted vibrations to nearby structures.

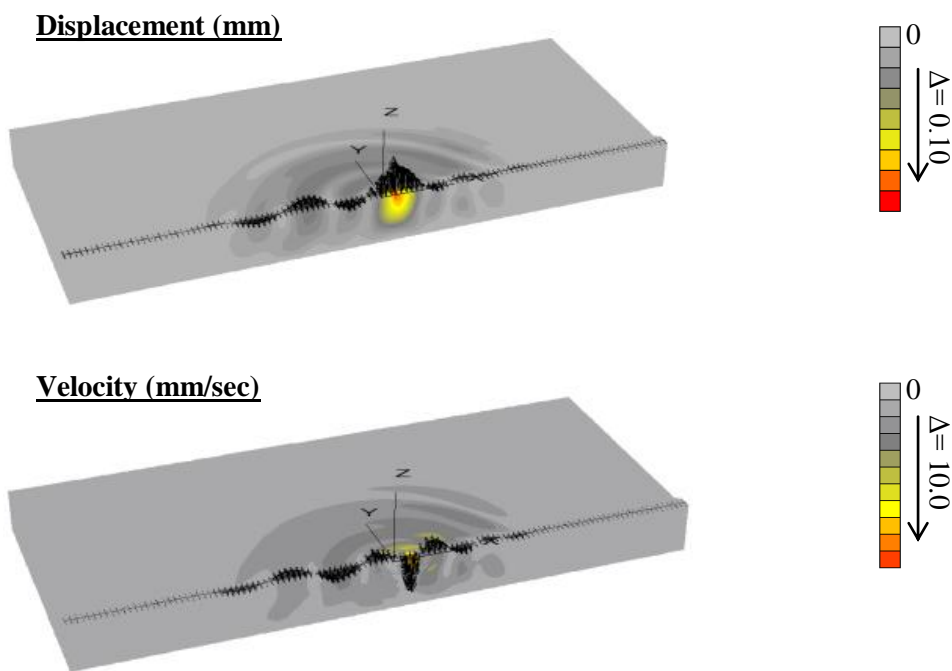


Figure 2-12: Response of the track/ground interaction model ($70 \times 30 \times 5$ m³) after three-period harmonic loading; $V=50$ Km/h and $f=10$ Hz

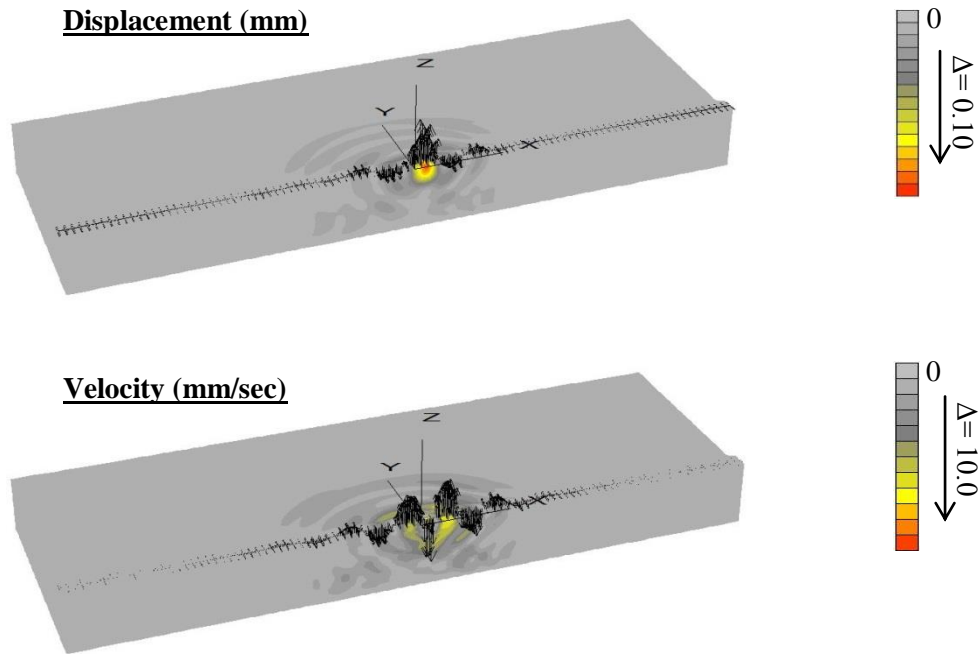


Figure 2-13: Response of the track/ground interaction model ($60 \times 20 \times 5 \text{ m}^3$) after three-period harmonic loading; $V=50 \text{ Km/h}$ and $f=20 \text{ Hz}$

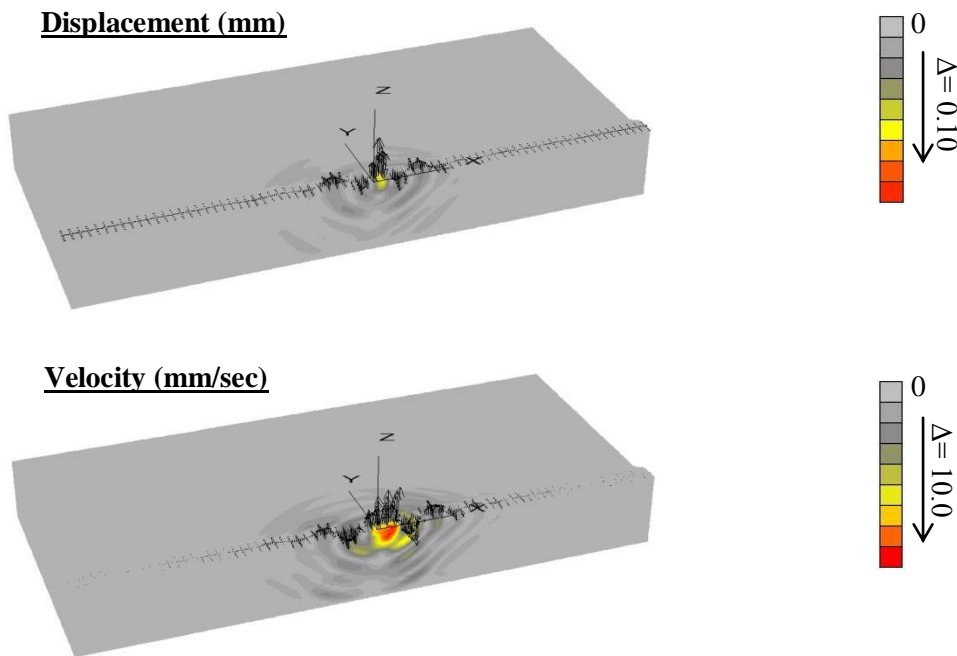


Figure 2-14: Response of the track/ground interaction model ($45 \times 20 \times 5 \text{ m}^3$) after three-period harmonic loading; $V=50 \text{ Km/h}$ and $f=30 \text{ Hz}$

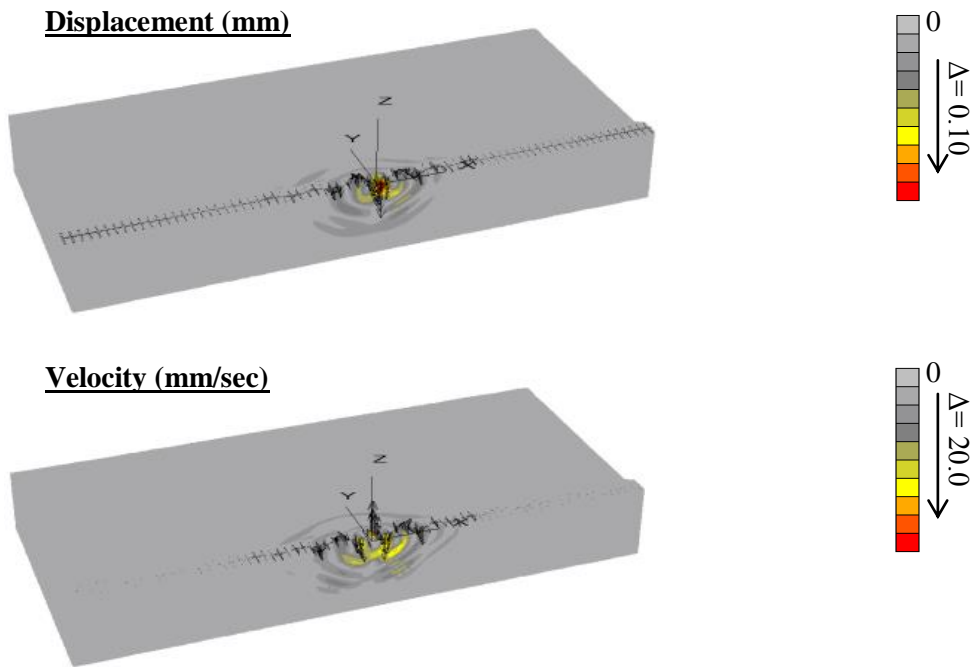


Figure 2-15: Response of the track/ground interaction model ($45 \times 20 \times 5 \text{ m}^3$) after three-period harmonic loading; $V=50 \text{ Km/h}$ and $f=40 \text{ Hz}$

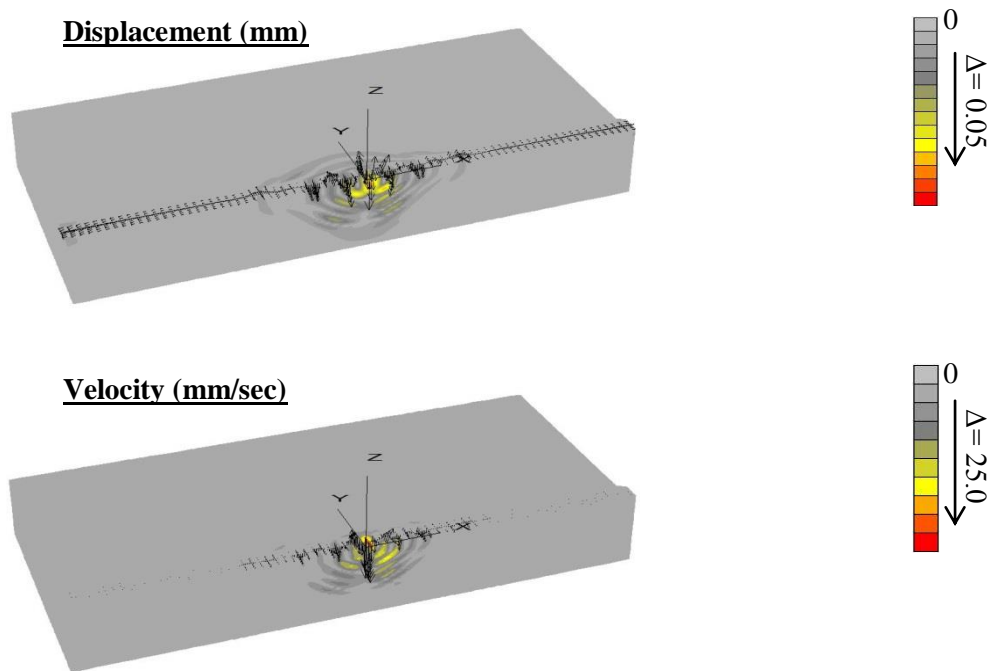


Figure 2-16: Response of the track/ground interaction model ($45 \times 20 \times 5 \text{ m}^3$) after three-period harmonic loading; $V=50 \text{ Km/h}$ and $f=50 \text{ Hz}$

Table 2-3 summarizes the peak values of the instantaneous displacement of the rail after three periods of harmonic loading (at $t=3T$) for various cases of linear frequency. The traveling velocity is fixed at $V=50$ Km/h. Another time the same trend is found; when the frequency decreases as it approaches f_s the dynamic response of the rail becomes more amplified. Indicatively, the passage from $f=50$ Hz to $f=10$ Hz excitation signal leads to an amplification ratio equals to 3.5.

Table 2-3: Peaks of the rail response at $t=3T$; $V=50$ Km/h

f [Hz]	Max(y_r) [mm]	f [Hz]	Max(y_r) [mm]
10	1.525	35	0.7708
15	1.519	40	0.8346
20	1.322	45	0.7273
25	1.316	50	0.4365
30	1.248		

4.1.2. Multi-frequency domain

Since the train induced excitation comprises the quasi-static as well as the dynamic contribution (rail roughness, track unevenness, transition zone ...), it will generate multiple harmonics. Consequently, the developed scheme is applied in the multi-frequency domain in which two scenarios are investigated. The first one concerns the case of single multi-frequency moving load while the second includes a vibration analysis of the case of multi-harmonic moving loads. Herein each temporal sequence is presented together with the corresponding Fourier spectrum obtained from FFT algorithm.

In the first scenario, two deterministic signals are considered. They are applied separately at the rolling surface of the infinite beam structure. The frequency content of each case of study is presented in table 2-4. Note that the first number in each cell refers to the linear frequency f_j while the second denotes for the corresponding amplitude P_j measured in [KN].

Table 2-4: Frequency content of the deterministic multi-frequency moving loads

Multi-frequency	$P_1(t)$	$P_2(t)$	$P_3(t)$	$P_4(t)$
Case 1	(10, 50)	(20, 30)	(35, 10)	(50, 10)
Case 2	(10, 50)	(15, 30)	(20, 20)	-

Thus the mathematical expression projected on the time axis t of the applied moving load $P(t)$ is given as follows:

$$P(t) = \text{imag} \left(\sum_j P_j e^{-i\omega_j t} \right) \quad (2.7a)$$

$$\omega_j = 2\pi f_j \quad (2.7b)$$

Then, the L-AMN scheme is used to investigate the rail response in the case of multiple time-variant moving loads ($P_1 \rightarrow P_4$) traveling simultaneously the rail at constant velocity V . Table 2-5 summarizes the loads characteristics (frequency & amplitude) of the case under consideration.

Table 2-5: Characteristics of the simultaneous harmonic moving loads

Moving load	X_r [m]	$(f_j$ [Hz], P_j [KN])
$P_1(t)$	0	(10, 50)
$P_2(t)$	-1	(20, 30)
$P_3(t)$	-4	(35, 10)
$P_4(t)$	-5	(50, 10)

Figure 2-17 depicts the dynamic response of the rail at the beam span ($X_r = -4$ m) for the two moving load cases of the first scenario. On the other hand, Fig. 2-18 shows the response of the rail at $X_r = 0$ and -4 m for the considered loading case of the second scenario. The results show that the rail/foundation interaction is complex. It involves several parameters, in particular the frequency content of the moving loads, and the natural frequency of the soil layer f_s . The loading frequencies as well as f_s determine the intensity of the dynamic amplification of the rail response. It is worth noting that, the sleeper passing frequency (V divided by the sleeper span) does not appear on the frequency analysis seen that the traveling velocity is elevated.

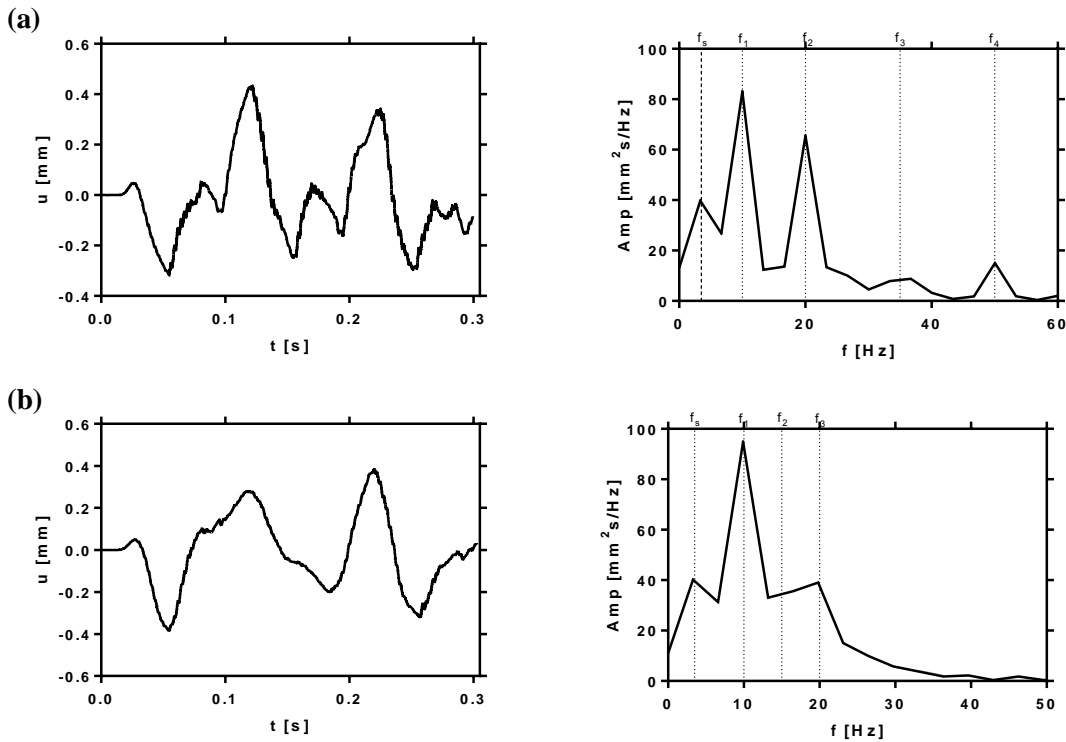


Figure 2-17: Dynamic response of the rail ($X_r=-4$ m) in the multi-frequency domain: first scenario $V=200$ Km/h; (a) case 1 (b) case 2

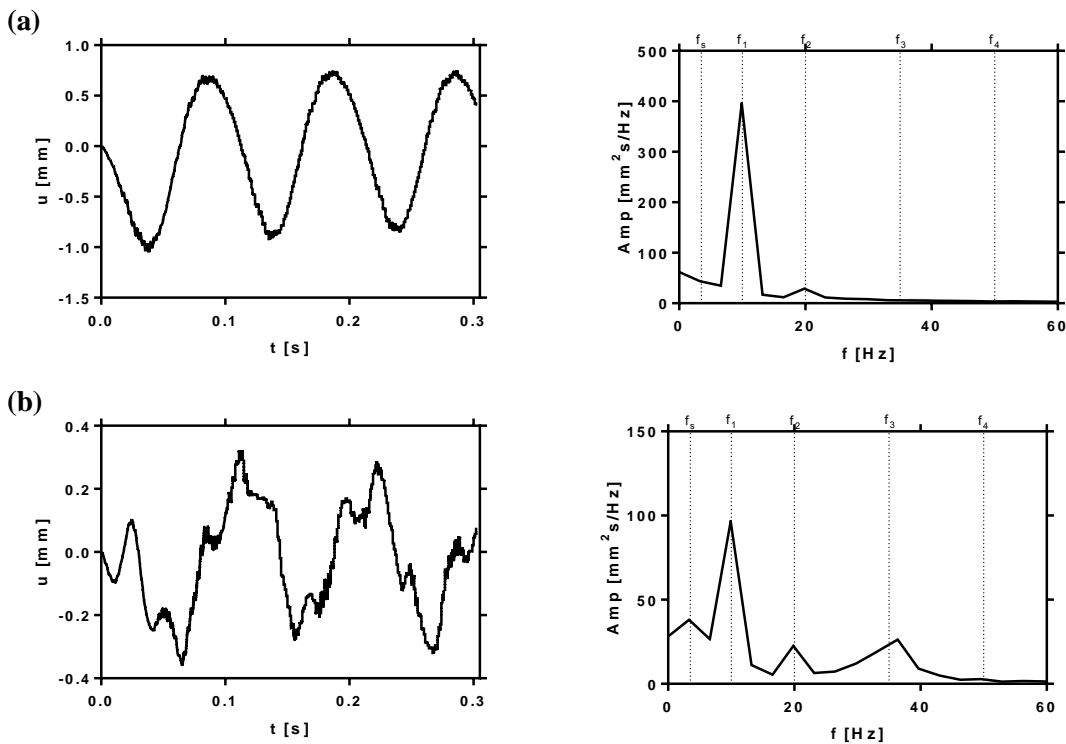


Figure 2-18: Dynamic response of the rail in the multi-frequency domain: Second scenario $V=200$ Km/h; (a) $X_r=0$ (b) $X_r=-4$ m

4.2. Super-Rayleigh range

In the field of aerodynamics, the shock wave which takes place in a fluid medium, initially at rest and subjected to supersonic moving object is a cone composed of overlapping spherical wave fronts. Several authors [3,33,35] have found some similarities with the response of a soil stratum when the excitation source moves at high velocity that crosses the threshold speed of the elastic medium; i.e. the Rayleigh wave speed C_R .

In order to stay within the speed range of HSL, the system is excited through the rail via a single harmonic load moving at constant velocity $V=300$ Km/h that slightly exceeds C_R . Figure 2-19 provides a 3D representation of the mobilized velocity at the soil surface resulting from three-period dynamic loading for two scenarios that of $f=10$ Hz and $f=20$ Hz. Herein, the induced energy is concentrated mainly inside a regular volume, i.e. a half of the Mach cone; in which the major induced velocity is located at the moving load position. Once again the obtained results intersect with that found in reference [33].

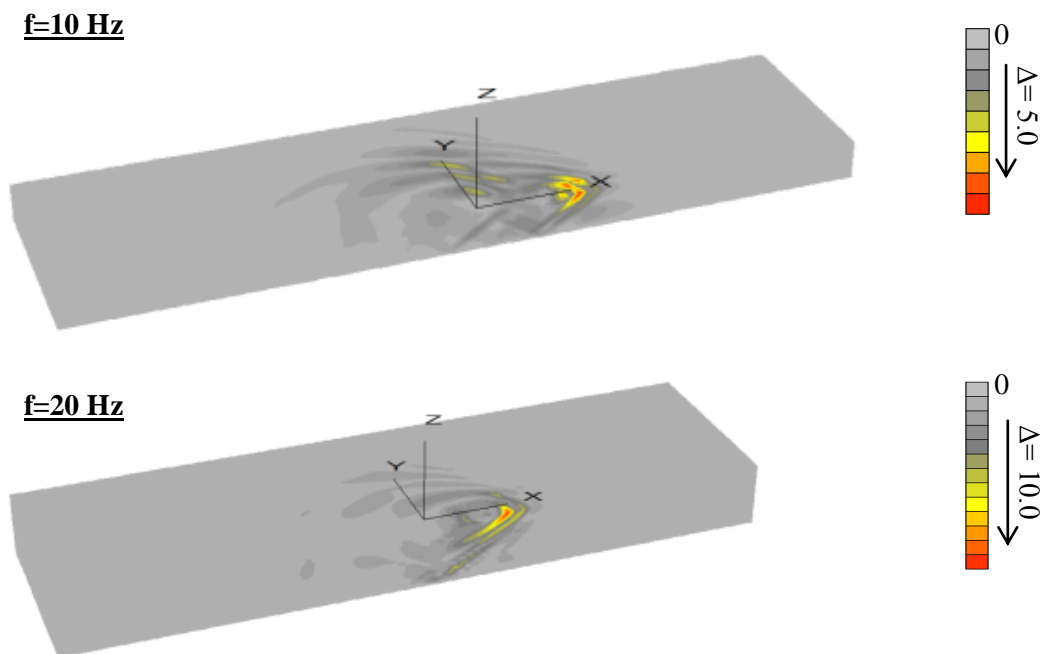


Figure 2-19: Mobilized velocity [mm/sec] at the soil surface after three-period harmonic loading; $V=300$ Km/h

To confirm the validation of the L-AMN adaptive scheme, the subsoil layer is considered to be more flexible; its Young's modulus is assumed to be one-fifth of that of the reference case. Subsequently a computational grid of dimensions $70 \times 20 \times 5 \text{ m}^3$ meshed at the center using 0.1^3 m^3 brick elements is used to find the soil surface dynamic response for the case of $V=350 \text{ Km/h}$ and $f=20 \text{ Hz}$. The obtained results are presented in Fig. 2-20. It can be observed that the same trends of the soil behavior are obtained; a half of the Mach cone appears clearly at the center of the model. Consequently, the developed model proves a strong ability to represent the track/ground interaction problem.

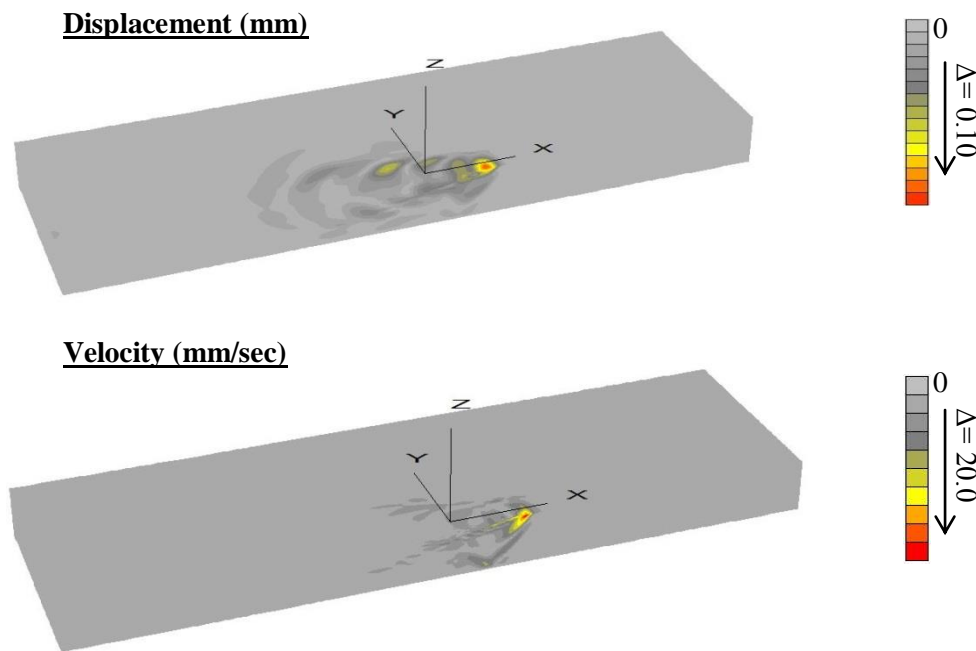


Figure 2-20: Soil response ($E_{\text{soil}}=0.2E_s$) in the super-Rayleigh range after three-period harmonic loading; $V=350 \text{ Km/h}$ and $f=20 \text{ Hz}$

5. Conclusions

The problem of induced waves by high-speed moving loads that propagate in media with complex geometry and material behavior was evoked in this chapter. An efficient approach was proposed in a fixed reference system aimed to overcome the lack of ability of the classical methods that formulated in the time domain which require a mesh refinement along the load path. A three dimensional numerical tool was developed on the basis of the finite difference method within the frame of an adaptive meshing scheme “L-AMN” which is based upon the

creation of load-attached moving nodes on the rail rolling surface. The study is performed in the perfectly elastic domain. However any kind of geometrical and mechanical anomalies comprising soil discontinuities and material non-linearity can be easily integrated in the present model without causing a considerable increase in the calculation time thanks to the use of an explicit numerical scheme (the central-difference method).

In order to capture the governing dynamic characteristics of the track/ground response that result from the mutual dynamic interactions between the model components, some considerations should be made especially on the discretization of the spatiotemporal coupled domain. It has been found that approximately 14 grid points per wavelength should be used to correctly discretize the foundation domain which exceeds that needed to resolve a stationary loading problem. On the other hand the influence of the rail-beam spatiotemporal mesh on the discrete representation of the time-variant moving load is studied; a ratio of 130 subdivisions per wavelength is found to ensure a satisfactory numerical convergence. They are used to specify the successive position of the moving node. Many numerical experiments have been performed in the sub-Rayleigh and super-Rayleigh ranges in order to validate the developed model. They clearly showed the capacity to reproduce the dynamic response of the track/ground system especially when the load velocity exceeds the Rayleigh wave speed of the subsoil layer in which a Mach cone appears at the center of the model.

References

- [1] ISO 2631-2:2003 - Vibrations et chocs mécaniques -- Évaluation de l'exposition des individus à des vibrations globales du corps -- Partie 2: Vibrations dans les bâtiments (1 Hz à 80 Hz). ISO 2003.
- [2] Heckl M, Hauck G, Wettschureck R. Structure-borne sound and vibration from rail traffic. *J Sound Vib* 1996;193:175–84. doi:10.1006/jsvi.1996.0257.
- [3] Sheng X, Jones CJC, Thompson DJ. A comparison of a theoretical model for quasi-statically and dynamically induced environmental vibration from trains with measurements. *J Sound Vib* 2003;267:621–35. doi:10.1016/S0022-460X(03)00728-4.
- [4] Suiker ASJ. *The Mechanical Behaviour of Ballasted Railway Tracks*. Delft: IOS Press; 2002.
- [5] Kaynia AM, Madshus C, Zackrisson P. Ground Vibration from High-Speed Trains: Prediction and Countermeasure. *J Geotech Geoenvironmental Eng* 2000;126. doi:10.1061/(ASCE)1090-0241(2000)126:6(531).
- [6] Madshus C, Kaynia AM. High-speed railway lines on soft ground: Dynamic behaviour at critical train speed. *J Sound Vib* 2000;231:689–701. doi:10.1006/jsvi.1999.2647.
- [7] Paolucci R, Maffei A, Scandella L, Stupazzini M, Vanini M. Numerical prediction of low-frequency ground vibrations induced by high-speed trains at Ledsgaard, Sweden. *Soil Dyn Earthq Eng* 2003;23:425–33. doi:10.1016/S0267-7261(03)00061-7.
- [8] Yang YB, Hung HH, Chang DW. Train-induced wave propagation in layered soils using finite/infinite element simulation. *Soil Dyn Earthq Eng* 2003;23:263–78. doi:10.1016/S0267-7261(03)00003-4.
- [9] Alves Costa P, Caçada R, Silva Cardoso A, Bodare A. Influence of soil non-linearity on the dynamic response of high-speed railway tracks. *Soil Dyn Earthq Eng* 2010;30:221–35. doi:10.1016/j.soildyn.2009.11.002.
- [10] Hall L. Simulations and analyses of train-induced ground vibrations in finite element models. *Soil Dyn Earthq Eng* 2003;23:403–13. doi:10.1016/S0267-7261(02)00209-9.
- [11] Galvín P, Romero A, Domínguez J. Vibrations induced by HST passage on ballast and non-ballast tracks. *Soil Dyn Earthq Eng* 2010;30:862–73. doi:10.1016/j.soildyn.2010.02.004.
- [12] Galvín P, Romero A, Domínguez J. Fully three-dimensional analysis of high-speed train-track-soil-structure dynamic interaction. *J Sound Vib* 2010;329:5147–63. doi:10.1016/j.jsv.2010.06.016.
- [13] Connolly D, Giannopoulos A, Forde MC. Numerical modelling of ground borne vibrations from high speed rail lines on embankments. *Soil Dyn Earthq Eng* 2013;46:13–9. doi:10.1016/j.soildyn.2012.12.003.

- [14] Connolly DP, Kouroussis G, Giannopoulos A, Verlinden O, Woodward PK, Forde MC. Assessment of railway vibrations using an efficient scoping model. *Soil Dyn Earthq Eng* 2014;58:37–47. doi:10.1016/j.soildyn.2013.12.003.
- [15] O'Brien J, Rizos DC. A 3D BEM-FEM methodology for simulation of high speed train induced vibrations. *Soil Dyn Earthq Eng* 2005;25:289–301. doi:10.1016/j.soildyn.2005.02.005.
- [16] Wu J-S, Lee M-L, Lai T-S. The dynamic analysis of a flat plate under a moving load by the finite element method. *Int J Numer Methods Eng* 1987;24:743–62. doi:10.1002/nme.1620240407.
- [17] Wu J-J, Whittaker AR, Cartmell MP. The use of finite element techniques for calculating the dynamic response of structures to moving loads. *Comput Struct* 2000;78:789–99. doi:10.1016/S0045-7949(00)00055-9.
- [18] Wu J-J. Use of equivalent beam models for the dynamic analyses of beamplates under moving forces. *Comput Struct* 2003;81:2749–66. doi:10.1016/S0045-7949(03)00341-9.
- [19] Krenk S, Kellezi L, Nielsen SRK, Kirkegaard PH. Finite elements and transmitting boundary conditions for moving loads. *Proc. 4th Eur. Conf. Struct. Dyn. Eurodyn99*, Balkema Publishers, A.A. / Taylor & Francis The Netherlands; 1999, p. 447–52.
- [20] Andersen L, Nielsen SRK, Krenk S. Numerical methods for analysis of structure and ground vibration from moving loads. *Comput Struct* 2007;85:43–58. doi:10.1016/j.compstruc.2006.08.061.
- [21] Zhai W, Song E. Three dimensional FEM of moving coordinates for the analysis of transient vibrations due to moving loads. *Comput Geotech* 2010;37:164–74. doi:10.1016/j.compgeo.2009.08.007.
- [22] El Kacimi A, Woodward PK, Laghrouche O, Medero G. Time domain 3D finite element modelling of train-induced vibration at high speed. *Comput Struct* 2013;118:66–73. doi:10.1016/j.compstruc.2012.07.011.
- [23] Lysmer J, Kuhlemeyer RL. Finite dynamic model for infinite media. *J Eng Mech Div* 1969;95:859–78.
- [24] Woodward PK, Griffiths DV. Influence of viscous damping in the dynamic analysis of an earth dam using simple constitutive models. *Comput Geotech* 1996;19:245–63. doi:10.1016/0266-352X(96)00002-X.
- [25] Semblat J-F, Pecker A. *Waves and vibrations in soils: earthquakes, traffic, shocks, construction works*. IUSS Press; 2009.
- [26] Tsai C-C, Park D, Chen C-W. Selection of the optimal frequencies of viscous damping formulation in nonlinear time-domain site response analysis. *Soil Dyn Earthq Eng* 2014;67:353–8. doi:10.1016/j.soildyn.2014.10.026.
- [27] Griffin MJ. *Handbook of Human Vibration*. Elsevier; 1996.

- [28] Kuhlemeyer RL, Lysmer J. Finite element method accuracy for wave propagation problems. *J Soil Mech Found Div* 1973;99.
- [29] Shih JY, Thompson DJ, Zervos A. The effect of boundary conditions, model size and damping models in the finite element modelling of a moving load on a track/ground system. *Soil Dyn Earthq Eng* 2016;89:12–27. doi:10.1016/j.soildyn.2016.07.004.
- [30] Zerwer A, Cascante G, Hutchinson J. Parameter Estimation in Finite Element Simulations of Rayleigh Waves. *J Geotech Geoenvironmental Eng* 2002;128. doi:10.1061/(ASCE)1090-0241(2002)128:3(250).
- [31] Belytschko T, Hughes TJR. An Overview of Semidiscretization and Time Integration Procedures. *Comput. Methods Transient Anal*. New York, Elsevier Science Publishers; 1983, p. 1–65.
- [32] Lefeuvre-Mesgouez G, Peplow AT, Le Houédec D. Surface vibration due to a sequence of high speed moving harmonic rectangular loads. *Soil Dyn Earthq Eng* 2002;22:459–73. doi:10.1016/S0267-7261(02)00034-9.
- [33] Paolucci R, Spinelli D. Ground motion induced by train passage. *J Eng Mech* 2006;132:201–10. doi:10.1061/(ASCE)0733-9399(2006)132:2(201).
- [34] Pariseau WG. *Design Analysis in Rock Mechanics*. Second Edition. CRC Press; 2011.
- [35] Lefeuvre-Mesgouez G, Mesgouez A. Three-dimensional dynamic response of a porous multilayered ground under moving loads of various distributions. *Adv Eng Softw* 2012;46:75–84. doi:10.1016/j.advengsoft.2010.09.006.

Chapter 3

Frequency and Velocity Dependent Simplified Model for Rail/Foundation Dynamics

ABSTRACT

This chapter presents an efficient and reliable numerical tool for the prediction of railway track dynamic response through the foundation interaction. It proposes an improvement of the well-known model: the infinite Euler-Bernoulli beam that rests on continuous series of linear spring-damper units. In particular it focuses on the track/subsoil dynamic interaction. Constitutive laws that govern the dynamic behavior of the discrete elements are proposed within the frame of a reference case comprising an infinite linear track resting on a classical ballasted formation. A three dimensional explicit finite difference code coupled with spatiotemporal adaptive meshing scheme is used to calibrate the dynamic impedances of the simplified beam model by exciting the two systems via the same time-dependent moving load. An iterative fitting procedure is carried out using the genetic algorithm. It allows the production of charts for the dynamic parameters for a wide range of loading frequency and velocity. The numerical experiments show an important capacity to achieve satisfactory results with significant reduction in computational effort. The obtained results emphasize the major impact of the excitation characteristics on the parameters of the discrete models that are widely used in the literature. The technique and the findings will be useful in railway track design.

Keywords: moving load, rail vibration, rail/foundation interaction, frequency and velocity dependent foundation, genetic algorithm, dynamic impedance

1. Introduction

Running trains on imperfect wheel/rail interface generate dynamic vibratory loads on the railway tracks; they cause vibrations of the track and surrounding soil that may seriously influence the living and work environment of the people. As pointed out by a number of authors [1–3], the track response is strongly influenced by the soil. It has been stated that the very soft soils yield completely different track behavior and ground-born vibration compared to normally stiff soils [2].

When dealing with soil-structure system subjected to dynamic loading, the soil can be compared to a frequency filtering device due to its selective amplification behavior. Several researches have been carried out to represent the soil parameters through specific numerical tools in order to accurately analyze the dynamic response of the soil-structure mutual interface. Mulliken and Karabalis [4] developed a discrete model composed of mass, frequency-independent springs and dashpots for the prediction of the dynamic interaction between adjacent rigid surface foundations through the soil elastic layer. Ju [5] has determined the equivalent mass, damping and stiffness matrices for an embedded foundation using the three-dimensional (3D) finite element method (FEM) coupled with the least-squares method. However the railway track/foundation coupled problem is classified among the most critical problems due to the complex dynamic interaction between the various system components. On the other hand, any erroneous hypothesis can lead to high environmental impact on the surrounding urban areas.

Numerical models with high complexity degree are widely reported in the literature. However, they are mainly concerned with the ground induced vibrations in the low frequency range. Despite the recent advances in numerical techniques, the infinite beam resting on continuous elastic foundation remains a frequent solution [6–10] for the assessment of the interaction forces acting at the rail.

Paolucci et al. [6] analyzed the ground vibrations induced by a passenger train at the site of Ledsgaard, Sweden through a spectral element discretization of the soil. They modeled the track and the embankment as a beam on elastic foundation, subjected to static loads moving at constant velocity. Yang et al. [7] studied the transmissibility of soils for vibrations induced by moving trains where the moving load effect is determined using the deflection curve of an infinitely elastically supported beam and directly applied on a soil stratum. Koh et al. [8] proposed a variant of the FEM called the moving element method (MEM) to perform a

dynamic analysis of train/track systems using rail-beam on continuous viscoelastic foundation in which four cases of moving vehicle are studied. Later, Ang and Dai [9] used the MEM to investigate the “jumping wheel” phenomenon in a high-speed train motion at constant velocity over a transition region where there is a sudden change of foundation stiffness. Tran et al. [10] proposed a reformulation of the MEM to find the vertical dynamic response of high speed rail systems involving accelerating/decelerating trains.

As a matter of fact, the use of continuous support eliminates the dynamic effect of sleepers. However, this hypothesis is considered suitable for slab tracks modeling whereas for ballasted tracks, it leads to ignore the sleeper passing frequency. To overcome this simplification, the rail is modeled with predefined elastic supports [11–14].

Zhai and Cai [11] as well as Kouroussis and Verlinden [14] analyzed a flexible track resting on regularly spaced lumped masses defining the sleepers. In their studies, three layers of discrete springs and dampers were used to model the elasticity and damping effect of the rail pads, the ballast and the subgrade respectively. Shear springs and dampers were introduced between the ballast masses in order to account for the shear coupling effects in the ballast. Lei and Noda [12] and Xia et al. [13] developed a dynamic computational model for the vehicle and track coupling system in which the rail was considered as a beam rested on a double layer of discrete viscoelastic units.

It is worth noting that, the previously mentioned studies omitted the existence of any correlation between the parameters of the discrete models and the frequency content and/or the velocity of the moving loads. On the other hand, to reproduce the foundation effect on the rail dynamic response, a reliable model is required in order to remedy the error resulting from the physical rail/foundation decoupling and to accurately simulate the time lag effect due to the wave propagation process in a solid medium. The present study aims at improving and adapting the well-known model i.e. the infinite Euler-Bernoulli beam that rests on continuous viscoelastic foundation, in order to correctly simulate the dynamic response of the rail under high speed moving loads. This goal is achieved by conducting a great number of numerical simulations based on a sophisticated 3D finite difference model for a wide range of selected loading frequency that can reach 50 Hz. The 3D model involves a high realistic simulation of force transmission from rail interface to the soil via an adaptive meshing scheme i.e. step-by-step procedure in the time domain based upon the creation of load-attached moving nodes on the rail rolling surface. The analysis is performed within the frame of a reference case

consisting of a classical straight ballasted track supported by a homogeneous soil layer underlain by a rigid substratum.

The obtained results are very useful to calibrate the parameters of the simplified beam model. An iterative curve fitting procedure based on the Genetic Algorithm (GA) is then applied in order to obtain the convergence between the output signals of the two models. This process leads to a frequency and velocity dependent prismatic beam model with constant material density. A major influence of the moving load characteristics on the parameters of the proposed train/track interaction “TTI model” is found.

The chapter is organized as follows: Section 2 describes the main components of the studied reference case as well as the developed 3D finite difference model. Section 3 explains the TTI model as a novel track/ground interaction predictive tool. Finally section 4 discusses and critically evaluates the obtained results.

2. Reference Case- 3D Modeling

The selected reference case consists of a conventional ballasted railway track resting at the top surface of a homogeneous clayey soil that represents a soft soil with a total depth $H=5$ m. The standard gauge track is composed of two parallel continuous welded rails discreetly supported by regularly spaced horizontal sleepers. The rail-sleeper interface is considered to be perfectly linear elastic. As shown in Figure 3-1, the track substructure consists of ballast and sub-ballast layers which form a transition zone to the subsoil.

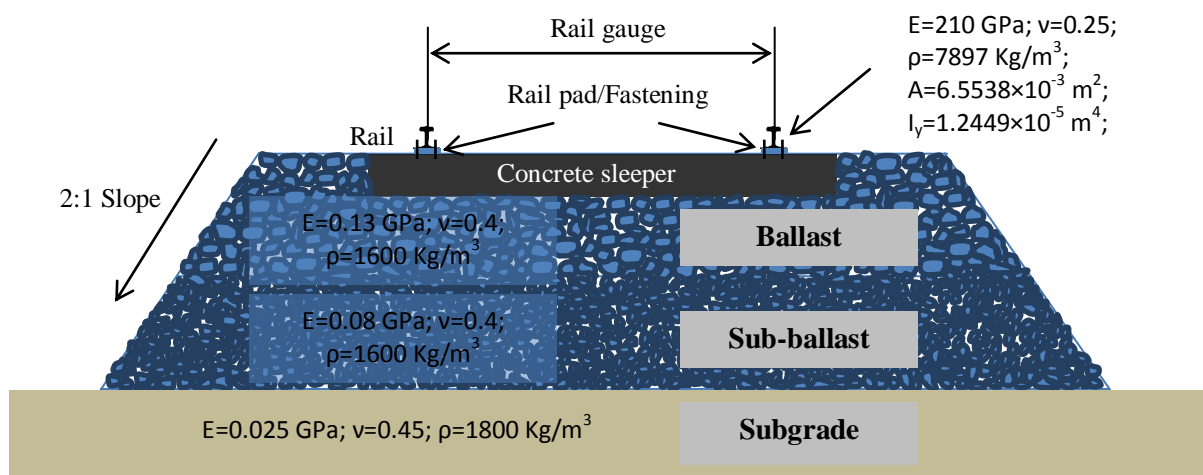


Figure 3-1: Components of the ballasted track structure

Figure 3-1 gives values of the track foundation elastic properties; where E , ν and ρ are the Young’s modulus, Poisson’s ratio and material density respectively. The mechanical

parameters of the rail are also given in which A and I_y are the area and the second moment of inertia of the rail cross section.

To simulate the dynamic response of the track/ground interaction problem, a truncated domain is considered in which the railway foundation is represented by 8 noded brick elements whereas the rail and sleepers are modeled by mean of elastic beam elements with six degrees of freedom per node. In order to prevent spurious reflections at the model boundary, an absorbing boundary condition insured by viscous elements is applied. In this study, the track structure is considered to be subjected to symmetrically applied load. Consequently, this hypothesis is used to enforce the symmetry condition along the track centerline. As the physical space is assumed to overly bedrock, fixed base boundary condition is applied, while its top surface is free. Figure 3-2 shows an illustrative example of the computational finite difference grid with the adopted boundary conditions.

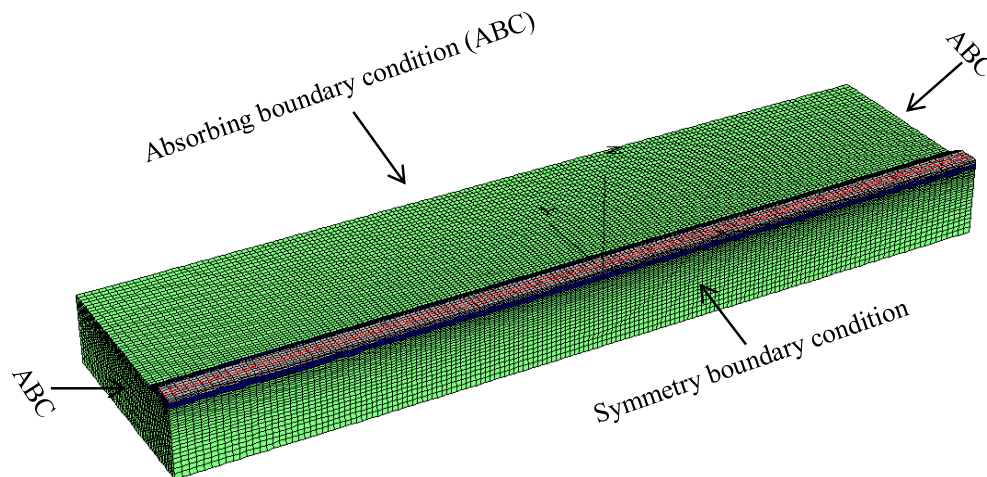
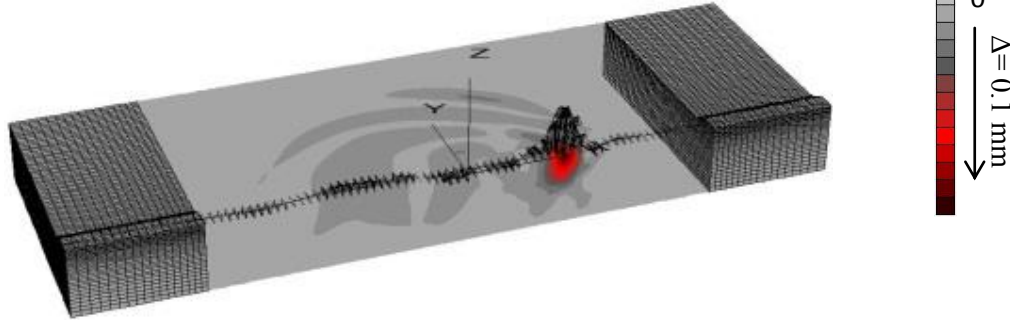


Figure 3-2: Computational finite difference grid: 194972 zones and 207972 grid points

The Load-Attached Moving Node (L-AMN) scheme which has been developed in chapter 2 is used to model the wheel/track interaction via a periodic adaptation of the spatial mesh. The proposed approach is efficiently implemented in the three-dimensional finite difference explicit code “FLAC^{3D},” in which a Matlab subroutine has been created to allow a rapid development of the generic input files. Further discussion on the L-AMN approach can be found in chapter 2, including the coupling of the adaptive formulation with the finite difference code for predicting ground vibration from railways.

During the numerical calculation, the vertical displacement of the rail y_r is recorded at selected predefined points including unloaded moving nodes; they are located at each time step according to the load attached moving reference X_r . Figure 3-3 shows a typical output of the interaction model comprising the spatial spread of the induced seismic waves and the rail dynamic response under high-speed moving load traveling the rail at constant velocity.

I- Spatial spread of the induced waves



II- Rail dynamic response

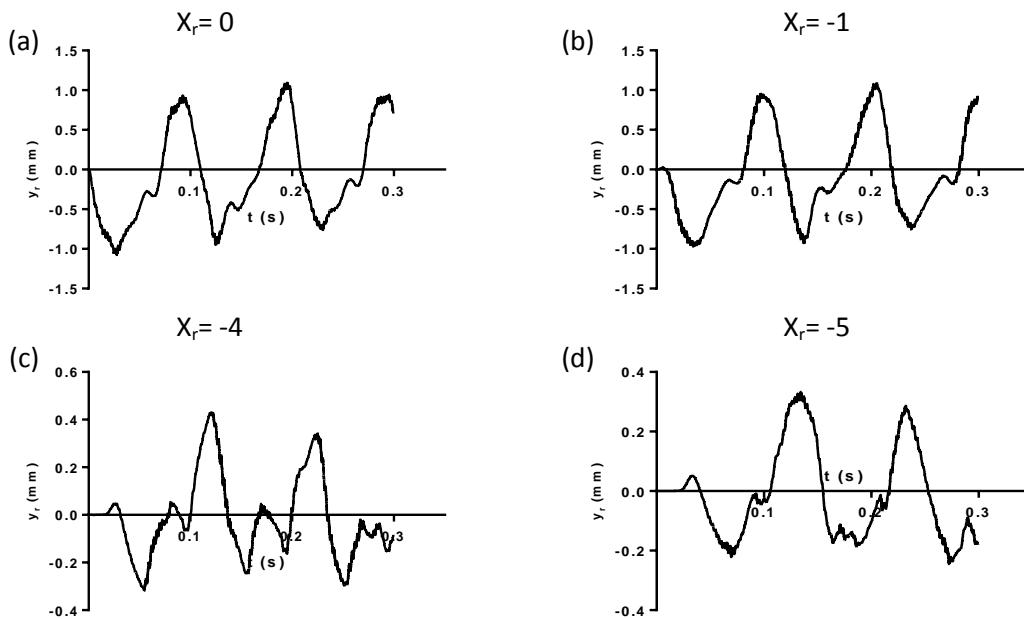


Figure 3-3: Dynamic response of the track/ground interaction model due to single moving load

3. TTI Predictive Tool for Rail Vibrations

Prediction of train-induced ground vibrations has to cope with the complexity of the mutual dynamic interactions between train, track formation and the subsoil. A classical solution based upon the sub-structuring approach [6,7,15] consisting of two calculation phases in which the first aims to study the train/track interaction using a Spring-viscous Damper-lumped Mass system (SDM model) which provides a simplified approach to account for the

dynamic stiffness of the embankment-subsoil medium. The second phase simulates the induced seismic waves that propagate in the substructure of the railway by applying the previously obtained reactions at the decoupling interface. Figure 3-4 summarizes the procedure for the evaluation of ground vibrations.

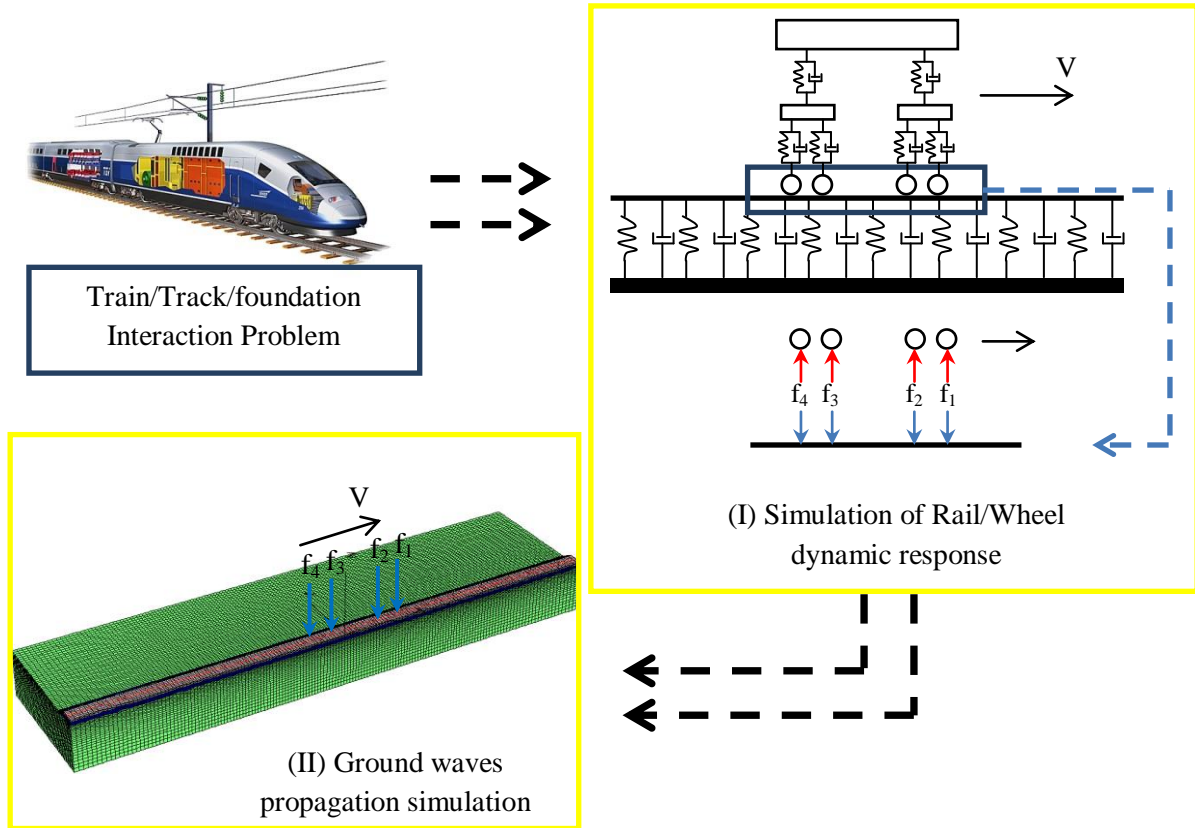


Figure 3-4: Sub-structuring approach for the assessment of ground vibrations

By focusing on the SDM models that are reported in the literature review, the effect of the frequency content and traveling velocity of the applied moving loads is generally neglected when selecting the equivalent dynamic impedances, which constitutes the main weakness of these models. Thus the purpose of the current study is to evaluate the sensitivity to loading frequency and/or velocity of the dynamic impedances used in simplified beam models.

The studied model constitutes from an infinite Euler-Bernoulli beam of constant mass per unit length m resting on a continuous viscoelastic layer comprising an infinite series of linear elastic vertical springs having a vertical rigidity per linear meter k . The damping of the equivalent material forming the foundation is integrated through linear viscous dampers η continuously distributed beneath the beam. Based on the solution of the one-dimensional wave equation, there is a dynamic equivalence between an end-excited semi-infinite bar and a single viscous dashpot. This shows that, the dynamic-stiffness relationship of a continuum

having an unlimited number of internal degrees-of-freedom can, in principle, be represented by a limited number of discrete elements.

A rigorous assessment of the dynamic impedances is obtained via a sensitivity analysis and iterative curve fitting procedure until reaching a good agreement between the predicted results of the simplified and the 3D models. Fig. 3-5 shows a schematic illustration of the adopted procedure for the assessment of the frequency and velocity dependent equivalent impedances of the rail foundation.

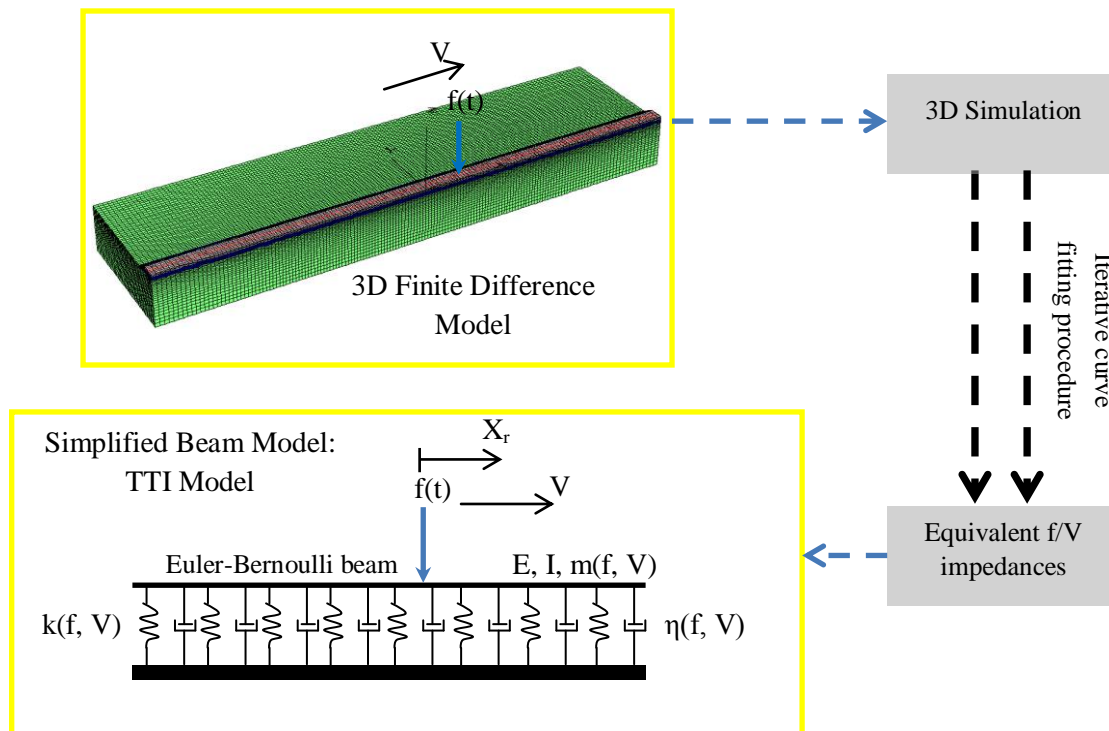


Figure 3-5: Calibration process of the simplified rail vibrations predictive tool

3.1.Preliminary study

The dynamic response of an infinite prismatic beam resting on continuous viscoelastic foundation and subjected to moving harmonic load $P(t)$ crossing the beam at constant velocity V is found analytically by Andersen et al. [16]. Where:

$$P(t) = P_0 e^{-i\omega t} \tag{3.1}$$

P_0 and ω are the amplitude and the angular frequency of the load respectively; $i = (-1)^{0.5}$.

The displacement field y_a of the infinite beam is expressed in the load-attached moving reference system X_r as follows:

$$y_a(X_r, t) = \begin{cases} A_1 e^{-\tau_1 X_r + i(\sigma_1 X_r - \omega t)} + A_2 e^{-\tau_2 X_r + i(\sigma_2 X_r - \omega t)} \\ A_3 e^{-\tau_3 X_r + i(\sigma_3 X_r - \omega t)} + A_4 e^{-\tau_4 X_r + i(\sigma_4 X_r - \omega t)} \end{cases} \quad (3.2)$$

Where A_j ($j=1, 2, 3, 4$) are the amplitude parameters to be determined using the conditions of continuity of the displacement, the bending moment and the shear force fields at the loading point; τ_j and σ_j are respectively the real and imaginary part of the j^{th} wave number. Physically τ_j represents the propagation and σ_j the attenuation of the j^{th} component of the propagated waves.

The purpose of this section is to achieve a reliable model allowing an accurate assessment of the rail dynamic response when the system excitation is a single harmonic moving load. The proposed plan is to determine the variation trend of the dynamic parameters (k, η, m) that lead to minimize the deviation of the predicted solution obtained with the simplified wave propagation model from that of the sophisticated 3D model. In the sequel, this model is called Train Track Interaction (TTI) model.

In order to solve this combinatorial optimization problem, we assume the discrete search space Ω , and a function g :

$$g: \Omega \rightarrow \mathfrak{R} \quad (3.3)$$

The general problem is to find:

$$\min_{\alpha \in \Omega} (g) \quad (3.4)$$

Where α is a vector of decision variables, and g is the objective function (also called fitness function).

In this study, a random research algorithm called “the Genetic Algorithm (GA)” is used to optimize the vector α . The adopted procedure is based upon the process of natural selection in which a set of individuals is created in solution space and these individuals reproduce to create one or more offspring, after which the offspring are mutated randomly, until a suitable solution is found. The GA is oriented by some genetic operators as shown in Figure 3-6, like selection, crossover and mutation in which the fittest individuals have more chance to be inherited into the next generation; the strong tend to adapt and survive and the weak tend to

die out. A more complete discussion of genetic algorithms, including extensions and related topics can be found in references [17,18].

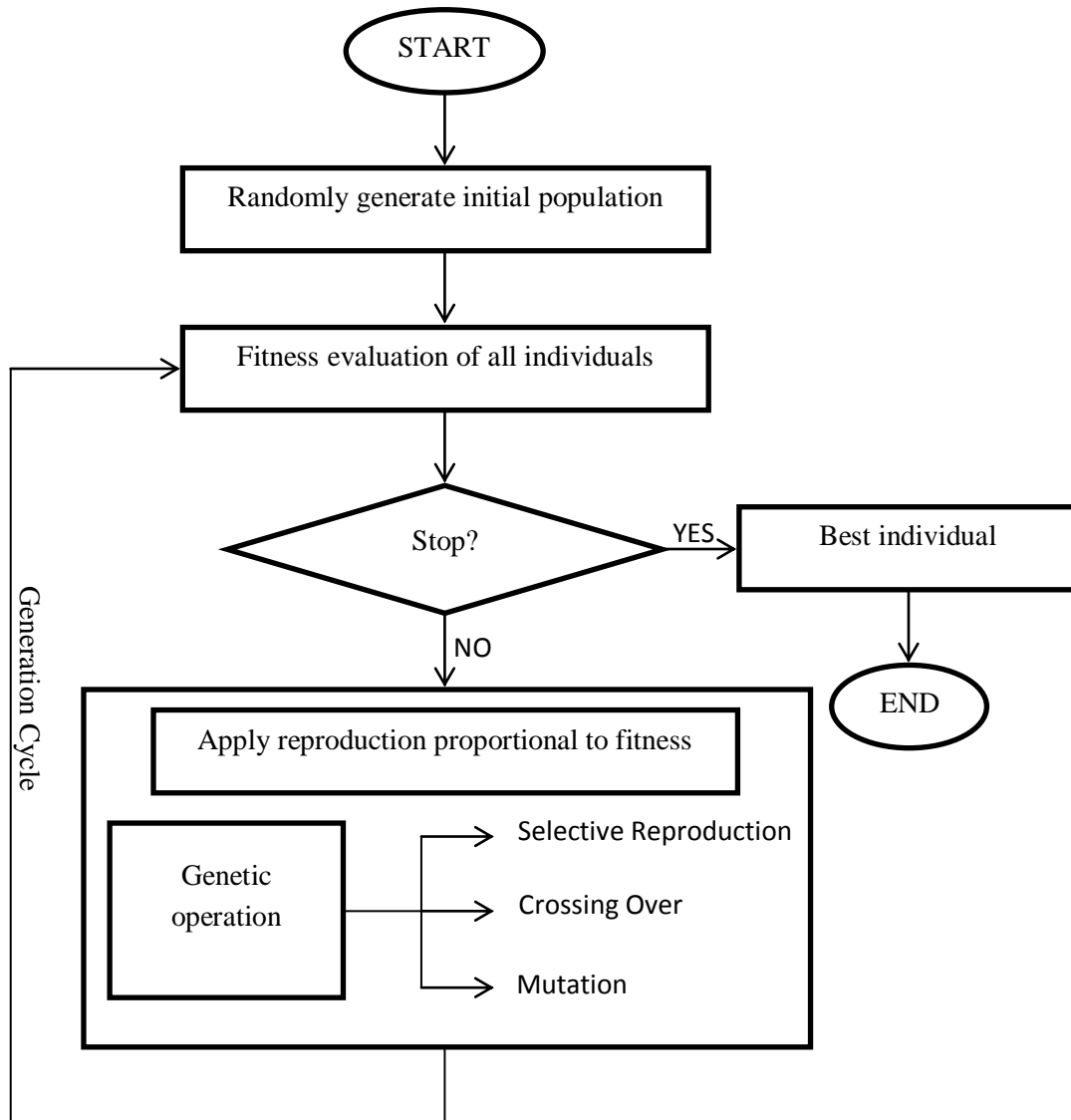


Figure 3-6: Flowchart of the Genetic Algorithm

The objective function g is taken as the square root of the usual mean squared error (MSE) calculated using a set of N_p points at the load position ($X_r=0$):

$$g = \sqrt{\frac{1}{N_p} \times \sum_{N_p} (y_r - \text{imag}(y_a))^2} \quad (3.5)$$

Where the applied harmonic load is considered to be the sine part of $P(t)$ (Eq. 3.1); that is why the imaginary part of the analytical solution has been appeared in the expression of the objective function (Eq. 3.5).

3.2.TTI Model- Dynamic impedances

In order to study the dynamic behavior of the discrete elements, 40 loading cases are taken into account; they correspond to 10 values of linear frequency f ranging from 5 to 50 Hz that fall within the frequency range highlighted in reference [19]. Moreover, 4 scenarios of traveling velocity V varying between 50 and 300 Km/h are studied. After applying each loading case which is characterized by a pair (f, V) to the 3D model, the dynamic response of the rail y_r is obtained that allows to launching of the iterative procedure for model parameters optimization.

The stiffness, damping and mass factors representing the dynamic components of rail foundation resistance are depicted in Fig. 3-7. It should be mentioned that, each triplet (k, η, m) that correspond to a pair (f, V) is obtained after reaching the convergence of the GA. Here, the evolution of an initial random population of 300 individuals is simulated over 100 generations.

The obtained results show that the shape of the curve representing the linear stiffness k of the equivalent foundation is generally increasing on the frequency and velocity axis. Conversely, the vibrating mass per unit length m tends to decrease simultaneously with f and V . Therefore the mobilized frequency f_0 (Eq. 3.6) of the simplified model tends to increase with the loading frequency and traveling velocity. Figure 3-7 illustrates also the variation of f_0 to load frequency ratio Φ over the plane (f, V) . It reflects a clear tendency of the dimensionless ratio to have a vertical asymptote in the vicinity of the subsoil natural frequency f_s which equals to 3.5 Hz (shear wave speed divided by the layer depth H). This fact highlights the capacity of the equivalent material to rigidify depending on the external loading mechanism.

$$f_0(f, V) = \frac{1}{2\pi} \sqrt{\frac{k}{m}} \quad (3.6)$$

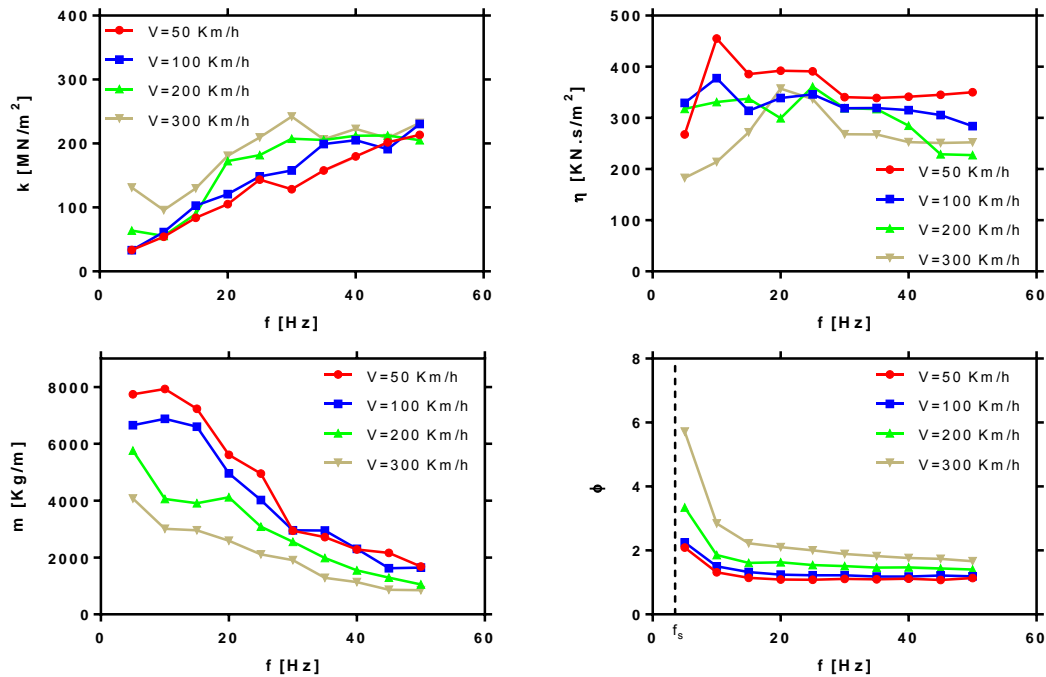


Figure 3-7: Dynamic components of the rail viscoelastic foundation

On the other hand, Figure 3-8 shows the optimal capacity of the TTI model to reproduce the mutual dynamic interactions in the track/foundation/subsoil system under high-speed moving harmonic load. The committed error in the calculated displacement field is expressed in terms of the normalized value of the objective function, Γ (Eq. 3.7), which is calculated at four discrete positions after the convergence of the optimization algorithm. The four nodes are located respectively at $X_r=0$ (load position), -1, -4 and -5 m (beam-rail span).

$$\Gamma(X_r) = \frac{g(X_r)}{\max[y_r(X_r)]} \quad (3.7)$$

The continuous viscoelastic foundation is found to give acceptable results at the load position in which the errors are ranging from 8 to 20%. Unfortunately, a dramatic decrease in the model reliability appears at the beam span. The calibration procedure reveals that the error in calculating displacement can reach 80%. This is due to the time lag effect that results from the wave propagation process in a solid medium.

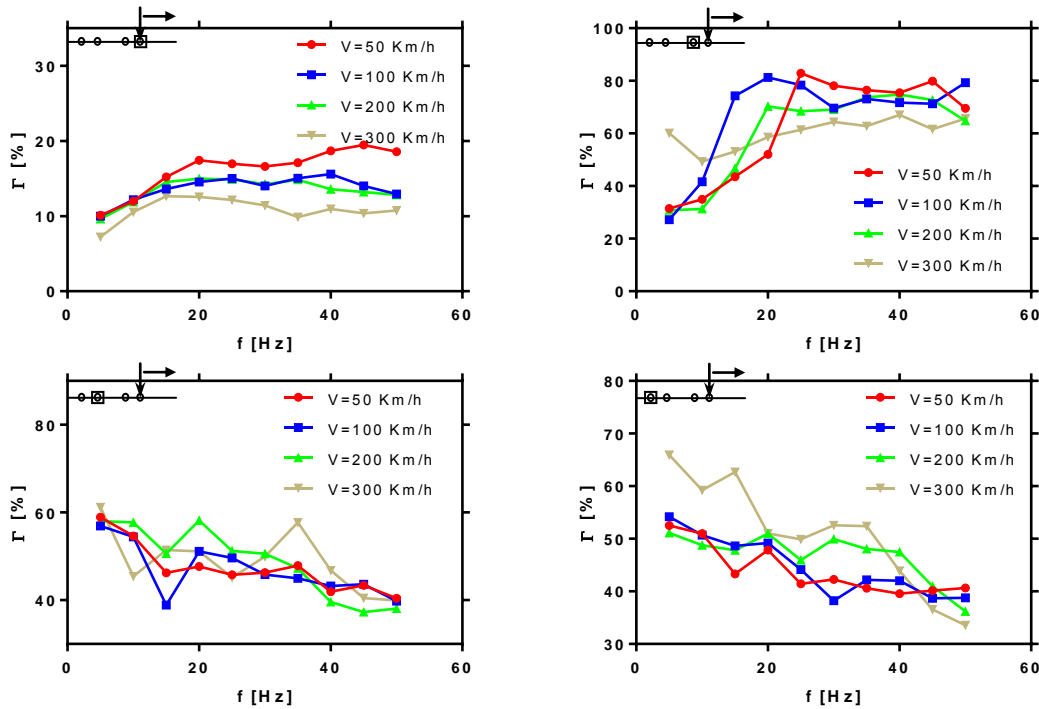


Figure 3-8: Optimal capacity of the viscoelastic foundation to represent the dynamic behavior of the track foundation

Figures 3-9 to 3-12 present the dynamic response of the TTI model compared to that of the 3D model at the load position ($X_r=0$); in which the two systems are excited simultaneously by the same harmonic moving load with amplitude equal to 100 KN. They correspond to load traveling velocity $V=50, 100, 200$ and 300 Km/h respectively.

An excellent agreement including amplitude similarity and phase synchronicity between the two predicted responses is easily noticed in the response of the attached-node to the moving load. This conclusion remains valid on the whole plan load frequency-load velocity.

The use of simplified model with improved input parameters is proved to be able to reliably reproduce the dynamic response of the rail even through the physical decoupling of the rail/foundation subsystems. The mutual dynamic interaction is taken into account implicitly through the laws of the discrete elements characteristics.

It's worth noting that the ratio between the required calculation time of the three-dimensional simulation and that of the simplified exceed for several cases 2000. Consequently, the use of the TTI model leads to avoid the manipulation of huge amount of numerical operations while maintaining a good accuracy level. This proves the efficiency of the TTI model which has been developed basically from one-dimensional discrete elements.

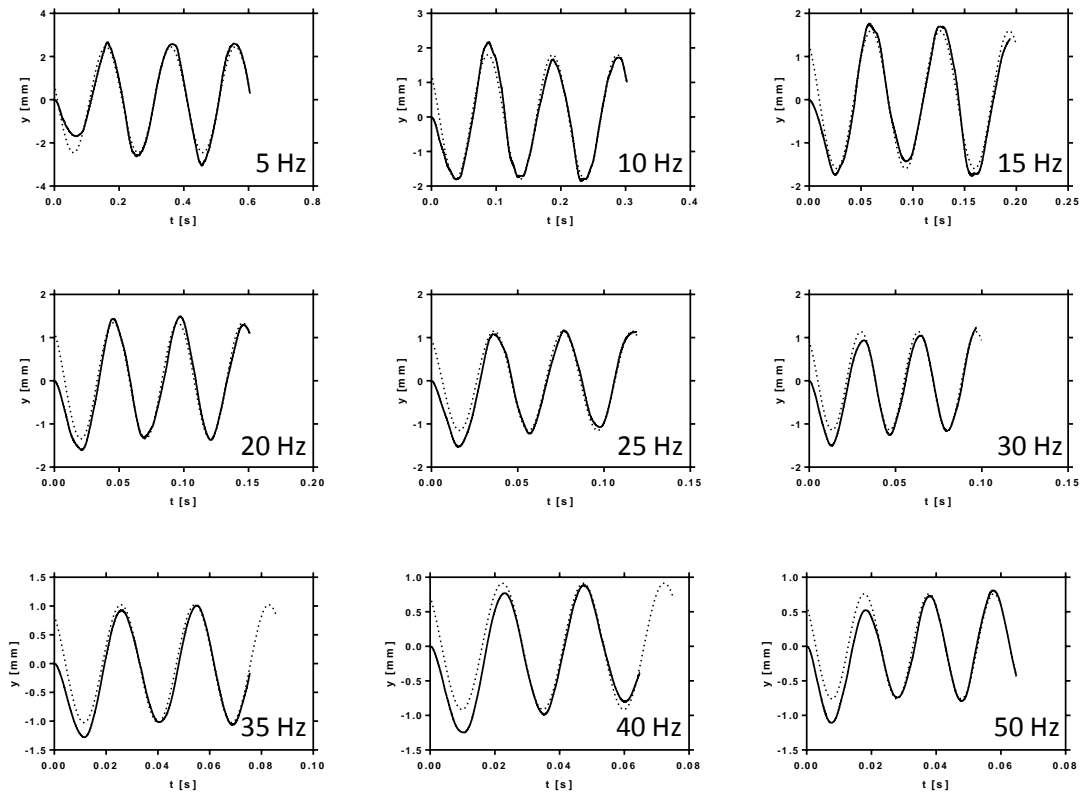


Figure 3-9: Dynamic response of the rail at $X_r=0$; case of harmonic load moving at $V=50$ Km/h. Solid line: 3D numerical system, dotted line: TTI model

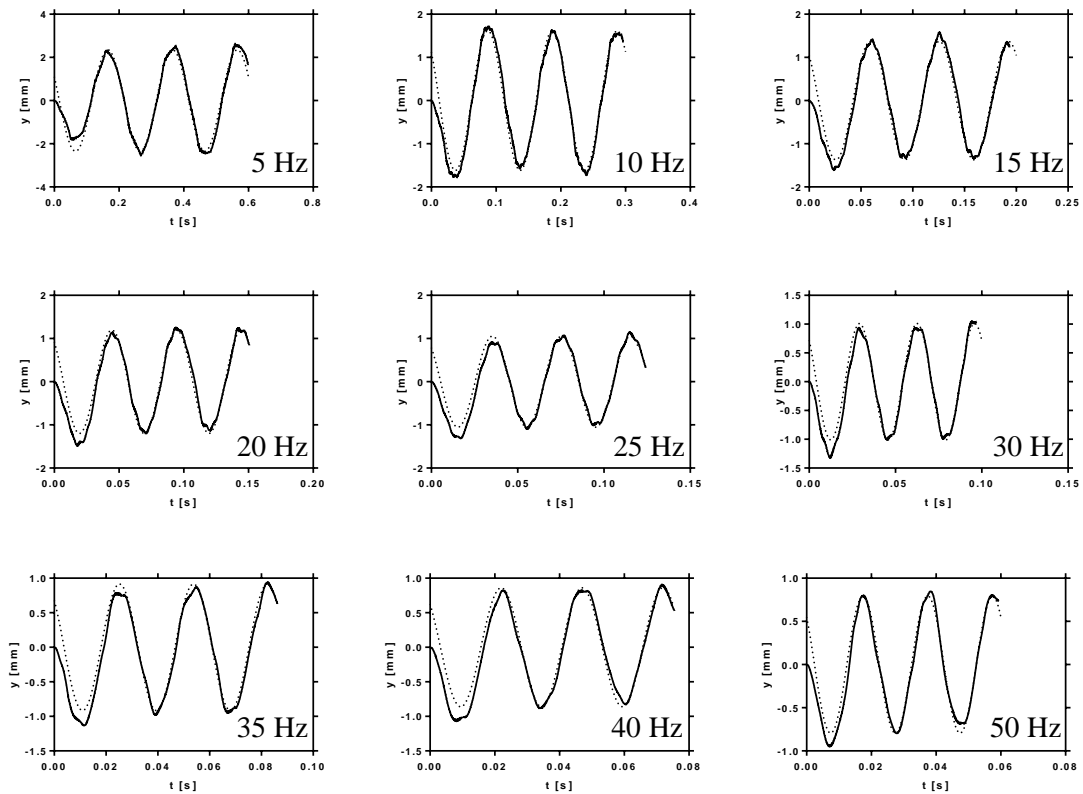


Figure 3-10: Dynamic response of the rail at $X_r=0$; case of harmonic load moving at $V=100$ Km/h. Solid line: 3D numerical system, dotted line: TTI model

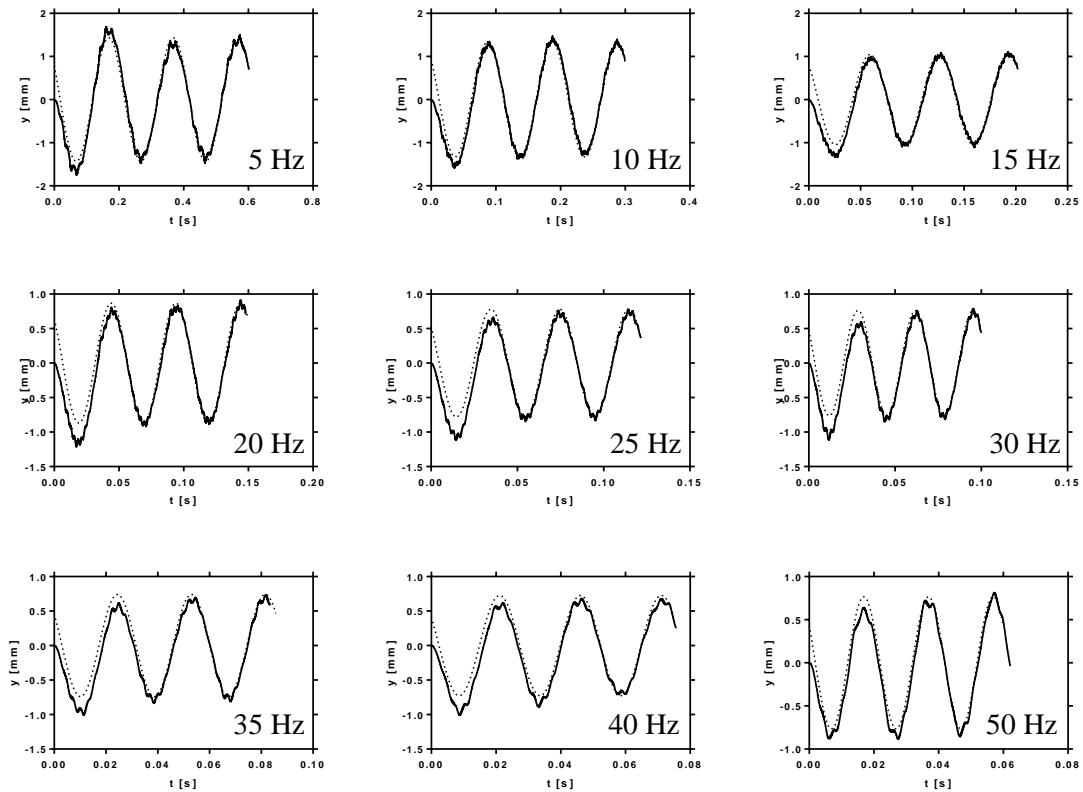


Figure 3-11: Dynamic response of the rail at $X_r=0$; case of harmonic load moving at $V=200$ Km/h. Solid line: 3D numerical system, dotted line: TTI model

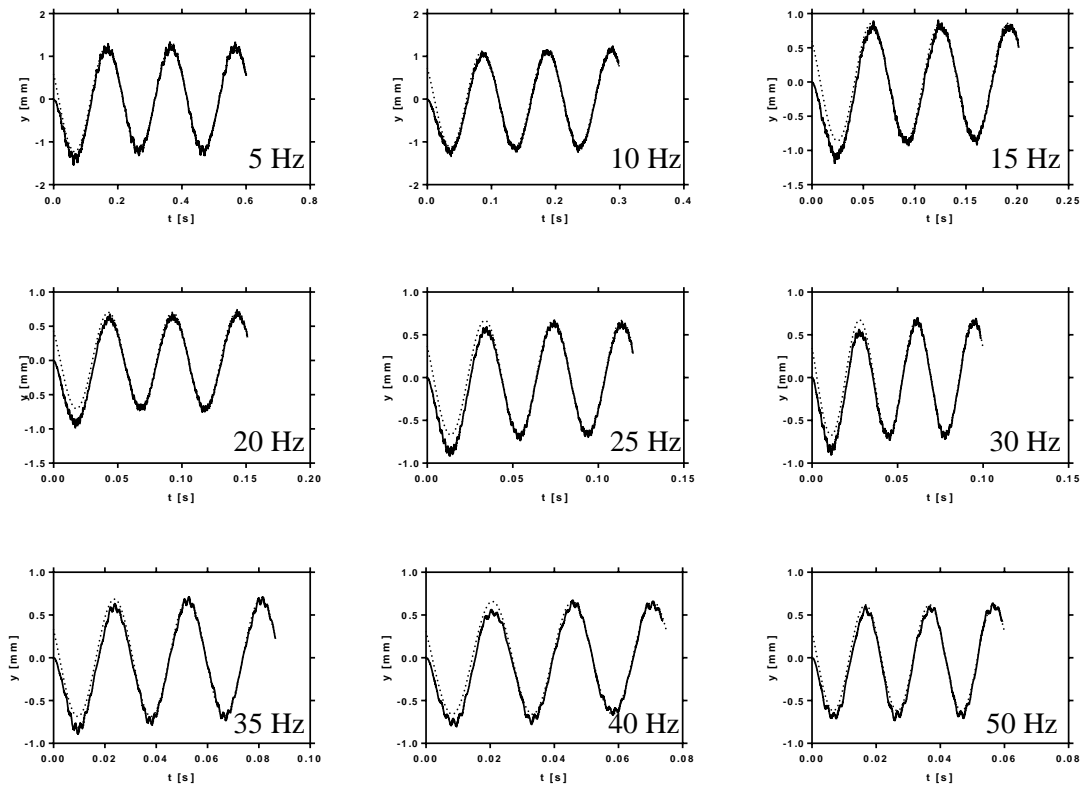


Figure 3-12: Dynamic response of the rail at $X_r=0$; case of harmonic load moving at $V=300$ Km/h. Solid line: 3D numerical system, dotted line: TTI model

4. Conclusions

This chapter included a simplified numerical model (TTI) for the simulation of train/track interaction problems in unbounded domain. The ballasted railway track is assumed to rest on an elastic half space. However any material/geometrical nonlinearity could be easily implemented in the TTI numerical model.

The model ensures the incorporation of the foundation dynamic effect in the response of the system via an adaptation process. A physical decoupling between the rail and the classical ballasted track formation is proposed. The rail-pads and the sleepers as well as the ballast, sub-ballast and subsoil layers are modeled by an equivalent continuous viscoelastic foundation that supports an infinite Euler-Bernoulli beam-rail. The dynamic impedances of the TTI model are investigated via a sensitivity analysis in the excitation frequency-load traveling velocity domain. Consequently, appropriate charts are determined using a random research algorithm “the genetic algorithm” that used to minimize the deviation of the predicted solution obtained with the simplified wave propagation model from that of a sophisticated 3D model. Herein, the excitation is a single harmonic moving load that traversed the rail at constant velocity. The continuous viscoelastic foundation is found to give acceptable results at the attached-node to the moving load in which the errors are ranging from 8 to 20%. Unfortunately, a dramatic decrease in the model reliability appears at the beam span in which the error can reach 80%. The developed model allows a high decrease in the computational cost where the required computation time can be reduced for several cases by a factor of 2000 with respect to an equivalent 3D advanced simulation.

The present study points out the significant importance of considering the track/soil dynamic interaction effect on the parameters of the SDM models, in particular this study focused on the case of the well-known model in the field of track dynamics: the infinite Euler-Bernoulli beam on continuous viscoelastic foundation. Generally, it can be concluded that a simplified calculation protocol should be preceded by a reliability study before being used in the vibratory analysis of the railways under high speed time-variant moving loads.

References

- [1] Madshus C, Kaynia AM. High-speed railway lines on soft ground: Dynamic behaviour at critical train speed. *J Sound Vib* 2000;231:689–701. doi:10.1006/jsvi.1999.2647.
- [2] Auersch L. The effect of critically moving loads on the vibrations of soft soils and isolated railway tracks. *J Sound Vib* 2008;310:587–607. doi:10.1016/j.jsv.2007.10.013.
- [3] Alves Costa P, Calçada R, Silva Cardoso A, Bodare A. Influence of soil non-linearity on the dynamic response of high-speed railway tracks. *Soil Dyn Earthq Eng* 2010;30:221–35. doi:10.1016/j.soildyn.2009.11.002.
- [4] Mulliken JS, Karabalis DL. Discrete model for dynamic through-the-soil coupling of 3-D foundations and structures. *Earthq Eng Struct Dyn* 1998;27:687–710. doi:10.1002/(SICI)1096-9845(199807)27:7<687::AID-EQE752>3.0.CO;2-O.
- [5] Ju SH. Evaluating foundation mass, damping and stiffness by the least-squares method. *Earthq Eng Struct Dyn* 2003;32:1431–42. doi:10.1002/eqe.285.
- [6] Paolucci R, Maffei A, Scandella L, Stupazzini M, Vanini M. Numerical prediction of low-frequency ground vibrations induced by high-speed trains at Ledsgaard, Sweden. *Soil Dyn Earthq Eng* 2003;23:425–33. doi:10.1016/S0267-7261(03)00061-7.
- [7] Yang YB, Hung HH, Chang DW. Train-induced wave propagation in layered soils using finite/infinite element simulation. *Soil Dyn Earthq Eng* 2003;23:263–78. doi:10.1016/S0267-7261(03)00003-4.
- [8] Koh CG, Ong JSY, Chua DKH, Feng J. Moving element method for train-track dynamics. *Int J Numer Methods Eng* 2003;56:1549–67. doi:10.1002/nme.624.
- [9] Ang KK, Dai J. Response analysis of high-speed rail system accounting for abrupt change of foundation stiffness. *J Sound Vib* 2013;332:2954–70. doi:10.1016/j.jsv.2013.01.005.
- [10] Tran MT, Ang KK, Luong VH. Vertical dynamic response of non-uniform motion of high-speed rails. *J Sound Vib* 2014;333:5427–42. doi:10.1016/j.jsv.2014.05.053.
- [11] Zhai W, Cai Z. Dynamic interaction between a lumped mass vehicle and a discretely supported continuous rail track. *Comput Struct* 1997;63:987–97. doi:10.1016/S0045-7949(96)00401-4.
- [12] Lei X, Noda N-A. Analyses of dynamic response of vehicle and track coupling system with random irregularity of track vertical profile. *J Sound Vib* 2002;258:147–65. doi:10.1006/jsvi.2002.5107.
- [13] Xia H, Cao YM, De Roeck G. Theoretical modeling and characteristic analysis of moving-train induced ground vibrations. *J Sound Vib* 2010;329:819–32. doi:10.1016/j.jsv.2009.10.007.
- [14] Kouroussis G, Verlinden O. Prediction of railway ground vibrations: Accuracy of a coupled lumped mass model for representing the track/soil interaction. *Soil Dyn Earthq Eng* 2015;69:220–6. doi:10.1016/j.soildyn.2014.11.007.

- [15] Kouroussis G, Verlinden O, Conti C. A two-step time simulation of ground vibrations induced by the railway traffic. *Proc Inst Mech Eng Part C J Mech Eng Sci* 2012;226:454–72. doi:10.1177/0954406211414483.
- [16] Andersen L, Nielsen SRK, Kirkegaard PH. Finite element modelling of infinite Euler beams on Kelvin foundations exposed to moving loads in convected co-ordinates. *J Sound Vib* 2001;241:587–604. doi:10.1006/jsvi.2000.3314.
- [17] Michalewicz Z. *Genetic Algorithms + Data Structures = Evolution Programs* (3rd Ed.). London, UK, UK: Springer-Verlag; 1996.
- [18] Reeves C. Genetic Algorithms. In: Glover F, Kochenberger GA, editors. *Handb. Metaheuristics*, Springer US; 2003, p. 55–82. doi:10.1007/0-306-48056-5_3.
- [19] Griffin MJ. *Handbook of Human Vibration*. Elsevier; 1996.

Conclusions and Further Work

This section summarizes the conclusions drawn from the present work and suggests areas where further work may be achieved.

1. Conclusions

This thesis deals with the numerical modeling of the track/ground interaction problems under high-speed time variant moving loads. It aims to provide reliable detailed and simplified predictive tools in the time domain to assess the vibration levels near HSL.

In this context, chapter 1 proposed a stable, consistent and numerically convergent innovative adaptive method (the PCU method) for the assessment of the dynamic response of infinite beams resting on continuous foundation under high speed moving loads. The key advantage of the proposed approach appears through the vanishing of the convective terms that lead to a numerical instability due to the induced negative numerical damping when linear elements are used in the FEM discretization. The case of viscoelastically damped foundation with high velocities that can reach the critical velocity of the beam is studied in the linear domain. The accuracy of the PCU method is investigated function of the adaptive scheme parameters. Two-time steps which precede the interpolation process performed using a fifth-order Hermite's interpolating polynomial (three points of interpolation) show a good numerical performance on the entire velocity axis at the studied frequency range. The use of progressive mesh doesn't present a constraint for the PCU method.

Chapter 2 presented an efficient approach to solve the problem of ground-induced waves by high-speed moving loads that propagate in media with complex geometry and material behavior. A 3D numerical tool is developed on the basis of the finite difference method within the frame of an adaptive meshing scheme "L-AMN" which is based upon the creation of load-attached moving nodes on the rail rolling surface. The convergence of the approach is studied with respect to the discretization parameters of the spatiotemporal coupled domain. It is found that approximately 14 grid points per wavelength should be used to correctly discretize the foundation domain which exceeds that needed to resolve a stationary loading problem. On the other hand the influence of the rail-beam spatiotemporal mesh on the discrete representation of the time-variant moving load is studied; a ratio of 130 subdivisions per wavelength is found

to ensure a satisfactory numerical convergence. Many numerical experiments are performed in the sub-Rayleigh and super-Rayleigh ranges in order to validate the developed model. They clearly show the capacity to assess the dynamic response of the track/ground system especially when the load velocity exceeds the Rayleigh wave speed of the subsoil layer in which a Mach cone appears at the center of the model.

The last chapter included a simplified numerical model (TTI) for the simulation of train/track interaction problems in unbounded domain. The model ensures the incorporation of the foundation dynamic effect in the response of the system via an adaptation process. A physical decoupling between the rail and the classical ballasted track formation is proposed. It gives rise to an equivalent continuous viscoelastic foundation that supports an infinite Euler-Bernoulli beam-rail. The dynamic impedances of the TTI model are investigated via a sensitivity analysis in the excitation frequency-load traveling velocity domain. Consequently, appropriate charts are determined using a random research algorithm “the genetic algorithm” that used to minimize the deviation of the predicted solution obtained with the simplified wave propagation model from that of a sophisticated 3D model. Herein, the excitation is a single harmonic moving load that traversed the rail at constant velocity. The continuous viscoelastic foundation is found to give acceptable results at the attached-node to the moving load in which the errors are ranging from 8 to 20%. Unfortunately, a dramatic decrease in the model reliability appears at the beam span in which the error can reach 80%. The developed model allows a high decrease in the computational cost where the required computation time can be reduced for several cases by a factor of 2000 with respect to an equivalent 3D advanced simulation.

2. Recommendations for Further Work

This work highlighted two reliable numerical models that can be used to assess the vibration levels at the rail and the surrounding soil. Special precautions have been taken during the simulation of the moving loads at their contacts with the rail in which two approaches have been proposed that of the PCU and the L-AMN.

In the first chapter, the simplified numerical model has been studied in the linear elastic domain. However, any kind of behavioral nonlinearity either at the wheel/rail interface or at the foundation can be easily integrated in the temporal formulation by adopting an appropriate iterative solver e.g. the Newton-Raphson method. On the other, to reduce the required time of

calculation, an appropriate absorbing boundary condition (ABC) can be applied at the model boundaries.

Similarly, in the second chapter, the detailed model (3D finite difference model) has been developed in the perfectly elastic domain. This does not preclude consideration of any kind of geometrical and mechanical anomalies comprising soil discontinuities and material non-linearity in the present model without causing a considerable increase in the calculation time thanks to the use of an explicit numerical scheme (the central-difference method). Moreover, this model represents an efficient tool to test/develop strategies (mitigation techniques) that would lead to acceptable vibration levels in urban areas via the damping of ground-borne vibrations near to HSL.

In the last chapter, an enhancement of the TTI model performance especially at span can be investigated via the introducing of additional parameters. On the other hand, the reliability of the simplified model as well as the parameters selection in the multi-frequency domain can be studied in subsequent works.

Appendix A

Matlab Code of the Periodic Configuration Update Method: Formulation in the Time Domain

1. USER INTERFACE

In the following, we present the user interface which is the space where interactions between users and calculating machine occur. It is allow effective operation and control of the calculation mechanism in which the dynamic parameters of the system, the beam spatial mesh and the numerical parameters are specified. Herein, a unique function “Gest_Cal” is called in order to start the numerical calculation.

```

%Dynamic parameters of the system
%-----
E=2e11;%Young's Modulus [pa]
I=3.06e-5;%Second moment of inertia [m^4]
mb=60.34;%Mass per linear meter [Kg/m]
Kb=1.6e7;%Stiffness of the foundation [N/m2]
Cb=0.1*2*sqrt(mb*Kb);%Damping of the foundation material [Ns/m2]
V=1.00*sqrt(sqrt(E*I*Kb/(mb^2)));%Travelling velocity [m/s]
P0=40000;%Load amplitude [N]
omega=2.0*sqrt(Kb/mb);%Angular frequency of the load [rd/s]

%Discretization of the beam
%-----
Ln1=100;%Length of the left part
Lnc1=10;%Length of the left central part
Lnc2=10;%Length of the right central part
Ln2=100;%Length of the right part
Lig=3.0;%Largest mesh size
Lfg=0.3;%Medium mesh size
Lfc1=0.3;%smallest mesh size

%Parameters of the numerical model
%-----
NT=100;%Number of periods of the moving harmonic load
dt=1.3e-5;%Infinitesimal time step
m=2;%Number of time steps that precede the interpolation process
dint=3;%Number of points integrated in the interpolation process

%Validation parameters
%-----
Tce=20;%Start of error calculation from Tceth period
Tdp=20;%Keep the beam configuration at the Tdpth response period
Ldif=10;%Half-length of the diffusion zone
rac=1000;%Keep the displacement d on span/ d>(Amp(dcenter)/rac)
fc=1000;%Cut-off frequency [Hz]
vaf=200;%Display the calculation progress every vaf steps

%Numerical solution
%-----
[arad,crail,dr,r,pde,S_Fou]=Gest_Cal(E,I,mb,Kb,Cb,V,Ln1,Lnc1,Lnc2,Ln2,
,Lig,Lfg,Lfc1,P0,omega,NT,dt,m,dint,Tce,Tdp,Ldif,rac,fc,vaf);

```

2. THE MOTHER FUNCTION “Gest_Cal”

This function serves to manage the numerical calculation in which it starts by the assessment of the global mass, damping and stiffness matrices (see Eq. 1.2) via the embedded function “Configuration”. Then, based on the user-defined interpolation parameters, the function “Matr_Fct_Int” calculate the matrix H (see Eq. 1.12) which is formed from the Hermitian polynomials used in the adaptation process of every node. Finally, the function “Adap_Num_Ana” is called to find the analytical and the numerical solutions of the studied structure.

```
function[arad,craill,dr,r,pde,S_Fou]=Gest_Cal(E,I,mb,Kb,Cb,V,Ln1,Lnc1,
Lnc2,Ln2,Lig,Lfg,Lfc1,P0,omega,NT,dt,m,dint,Tce,Tdp,Ldif,rac,fc,vaf)
arad=zeros(1,4);
fprintf('*****
****');
fprintf('\n');fprintf('\t\t\t\t\tCalcul des Matrices M, C, K\n');
fprintf('*****
****');
fprintf('\n');
[M,C,K,pt,n1,nc1,~,~,cox,cor,T_conf]=Configuration(E,I,mb,Kb,Cb,Ln1,
Lnc1,Lnc2,Ln2,Lig,Lfg,Lfc1);
if V==0
    MNi=zeros;dMNi=zeros;bih=0;bsih=0;T_int=0;
else
    [MNi,dMNi,bih,bsih,T_int]=Matr_Fct_Int(cox,pt,dint);
end
fprintf('statut: Validé\n');
fprintf('*****
****');
fprintf('\n');fprintf('\t\t\t\t\tDébut du Calcul Numérique\n');
fprintf('*****
****');
fprintf('\n');
[~,~,~,~,~,~,dr,r,craill,~,ermaxc,ermaxt,pde,S_Fou,T_ex_adap]=Adap_Num
_Ana(M,C,K,MNi,dMNi,E,I,mb,Kb,Cb,V,P0,omega,n1,nc1,pt,cor,bih,bsih,
NT,m,dt,Tce,Tdp,Ldif,rac,fc,vaf,dint);
arad(1,1)=V/sqrt(sqrt(E*I*Kb/(mb^2)));arad(1,2)=ermaxc;arad(1,3)=erm
axt;arad(1,4)=T_conf+T_int+T_ex_adap;
fprintf('*****
****');
fprintf('\n');
fprintf('statut: Validé\n');
fprintf('*****
****');
fprintf('\n');
end
```

3. BASIC SUBROUTINES

In this part, we present the master subroutines which perform the main tasks of numerical calculation including the matrices generation, the stationary- loading state calculation, the adaptation process (see Eq. 1.15 and 1.16) and the analytical solution (see Eq. 1.18).

3.1. Configuration

```
function[M,C,K,pt,n1,nc1,Lre,Lto,cox,cor,T_conf]=Configuration(E,I,m
b,Kb,Cb,Ln1,Lnc1,Lnc2,Ln2,Lig,Lfg,Lfc1)
tic
x0=[0.5 1];
[x]=Serie_Geo(Ln1,Lig,Lfg,x0);
n1=round(x(2));
r1=(Lfg/Lig)^(1/n1);
L01=Lig;
if Lig==Lfg
L1=(n1+1)*Lig;
else
L1=(L01*(1-(r1)^(n1+1)))/(1-r1);
end
Lil=zeros(n1+1,1);
for i=1:n1+1
    Lil(i,1)=L01*(r1)^(i-1);
end
[x]=Serie_Geo(Lnc1,Lfg,Lfc1,x0);
nc1=round(x(2));
rc1=(Lfc1/Lfg)^(1/nc1);
L0c1=Lfg;
if Lfg==Lfc1
Lc1=(nc1+1)*Lfg;
else
Lc1=(L0c1*(1-(rc1)^(nc1+1)))/(1-rc1);
end
Lic1=zeros(nc1+1,1);
for i=1:nc1+1
    Lic1(i,1)=L0c1*(rc1)^(i-1);
end
[x]=Serie_Geo(Lnc2,Lfc1,Lfg,x0);
nc2=round(x(2));
rc2=(Lfg/Lfc1)^(1/nc2);
L0c2=Lfc1;
if Lfc1==Lfg
Lc2=(nc2+1)*Lfc1;
else
Lc2=(L0c2*(1-(rc2)^(nc2+1)))/(1-rc2);
end
Lic2=zeros(nc2+1,1);
for i=1:nc2+1
    Lic2(i,1)=L0c2*(rc2)^(i-1);
end
[x]=Serie_Geo(Ln2,Lfg,Lig,x0);
n2=round(x(2));
```

Matlab Code of the PCU Method: Formulation in the Time Domain

```

r2=(Lig/Lfg)^(1/n2);
L02=Lfg;
if Lfg==Lig
L2=(n2+1)*Lfg;
else
L2=(L02*(1-(r2)^(n2+1)))/(1-r2);
end
Li2=zeros(n2+1,1);
for i=1:n2+1
    Li2(i,1)=L02*(r2)^(i-1);
end
pt=n1+nc1+nc2+n2+4;
Lre=zeros(pt,1);
for i=1:n1+1
    Lre(i,1)=Lil(i,1);
end
for i=n1+2:n1+nc1+2
    Lre(i,1)=Lic1(i-(n1+1),1);
end
for i=n1+nc1+3:n1+nc1+nc2+3
    Lre(i,1)=Lic2(i-(n1+nc1+2),1);
end
for i=n1+nc1+nc2+4:n1+nc1+nc2+n2+4
    Lre(i,1)=Li2(i-(n1+nc1+nc2+3),1);
end
Lto=L1+Lc1+Lc2+L2;
cox=zeros(1,pt+1);
for j=2:pt+1
    cox(1,j)=cox(1,j-1)+Lre(j-1,1);
end
cor=zeros(1,pt+1);
for j=1:pt+1
    cor(1,j)=cox(1,j)-cox(1,n1+nc1+3);
end
nn=2;
ndl=2;
syms r
M=zeros((pt+1)*ndl,(pt+1)*ndl);
C=zeros((pt+1)*ndl,(pt+1)*ndl);
K=zeros((pt+1)*ndl,(pt+1)*ndl);
if Lig==Lfg
N1=(1/((Lig)^3))*(2*(r^3)-3*(r^2)*(Lig)...
+((Lig)^3));
N2=(1/((Lig)^3))*((r^3)*(Lig)...
-2*(r^2)*((Lig)^2)+r*((Lig)^3));
N3=(1/((Lig)^3))*(-2*(r^3)+3*(r^2)*(Lig));
N4=(1/((Lig)^3))*((r^3)*(Lig)-(r^2)*((Lig)^2));
N=[N1 N2 N3 N4];
d2N=diff(diff(N,r),r);
Meg=mb*int(N'*N,r,0,Lig);
Ceg=Cb*int(N'*N,r,0,Lig);
Keg=E*I*int(d2N'*d2N,r,0,Lig)+Kb*int(N'*N,r,0,Lig);
end
if Lfg==Lfc1
N1=(1/((Lfg)^3))*(2*(r^3)-3*(r^2)*(Lfg)...
+((Lfg)^3));

```

Matlab Code of the PCU Method: Formulation in the Time Domain

```

N2=(1/((Lfg)^3))*(r^3)*(Lfg)...
-2*(r^2)*((Lfg)^2)+r*((Lfg)^3);
N3=(1/((Lfg)^3))*(-2*(r^3)+3*(r^2)*(Lfg));
N4=(1/((Lfg)^3))*((r^3)*(Lfg)-(r^2)*((Lfg)^2));
N=[N1 N2 N3 N4];
d2N=diff(diff(N,r),r);
Mec=mb*int(N'*N,r,0,Lfg);
Cec=Cb*int(N'*N,r,0,Lfg);
Kec=E*I*int(d2N'*d2N,r,0,Lfg)+Kb*int(N'*N,r,0,Lfg);
end
for elmn=1:pt
if (elmn>=1 && elmn<=(n1+1) && Lig==Lfg)
    Me=Meg;Ce=Ceg;Ke=Keg;
else
    if (elmn>=(n1+2) && elmn<=(n1+nc1+nc2+3) && Lfg==Lfc1)
        Me=Mec;Ce=Cec;Ke=Kec;
    else
        if (elmn>=(n1+nc1+nc2+4) && elmn<=(n1+nc1+nc2+n2+4) &&
Lig==Lfg)
            Me=Meg;Ce=Ceg;Ke=Keg;
        else
N1=(1/((Lre(elmn,1))^3))*(2*(r^3)-3*(r^2)*(Lre(elmn,1))...
+((Lre(elmn,1))^3));
N2=(1/((Lre(elmn,1))^3))*(r^3)*(Lre(elmn,1))...
-2*(r^2)*((Lre(elmn,1))^2)+r*((Lre(elmn,1))^3);
N3=(1/((Lre(elmn,1))^3))*(-2*(r^3)+3*(r^2)*(Lre(elmn,1)));
N4=(1/((Lre(elmn,1))^3))*((r^3)*(Lre(elmn,1))-
(r^2)*((Lre(elmn,1))^2));
N=[N1 N2 N3 N4];
d2N=diff(diff(N,r),r);
Me=mb*int(N'*N,r,0,Lre(elmn,1));
Ce=Cb*int(N'*N,r,0,Lre(elmn,1));
Ke=E*I*int(d2N'*d2N,r,0,Lre(elmn,1))+Kb*int(N'*N,r,0,Lre(elmn,1));
end
end
end
for a=1:nn
    for i=1:ndl
        for b=1:nn
            for k=1:ndl
                rw=ndl*(elmn-2+a)+i;
                cl=ndl*(elmn-2+b)+k;
                M(rw,cl)=M(rw,cl)+Me(ndl*(a-1)+i,ndl*(b-1)+k);
                C(rw,cl)=C(rw,cl)+Ce(ndl*(a-1)+i,ndl*(b-1)+k);
                K(rw,cl)=K(rw,cl)+Ke(ndl*(a-1)+i,ndl*(b-1)+k);
            end
        end
    end
end
end
end
T_conf=toc;
end

```

3.2. *Matr_Fct_Int*

```

function [MNi,dMNi,biih,bsih,T_int]=Matr_Fct_Int(cox,pt,dint)
tic
[MNi]=sym('X', [pt 2*dint]);
syms X
cori=zeros(dint,1);
if dint==2
    biih=1;bsih=pt;
else
biih=((dint+1)/2);bsih=pt-((dint-3)/2);
end
if dint>=3
for jph=1:biih-1
[Ni]=Poly_Hermite([0;cox(1,jph+1)-cox(1,jph)]);
for jN=1:4
    MNi(jph,jN)=Ni(1,jN);
end
for jN=5:2*dint
    MNi(jph,jN)='0';
end
end
end
for jph=biih:bsih
if dint==2
    cori=[0;cox(1,jph+1)-cox(1,jph)];
else
    for icor=1:dint
        cori(icolor,1)=cox(1,jph-((dint+1)/2)+icolor)-cox(1,jph);
    end
end
[Ni]=Poly_Hermite(cori);
for jN=1:2*dint
    MNi(jph,jN)=Ni(1,jN);
end
end
if dint>=5
for jph=bsih+1:pt
[Ni]=Poly_Hermite([0;cox(1,jph+1)-cox(1,jph)]);
for jN=1:4
    MNi(jph,jN)=Ni(1,jN);
end
for jN=5:2*dint
    MNi(jph,jN)='0';
end
end
end
end
dMNi=diff(MNi,X);
T_int=toc;

end

```


Matlab Code of the PCU Method: Formulation in the Time Domain

```

    acclp(:,2) = a0*(deplp(:,2)-deplp(:,1))-a2*velp(:,1)-
a3*acclp(:,1);
    velp(:,2) = velp(:,1)+a6*acclp(:,1)+a7*acclp(:,2) ;
    end
    if v~=0
[deplau(:,1),velau(:,1),acclau(:,1)]=Inter_Hermite(pt,dint,VMNi,VdMN
i,biih,bsih,deplp(:,2),velp(:,2),acclp(:,2));
    deplp(:,2)=deplau;velp(:,2)=velau;acclp(:,2)=acclau;
    end
    if rem(i-(floor(i/ndel)*ndel),nw)==0

depl(:,iw+1)=deplp(:,2);vel(:,iw+1)=velp(:,2);accl(:,iw+1)=acclp(:,2
);
    Tt(1,iw+1)=t2/(2*pi()/(omegao));
    drr(iw+1,1)=t2/(2*pi()/(omegao));drr(iw+1,2)=deplp(2*(n1+nc1+3)-
1,2);
    drr(iw+1,3)=imag(Cham_Depl(alphaan,betaan,Amp,omegao,0,t2));
    iw=iw+1;
    end
    eltime=toc;
    T_ex_adap=T_ex_adap+eltime;
    e=nt-i;
    if e==0
    fprintf('Le run est fini\n');
    else
        if rem(e,vaf)==0
        if (eltime*e/3600)>=1
            fprintf('Le temps du calcul approximatif qui reste= %3.3f
heures\n',round(eltime*e*10^3/3600)/10^3);
        else
            if (eltime*e/60)>=1
                fprintf('Le temps du calcul approximatif qui reste=
%2.3f minutes\n',round(eltime*e*10^3/60)/10^3);
            else
                fprintf('Le temps du calcul approximatif qui reste=
%2.3f secondes\n',round(eltime*e*10^3)/10^3);
            end
        end
        end
        fprintf('Il te reste: %d étapes\n',e);
        fprintf('\n');
    end
    end
end
T_ex_adap=T_ex_adap+T_aff;
Xr=zeros((pt+1),length(depl(1,:)));ROr=zeros((pt+1),length(depl(1,:
)));
for i=1:(pt+1)
    for j=1:length(depl(1,:))
        Xr(i,j)=depl(2*i-1,j);
        ROr(i,j)=depl(2*i,j);
    end
end
end
[pik1,locv1]=findpeaks(drr(:,2));[pik2,locv2]=findpeaks(-drr(:,2));
TFp1=isempty(locv1);TFp2=isempty(locv2);
if TFp1==0 && TFp2==0
rde=abs(pik1(1,1)/pik2(length(pik2(:,1)),1));

```

Matlab Code of the PCU Method: Formulation in the Time Domain

```
    if rde<=10 && rde>=0.1
    [~,loc1]=findpeaks(drr(:,3));[~,loc2]=findpeaks(-drr(:,3));
    amd=max(drr(:,3));
    if drr(loc1(1,1),1)>drr(loc2(1,1),1)
        loc=loc2;
    else
        loc=loc1;
    end
    if Tce>length(loc(:,1))
    Taco=length(loc(:,1));
    else
    Taco=Tce;
    end
    Tres=(drr(loc(Taco,1),1)-drr(loc(Taco-1,1),1))*2*pi()/omegao;
    Tact=drr(loc(Taco,1),1);
    [ermaxc]=Tole_Cent(drr,ldr,Tact,omegao,Tres);
    [ermaxt]=Tole_Late(pt,cor,ldr,Ldif,Tact,omegao,alphaan,betaan,Amp,Tt
    ,Xr,amd,rac);
    [pde]=Verif_Sta(drr,loc,ldr,Tres,omegao);
    [craill]=Depl_Pou(ldr,pt,Tdp,loc,Tt,drr,Xr,alphaan,betaan,Amp,omegao,
    cor);
    [freqRng,Am_Fou_n]=Ser_Fourier(drr(:,2),deltat*nw,fc);
    [~,Am_Fou_a]=Ser_Fourier(drr(:,3),deltat*nw,fc);
    for i=1:length(Am_Fou_n(:,1))
    S_Fou(i,1)=freqRng(1,i);S_Fou(i,2)=Am_Fou_n(i,1);S_Fou(i,3)=Am_Fou_a
    (i,1);
    end
        else
        Tres=0;
        ermaxc=101;
        ermaxt=101;
        pde=zeros(1,2);
        craill=zeros(pt+1,2);
        S_Fou=zeros(1,3);
        end
    else
        Tres=0;
        ermaxc=101;
        ermaxt=101;
        pde=zeros(1,2);
        craill=zeros(pt+1,2);
        S_Fou=zeros(1,3);
    end
end
end
```

3.4. *Nomb_Ond*

```
function [alpha,beta,Amp]=Nomb_Ond(E,I,mb,Kb,Cb,V,P0,omega)
nondes=zeros(4,2);
ind=-100;
inom=1;
eta=zeros(4,1);
V0=sqrt(sqrt(E*I*Kb/(mb^2)));
omega0=sqrt(Kb/mb);
gama0=2*sqrt(mb*Kb);
psi=Cb/gama0;
```

Matlab Code of the PCU Method: Formulation in the Time Domain

```

v=V/V0;
OMEGA=omega/omega0;
f=@(K) (K^4) - (v^2*((omega0/V0)^2))* (K^2) - ...
((1i*4*psi*v*(omega0^2)*Kb)/(gama0*(V0^3)))+ ...
(2*OMEGA*v*((omega0/V0)^3))*K+ ...
(((omega0/V0)^4) - (OMEGA^2)*((omega0/V0)^4)) - ...
((1i*4*OMEGA*(omega0^3)*Kb*psi)/(gama0*(V0^4)));
c=@(x) complex(x(1),x(2));
g=@(x) abs(f(c(x)));
K0=[1,1];
Sau=c(fminsearch(g,K0,optimset('TolX',1e-15)));
S=Cas_Lim(Sau);
nondes(inom,1)=real(S);
nondes(inom,2)=imag(S);
while ind<=100
if ind==0
else
K0(1,1)=ind/10;
K0(1,2)=ind/10;
Sau=c(fminsearch(g,K0,optimset('TolX',1e-15)));
S=Cas_Lim(Sau);
for ik=1:inom
if abs(real(S)-nondes(ik,1))<=1e-12 && abs(imag(S)-
nondes(ik,2))<=1e-12
indik=0;
break
else
indik=1;
end
end
if indik==1
inom=inom+1;
nondes(inom,1)=real(S);
nondes(inom,2)=imag(S);
end
K0(1,1)=ind/10;
K0(1,2)=-ind/10;
Sau=c(fminsearch(g,K0,optimset('TolX',1e-15)));
S=Cas_Lim(Sau);
for ik=1:inom
if abs(real(S)-nondes(ik,1))<=1e-12 && abs(imag(S)-
nondes(ik,2))<=1e-12
indik=0;
break
else
indik=1;
end
end
if indik==1
inom=inom+1;
nondes(inom,1)=real(S);
nondes(inom,2)=imag(S);
end
end
end
ind=ind+1;
end

```

```
[alpha,beta]= Attri_Coef(nondes);
for ik=1:4
eta(ik,1)=-beta(ik,1)+1i*alpha(ik,1);
end
Mco=[1,1,-1,-1;eta(1,1),eta(2,1),-eta(3,1),-
eta(4,1);(eta(1,1)^2),...
(eta(2,1)^2),-(eta(3,1)^2),-
(eta(4,1)^2);(eta(1,1)^3),(eta(2,1)^3),...
-(eta(3,1)^3),-(eta(4,1))^3];
Psm=[0;0;0;P0/(E*I)];
Amp=Mco\Psm;
end
```

4. AUXILIARY SUBROUTINES

In this part, the auxiliary subroutines are presented in which they are dedicated to perform auxiliary tasks within the basic subroutines.

4.1. *Spatial mesh of the beam*

A single function “Serie_Geo” is presented in this section, which is designed to calculate the items of a geometric series. It is used to perform the progressive mesh of the beam according to Eq. 1.22.

4.1.1. Serie_Geo

```
function [x]=Serie_Geo(L,L0,Lf,x0)
options = optimset('Display','off');
[x]=fsolve(@calc,x0,options);
function fcns=calc(x)
if L0==Lf
fcns(1)=(L/L0)-(x(2)+1);
else
fcns(1)=(L/L0)-(1-(x(1)^(x(2)+1)))/(1-x(1));
end
fcns(2)=(Lf/L0)-(x(1)^x(2));
end
end
```

4.2. *Interpolation process*

The auxiliary subroutines presented in this section contribute to the interpolation process which aims to compensate the distance lag δx that results from the stationary- loading state calculation. The function “Optima” is developed to round the total time of calculation T_t to be multiple of Δt , while “Poly_Hermite” serves to find the generalized interpolating polynomial of Hermite of a beam section according to Eq. 1.3 and Fig. 1-2. The function

“Matr_Fct_Int_dx” serves to evaluate the matrix H (see Eq. 1.12). The recapitulative function “Inter_Hermite” is designed to find the new configuration of the beam according to Eq. 1.15 and 16, in order to re-inject it in the system (Eq. 1.1) as a new initial condition.

4.2.1. Optima

```
function [omegao,ti,ndel,deltat,nw]=Optima(V,NT,m,omega,dt)
if V==0
    omegao=2*pi()/(dt*round(2*pi()/(omega*dt)));
    ti=0;tf=round((NT*(2*pi())/omegao)*10^5)*10^-5;
    ndel=round((tf-ti)/(NT*dt));
    deltat=dt;
else
    omegao=2*pi()/(m*dt*round(2*pi()/(omega*m*dt)));
    ti=0;tf=round((NT*(2*pi())/omegao)*10^5)*10^-5;
    ndel=round((tf-ti)/(NT*m*dt));
    deltat=m*dt;
end

if (ndel/200)<=1.5
    nw=1;
else
    nw=floor(ndel/200)+1;
end
end
```

4.2.2. Poly_Hermite

```
function [Ni]=Poly_Hermite(x)
qv=sym('X', [length(x(:,1)) length(x(:,1))]);
Ni=sym('X', [1 2*length(x(:,1))]);
syms X
for iq=1:length(x(:,1))
    for iqq=1:length(x(:,1))
        if iqq~=iq
            qv(iqq,iq)=((X-x(iqq,1))/(x(iq,1)-x(iqq,1)))^2);
        end
    end
    end
qv(iq,iq)='1';
end
q=prod(qv);
dq=diff(q,X);
for iq=1:length(x(:,1))
    Ni(1,iq)=q(1,iq)*(1-(X-
x(iq,1))*double(subs(dq(1,iq),'X',x(iq,1))));
end
for iq=length(x(:,1))+1:2*length(x(:,1))
    Ni(1,iq)=q(1,iq-length(x(:,1)))*(X-x(iq-length(x(:,1)),1));
end
end
```

4.2.3. Matr_Fct_Int_dx

```
function [VMNi,VdMNi,T_aff]=Matr_Fct_Int_dx(MNi,dMNi,dx)
tic
VMNi=double(subs(MNi,'X',dx));
VdMNi=double(subs(dMNi,'X',dx));
T_aff=toc;
end
```

4.2.4. Inter_Hermite

```
function[deplf,velf,acclf]=Inter_Hermite(pt,dint,VMNi,VdMNi,biih,bsih,depl,vel,accl)
deplf=zeros(2*(pt+1),1);velf=zeros(2*(pt+1),1);acclf=zeros(2*(pt+1),1);
Di=zeros(2*dint,pt);Vi=zeros(2*dint,pt);Ai=zeros(2*dint,pt);
if dint>=3
for jin=1:biih-1
for iin=1:2
Di(iin,jin)=depl(2*(jin+iin-1)-1,1);
Vi(iin,jin)=vel(2*(jin+iin-1)-1,1);
Ai(iin,jin)=accl(2*(jin+iin-1)-1,1);
end
for iin=3:4
Di(iin,jin)=depl(2*(jin+iin-3),1);
Vi(iin,jin)=vel(2*(jin+iin-3),1);
Ai(iin,jin)=accl(2*(jin+iin-3),1);
end
end
end

for jin=biih:bsih
if dint==2
for iin=1:2
Di(iin,jin)=depl(2*(jin+iin-1)-1,1);
Vi(iin,jin)=vel(2*(jin+iin-1)-1,1);
Ai(iin,jin)=accl(2*(jin+iin-1)-1,1);
end
for iin=3:4
Di(iin,jin)=depl(2*(jin+iin-3),1);
Vi(iin,jin)=vel(2*(jin+iin-3),1);
Ai(iin,jin)=accl(2*(jin+iin-3),1);
end
else
for iin=1:dint
Di(iin,jin)=depl(2*(jin-((dint+1)/2)+iin)-1,1);
Vi(iin,jin)=vel(2*(jin-((dint+1)/2)+iin)-1,1);
Ai(iin,jin)=accl(2*(jin-((dint+1)/2)+iin)-1,1);
end
for iin=dint+1:2*dint
Di(iin,jin)=depl(2*(jin-((dint+1)/2)+iin-dint),1);
Vi(iin,jin)=vel(2*(jin-((dint+1)/2)+iin-dint),1);
Ai(iin,jin)=accl(2*(jin-((dint+1)/2)+iin-dint),1);
end
end
end
```

```

end
if dint>=5
for jin=bsih+1:pt
    for iin=1:2
Di(iin,jin)=depl(2*(jin+iin-1)-1,1);
Vi(iin,jin)=vel(2*(jin+iin-1)-1,1);
Ai(iin,jin)=accl(2*(jin+iin-1)-1,1);
        end
        for iin=3:4
Di(iin,jin)=depl(2*(jin+iin-3),1);
Vi(iin,jin)=vel(2*(jin+iin-3),1);
Ai(iin,jin)=accl(2*(jin+iin-3),1);
        end
    end
end
auX1=sum(VMNi.*Di',2); auX2=sum(VdMNi.*Di',2);
for iin=1:pt
    deplf(2*iin-1,1)=auX1(iin,1);
    deplf(2*iin,1)=auX2(iin,1);
end
auX1=sum(VMNi.*Vi',2); auX2=sum(VdMNi.*Vi',2);
for iin=1:pt
    velf(2*iin-1,1)=auX1(iin,1);
    velf(2*iin,1)=auX2(iin,1);
end
auX1=sum(VMNi.*Ai',2); auX2=sum(VdMNi.*Ai',2);
for iin=1:pt
    acclf(2*iin-1,1)=auX1(iin,1);
    acclf(2*iin,1)=auX2(iin,1);
end
deplf(2*(pt+1)-1,1)=depl(2*(pt+1)-1,1); deplf(2*(pt+1),1)=depl(2*(pt+1),1);
velf(2*(pt+1)-1,1)=vel(2*(pt+1)-1,1); velf(2*(pt+1),1)=vel(2*(pt+1),1);
acclf(2*(pt+1)-1,1)=accl(2*(pt+1)-1,1); acclf(2*(pt+1),1)=accl(2*(pt+1),1);
end

```

4.3. Convergence investigation of the PCU method

The following functions are developed in order to test the performance and accuracy of the proposed method. They aim to compare the dynamic response of an infinite beam resting on a viscoelastic foundation subjected to a single moving harmonic load crossing the beam with a constant velocity V found analytically to that provided by the numerical method.

The function “Tole_Cent” and “Tole_Late” are designed to calculate the value of Γ_1 (maximum of Eq. 1.20) and Γ_2 (maximum of Eq. 1.21) respectively. These two error estimators are widely used in the numerical investigation. The function “Verif_Sta” is

dedicated to find the difference between the obtained numerical solution and the exact solution of the differential equations according to excitation time.

4.3.1. Tole_Cent

```
function [ermaxc]=Tole_Cent(drr,ldr,Tact,omegao,Tres)
Tac=Tact;
Tacmin=(Tac*(2*pi()/omegao)-0.125*Tres)/(2*pi()/omegao);
if (Tac*(2*pi()/omegao)+0.125*Tres)/(2*pi()/omegao)<=drr(ldr,1)
Tacmax=(Tac*(2*pi()/omegao)+0.125*Tres)/(2*pi()/omegao);
else
Tacmax=drr(ldr,1);
end
delaic=zeros(ldr,2);cerr=zeros;ikl=1;
while Tac<=drr(ldr,1)
for i=1:ldr
delaic(i,1)=abs(drr(i,1)-Tacmin);
delaic(i,2)=abs(drr(i,1)-Tacmax);
end
indm1 = find(delaic(:,1) == min(delaic(:,1)));dex1=indm1;
indm2 = find(delaic(:,2) == min(delaic(:,2)));dex2=indm2;
if length(dex1)==1
bin=dex1;
else
bin=dex1(1,1);
end
if length(dex2)==1
bsu=dex2;
else
bsu=dex2(1,1);
end
erna=zeros(bsu-bin+1,1);
for ikj=bin:bsu
erna(ikj-bin+1,1)=abs((drr(ikj,2)-drr(ikj,3))/drr(ikj,3))*100;
end
cerr(ikl,1)=Tac;cerr(ikl,2)=max(erna(:,1));
Tac=Tac+(0.5*Tres/(2*pi()/omegao));
Tacmin=(Tac*(2*pi()/omegao)-0.125*Tres)/(2*pi()/omegao);
if Tac+(0.125*Tres/(2*pi()/omegao))>drr(ldr,1)
Tacmax=drr(ldr,1);
else
Tacmax=(Tac*(2*pi()/omegao)+0.125*Tres)/(2*pi()/omegao);
end
ikl=ikl+1;
end
ermaxc=max(cerr(:,2));
end
```

4.3.2. Tole_Late

```
function[ermaxt]=Tole_Late(pt,cor,ldr,Ldif,Tact,omega,alphaan,betaan
,Amp,Tt,Xr,amd,rac)
delait=zeros(2,pt+1);
for jtra=1:pt+1
```

Matlab Code of the PCU Method: Formulation in the Time Domain

```

    delait(1,jtra)=abs(cor(1,jtra)-(-Ldif));
    delait(2,jtra)=abs(cor(1,jtra)-(+Ldif));
end
indt1 = find(delait(1,:) == min(delait(1,:)));dextr1=indt1;
indt2 = find(delait(2,:) == min(delait(2,:)));dextr2=indt2;
if length(dextr1)==1
    bg=dextr1;
else
    bg=dextr1(1,1);
end
if length(dextr2)==1
    bd=dextr2;
else
    bd=dextr2(1,1);
end
Tactr=Tact;
daiTtr=zeros(1,ldr);
for j=1:ldr
    daiTtr(1,j)=abs(Tt(1,j)-Tactr);
end
indTtr = find(daiTtr(1,:) == min(daiTtr(1,:)));
dexTtr=indTtr;
if length(dexTtr)==1
    bindt=dexTtr;
else
    bindt=dexTtr(1,1);
end
cerrt=zeros(ldr-bindt+1,5);
for ktra=bindt:ldr
    crailce=zeros(bd-bg+1,2);
    for i=bg:bd
        crailce(i-bg+1,1)=Xr(i,ktra);
        crailce(i-
bg+1,2)=imag(Cham_Depl(alphaan,betaan,Amp,omega,cor(1,i),Tt(1,ktra)*
2*pi()/omega));
    end

[pikp,loctp]=findpeaks(crailce(:,1));ernatp=zeros(length(loctp(:,1))
,2);
ppmax=max(abs(pikp));
for itra=1:length(loctp(:,1))
    ernatp(itra,1)=abs((crailce(loctp(itra,1),1)-
crailce(loctp(itra,1),2)));
    ernatp(itra,2)=(ernatp(itra,1)*100)/ppmax;
end
[pikn,loctn]=findpeaks(-
crailce(:,1));ernatn=zeros(length(loctn(:,1)),2);
pnmax=max(abs(pikn));
for itra=1:length(loctn(:,1))
    ernatn(itra,1)=abs((crailce(loctn(itra,1),1)-
crailce(loctn(itra,1),2)));
    ernatn(itra,2)=(ernatn(itra,1)*100)/pnmax;
end
TF1=isempty(ernatp);TF2=isempty(ernatn);
if TF1==0
    cerrt(ktra,2)=ppmax;

```

Matlab Code of the PCU Method: Formulation in the Time Domain

```
    if ppmax>=(amd/rac)
cerrt(ktra,1)=max(ernatp(:,2));
    else
        cerrt(ktra,1)=0;
    end
else
    cerrt(ktra,1)=0;cerrt(ktra,2)=0;
end
if TF2==0
    cerrt(ktra,4)=pnmax;
    if pnmax>=(amd/rac)
cerrt(ktra,3)=max(ernatn(:,2));
    else
        cerrt(ktra,3)=0;
    end
else
    cerrt(ktra,3)=0;cerrt(ktra,4)=0;
end
cerrt(ktra,5)=max(cerrt(ktra,1),cerrt(ktra,3));
end
ermaxt=max(cerrt(:,5));
end
```

4.3.3. Verif_Sta

```
function [pde]=Verif_Sta(drr,loc,ldr,Tres,omegao)
pde=zeros;
pde(1,1)=0;pde(1,2)=100;
Tpde=drr(loc(1,1),1);
delaic=zeros(ldr,1);ist=2;
while Tpde<=drr(ldr,1)
for i=1:ldr
    delaic(i,1)=abs(drr(i,1)-Tpde);
end
indm1 = find(delaic(:,1) == min(delaic(:,1)));dex1=indm1;
if length(dex1)==1
    bin=dex1;
else
    bin=dex1(1,1);
end
pde(ist,1)=Tpde;
pde(ist,2)=abs((drr(bin,2)-drr(bin,3))*100/drr(bin,3));
Tpde=Tpde+(0.5*Tres/(2*pi()/omegao));
ist=ist+1;
end
end
```

4.4. Analytical solution

The following auxiliary functions “Cas_Lim” and “Attri_Coef” are dedicated to verify the convergence condition during the iterative resolution of the system of nonlinear equations that derived from the continuity conditions of Eq. 1.18 and to assign to each wavenumber an index

j according to the direction of propagation of the wave respectively. “Cham_Depl” is developed to evaluate the Eq. 1.18 for a given spatiotemporal state.

4.4.1. Cas_Lim

```
function S=Cas_Lim(Sau)
if abs(real(Sau))<10^-15
    if abs(imag(Sau))<10^-15
        S=(0)+1i*(0);
    else
        S=0+1i*imag(Sau);
    end
else
    if abs(imag(Sau))<10^-15
        S=real(Sau)+1i*0;
    else
        S=real(Sau)+1i*imag(Sau);
    end
end
end
```

4.4.2. Attri_Coef

```
function [alpha,beta]= Attri_Coef(nondes)
alpha=zeros(4,1);beta=zeros(4,1);
for ik=1:4
    if nondes(ik,1)>0
        if (nondes(ik,2)>0 || nondes(ik,2)==0)
            in2=ik;
            alpha(2,1)=nondes(ik,1);
            beta(2,1)=nondes(ik,2);
        end
    end
end
for ik=1:4
    if nondes(ik,1)<0
        if (nondes(ik,2)<0 || nondes(ik,2)==0)
            in4=ik;
            alpha(4,1)=nondes(ik,1);
            beta(4,1)=nondes(ik,2);
        end
    end
end
for ik=1:4
    if ik==in2 || ik==in4
    else
        if nondes(ik,2)>0
            alpha(1,1)=nondes(ik,1);
            beta(1,1)=nondes(ik,2);
        else
            alpha(3,1)=nondes(ik,1);
            beta(3,1)=nondes(ik,2);
        end
    end
end
```

```

                                end
                                end

end
end

```

4.4.3. Cham_Depl

```

function u=Cham_Depl(alpha,beta,Amp,ome,x,t)
if x>=0
    u=Amp(1,1)*exp(-beta(1,1)*x+1i*(alpha(1,1)*x-ome*t))...
    +Amp(2,1)*exp(-beta(2,1)*x+1i*(alpha(2,1)*x-ome*t));
else
    u=Amp(3,1)*exp(-beta(3,1)*x+1i*(alpha(3,1)*x-ome*t))...
    +Amp(4,1)*exp(-beta(4,1)*x+1i*(alpha(4,1)*x-ome*t));
end
end

```

4.5. *Output results*

Herein, the function “Depl_Pou” is used to capture the instantaneous dynamic response of the meshed beam at a user-defined instant. In the other hand “Ser_Fourier” serves to find for a temporal series the corresponding discrete Fourier transform which is computed after applying the FFT algorithm.

4.5.1. Depl_Pou

```

function[crail]=Depl_Pou(ldr,pt,Tdp,loc,Tt,dr, Xr,alphaan,betaan,Amp
,omegao,cor)
daiT=zeros(1,ldr);crail=zeros(pt+1,2);
if Tdp>length(loc(:,1))
    Tdpc=length(loc(:,1));
else
    Tdpc=Tdp;
end
for j=1:ldr
daiT(1,j)=abs(Tt(1,j)-dr(loc(Tdpc,1),1));
end
indmp = find(daiT(1,:) == min(daiT(1,:)));dext=indmp;
if length(dext)==1
    binc=dext;
else
    binc=dext(1,1);
end
for i=1:pt+1
    crail(i,1)=Xr(i,binc);

crail(i,2)=imag(Cham_Depl(alphaan,betaan,Amp,omegao,cor(1,i),Tt(1,bi
nc))*2*pi()/omegao);
end
end

```

4.5.2. Ser_Fourier

```
function [Freq_Fou,Am_Fou]=Ser_Fourier(x,deltim,fc)
Fs=round(1/deltim);
N=length(x);
k=0:N-1;
T=N/Fs;
freqRng=k/T;
YfreqD=fft(x)/N;
cutOff=ceil(N/2);
YfreqD=YfreqD(1:cutOff);
freqRng=freqRng(1:cutOff);
delaic=zeros(1,length(freqRng(1,:)));
for j=1:length(freqRng(1,:))
    delaic(1,j)=abs(freqRng(1,j)-fc);
end
indm1 = find(delaic(1,:) == min(delaic(1,:)));dex1=indm1;
if length(dex1)==1
    bin=dex1;
else
    bin=dex1(1,1);
end
Freq_Fou=zeros(1,bin);Yfreq_Fou=zeros(bin,1);
for i=1:bin
    Freq_Fou(1,i)=freqRng(1,i);
    Yfreq_Fou(i,1)=YfreqD(i,1);
end
Am_Fou=abs(Yfreq_Fou);
end
```


Appendix B

Matlab Code of the L-AMN Adaptive Meshing Scheme: 3D Finite Difference Modeling

1. User Interface

```

clear
clc
%%%%%%%%%%%%%%%%%%%%%%%%%%%%%%%%%%%%%%%%%%%%%%%%%%%%%%%%%%%%%%%%%%%%%%%%
%                               Géométrie du Modèle 3D
%%%%%%%%%%%%%%%%%%%%%%%%%%%%%%%%%%%%%%%%%%%%%%%%%%%%%%%%%%%%%%%%%%%%%%%%
%                               Dimensions de l'Embankment
le1d=2.85;%Moitié de la largeur inférieur de l'Embankment [m]
le2d=1.45;%Moitié de la largeur supérieur de l'Embankment [m]
he=0.7;%Hauteur de l'Embankment [m]
hb=0.3;%Epaisseur de la couche du ballast
%                               Dimensions du massif du sol
Lm=100;%Longueur du massif du sol (direction de passage) [m]
lmd=25;%Moitié de la largeur du massif du sol [m]
Hm=5;%Hauteur du massif du sol [m]
%Zone centrale du modèle (suivant x)
Lc=30;%Maillage raffiné dans cette zone [m]
%                               Géométrie de la Voie Ferrée
drp=0.7175;%Position du rail+ % à l'axe de l'embankment [m]
Est=0.6;%Distance entre les traverses (Entraxe) [m]
Ltr=2.6;%Longueur d'une traverse [m]
%%%%%%%%%%%%%%%%%%%%%%%%%%%%%%%%%%%%%%%%%%%%%%%%%%%%%%%%%%%%%%%%%%%%%%%%
%                               Maillage du Modèle 3D
%%%%%%%%%%%%%%%%%%%%%%%%%%%%%%%%%%%%%%%%%%%%%%%%%%%%%%%%%%%%%%%%%%%%%%%%
%                               Maillage de l'Embankment-Sol
%Maillage suivant X [m]
Lz1xi=0.5;Lz1xf=0.5;%Suivant X (Passage des forces)
Lz2xf=1.0;%Suivant X (Zone de stabilisation)
%Maillage suivant Y [m]
Lz1yi=0.25;Lz1yf=0.25;%Suivant Y (Lateral Embankment)
Lz3yf=0.25;%Suivant Y (Lateral Embankment)
Lz9yf=0.5;%Suivant Y (Massif du sol)
%Maillage suivant Z [m]
Lz1zi=0.1;Lz1zf=0.1;%Suivant Z (Profondeur Embankment)
Lz5zf=0.4;%Suivant Z (Massif du sol)
%                               Maillage de la Voie Ferrée
Nes=4;%Nombre des EF par span []
Netc=3;%Nombre des EF par demi-partie centrale d'une traverse []
Nete=2;%Nombre des EF par partie extreme d'une traverse []
%%%%%%%%%%%%%%%%%%%%%%%%%%%%%%%%%%%%%%%%%%%%%%%%%%%%%%%%%%%%%%%%%%%%%%%%
%                               Paramètres Méca-Dynamiques du Modèle 3D
%%%%%%%%%%%%%%%%%%%%%%%%%%%%%%%%%%%%%%%%%%%%%%%%%%%%%%%%%%%%%%%%%%%%%%%%
%*****Rail en acier (Matériau élastique linéaire)*****
Er=2.1e11;%Module de Young [N/m^2]
nr=0.25;%Coefficient de Poisson []
ror=7897;%Densité [Kg/m^3]
Ar=6.5538e-3;%Aire de la section transversale [m^2]
Iiyr=1.2449e-5;%Moment d'inertie % y [m^4]
Iizr=4.5261e-6;%Moment d'inertie % z [m^4]
Iixr=1.6975e-5;%Moment d'inertie % x [m^4]
Dr=0.04;%Fraction de l'Amortissement Critique []
%*****Railpad (Matériau élastique linéaire)*****
K_RP=150e6;%Rigidité ponctuelle du Railpad (N/m)
%*****Traverses en Béton (Matériau élastique linéaire)*****
Esl=30e9;%Module de Young [N/m2]
nsl=0.25;%Coefficient de Poisson []
rosl=2395;%Densité [Kg/m^3]
Asl=4.8175e-2;%Aire de la section transversale [m^2]
Iiysl=1.6871e-4;%Moment d'inertie % y [m^4]
Iizsl=2.2170e-4;%Moment d'inertie % z [m^4]
Iixsl=3.9042e-4;%Moment d'inertie % x [m^4]

```

Matlab Code of the L-AMN Adaptive Meshing Scheme: 3D Finite Difference Modeling

```
Dsl=0.04;%Fraction de l'Amortissement Critique []
%*****Ballast (Matériau élastique linéaire)*****
Eb=130e6;%Module de Young [N/m^2]
nb=0.4;%Coefficient de Poisson []
rob=1600;%Densité [Kg/m^3]
Db=0.04;%Fraction de l'Amortissement Critique []
%*****Sub-Ballast (Matériau élastique linéaire)*****
Esb=80e6;%Module de Young [N/m^2]
nsb=0.4;%Coefficient de Poisson []
rosb=1600;%Densité [Kg/m^3]
Dsb=0.04;%Fraction de l'Amortissement Critique []
%*****Sol (Matériau élastique linéaire)*****
Es=25e6;%Module de Young [N/m^2]
ns=0.45;%Coefficient de Poisson []
ros=1800;%Densité [Kg/m^3]
Ds=0.01;%Fraction de l'Amortissement Critique []
%%%%%%%%%%%%%%%%%%%%%%%%%%%%%%%%%%%%%%%%%%%%%%%%%%%%%%%%%%%%%%%%%%%%%%%%%%%%%%
%
%          Fonction de Chargement P(t)=Pch*sin(-2*pi*f*t)
%%%%%%%%%%%%%%%%%%%%%%%%%%%%%%%%%%%%%%%%%%%%%%%%%%%%%%%%%%%%%%%%%%%%%%%%%%%%%%
Pch=100e3;%L'amplitude de chargement [N]
fch=10;%La fréquence de chargement [Hz]
V=300*10/36;%Vitesse de passage de la charge [m/s]
Nt=3;%Nombre des périodes de chargement
%%%%%%%%%%%%%%%%%%%%%%%%%%%%%%%%%%%%%%%%%%%%%%%%%%%%%%%%%%%%%%%%%%%%%%%%%%%%%%
%
%          Position des points de vérification
%%%%%%%%%%%%%%%%%%%%%%%%%%%%%%%%%%%%%%%%%%%%%%%%%%%%%%%%%%%%%%%%%%%%%%%%%%%%%%
Lb=1;%Distance entre les points 1 et 2 (simi. 3 et 4) [m]
Lec=3;%Distance entre les points 2 et 3 [m]
%%%%%%%%%%%%%%%%%%%%%%%%%%%%%%%%%%%%%%%%%%%%%%%%%%%%%%%%%%%%%%%%%%%%%%%%%%%%%%
%
%          Paramètres Numériques
%%%%%%%%%%%%%%%%%%%%%%%%%%%%%%%%%%%%%%%%%%%%%%%%%%%%%%%%%%%%%%%%%%%%%%%%%%%%%%
Mro=1e-5;%Ratio mécanique des forces non-équilibrées
sx=3;%Nombre des sous-intervalles spatiales dans chaque EF/rail
sv=50;%Nombre des sous-intervalles temporels dans chaque sous-inte. EF/rail
%%%%%%%%%%%%%%%%%%%%%%%%%%%%%%%%%%%%%%%%%%%%%%%%%%%%%%%%%%%%%%%%%%%%%%%%%%%%%%
%
%          Codage_Flac3D
%%%%%%%%%%%%%%%%%%%%%%%%%%%%%%%%%%%%%%%%%%%%%%%%%%%%%%%%%%%%%%%%%%%%%%%%%%%%%%
%Suppression des fichiers existantes
Ava_Calc
%Création des noeuds du modèle 3D
[Pz,Infz]=Const_Mod(Lm,lmd,Hm,Lc,le1d,le2d,he,Lz1xi,Lz1xf,Lz1yi,Lz1yf,Lz1zi
,Lz1zf,Lz2xf,Lz3yf,Lz5zf,Lz9yf);
%Ecriture du code
%Calcul des Contraintes Statiques dans le Modèle 3D
[Fo_Cont,delxa,Nrp,Nch,Nfch]=Codage(Pch,fch,V,Nt,sx,sv,Pz,Infz,hb,Lb,Lec,dr
p,ltr,Est,Nes,Netc,Nete,K_RP,Es1,nsl,rosl,Asl,Iiysl,Iizsl,Iixsl,Er,nr,ror,A
r,Iiyr,Iizr,Iixr,Es,ns,ros,Eb,nb,rob,Esb,nsb,rosb,Mro);
%Réponse Dynamique du Modèle 3D
Load_In(Fo_Cont,Pz,delxa,Nch,Nfch,V,Dr,Dsl,Db,Dsb,Es,ns,ros,fch,Ds,sv,sx);
Load_Apl(Er,nr,ror,Ar,Iixr,Iiyr,Iizr,Dr);
Fonc_Pass;
```

2. Function 1: Const_Mod

```

function [Pz, Infz]=Const_Mod(Lm, lmd, Hm, Lc, le1d, le2d, he, Lz1xi, Lz1xf,
Lz1yi, Lz1yf, Lz1zi, Lz1zf, Lz2xf, Lz3yf, Lz5zf, Lz9yf)
lm=2*lmd; le1=2*le1d; le2=2*le2d;
%Déclaration des matrices
Pz1=zeros(4,3);Pz2=zeros(4,3);
Pz3=zeros(4,3);Pz4=zeros(4,3);
Pz5=zeros(4,3);Pz6=zeros(4,3);
Pz7=zeros(4,3);Pz8=zeros(4,3);
Pz9=zeros(4,3);Pz10=zeros(4,3);
Infz1=zeros(3,2);Infz2=zeros(3,2);
Infz3=zeros(3,2);Infz4=zeros(3,2);
Infz5=zeros(3,2);Infz6=zeros(3,2);
Infz7=zeros(3,2);Infz8=zeros(3,2);
Infz9=zeros(3,2);Infz10=zeros(3,2);
Pz=zeros(4,3,10);Infz=zeros(3,2,10);
%Zone 1:Brick mesh
[nz1x, rz1x, Ltz1x, ~]=Maillage((Lc/2), Lz1xi, Lz1xf);
[nz1y, rz1y, Ltz1y, ~]=Maillage((le2/2), Lz1yi, Lz1yf);
[nz1z, rz1z, Ltz1z, ~]=Maillage(he, Lz1zi, Lz1zf);
Pz1(1,1)=0;Pz1(1,2)=0;Pz1(1,3)=0;
Pz1(2,1)=0;Pz1(2,2)=Ltz1y;Pz1(2,3)=0;
Pz1(3,1)=Ltz1x;Pz1(3,2)=0;Pz1(3,3)=0;
Pz1(4,1)=0;Pz1(4,2)=0;Pz1(4,3)=-Ltz1z;
Infz1(1,1)=nz1y;Infz1(1,2)=rz1y;
Infz1(2,1)=nz1x;Infz1(2,2)=rz1x;
Infz1(3,1)=nz1z;Infz1(3,2)=rz1z;
%Zone 2:Brick mesh
[nz2x, rz2x, Ltz2x, ~]=Maillage((Lm-Lc)/2, Lz1xf, Lz2xf);
Pz2(1,1)=Ltz1x;Pz2(1,2)=0;Pz2(1,3)=0;
Pz2(2,1)=Ltz1x;Pz2(2,2)=Ltz1y;Pz2(2,3)=0;
Pz2(3,1)=Ltz1x+Ltz2x;Pz2(3,2)=0;Pz2(3,3)=0;
Pz2(4,1)=Ltz1x;Pz2(4,2)=0;Pz2(4,3)=-Ltz1z;
Infz2(1,1)=nz1y;Infz2(1,2)=rz1y;
Infz2(2,1)=nz2x;Infz2(2,2)=rz2x;
Infz2(3,1)=nz1z;Infz2(3,2)=rz1z;
%Zone 3:Wedge mesh
[nz3y, rz3y, Ltz3y, ~]=Maillage((le1-le2)/2, Lz1yf, Lz3yf);
Pz3(1,1)=0;Pz3(1,2)=Ltz1y;Pz3(1,3)=-Ltz1z;
Pz3(2,1)=0;Pz3(2,2)=Ltz1y;Pz3(2,3)=0;
Pz3(3,1)=Ltz1x;Pz3(3,2)=Ltz1y;Pz3(3,3)=-Ltz1z;
Pz3(4,1)=0;Pz3(4,2)=Ltz1y+Ltz3y;Pz3(4,3)=-Ltz1z;
Infz3(1,1)=nz1z;Infz3(1,2)=rz1z;
Infz3(2,1)=nz1x;Infz3(2,2)=rz1x;
Infz3(3,1)=nz3y;Infz3(3,2)=rz3y;
%Zone 4:Wedge mesh
Pz4(1,1)=Ltz1x;Pz4(1,2)=Ltz1y;Pz4(1,3)=-Ltz1z;
Pz4(2,1)=Ltz1x;Pz4(2,2)=Ltz1y;Pz4(2,3)=0;
Pz4(3,1)=Ltz1x+Ltz2x;Pz4(3,2)=Ltz1y;Pz4(3,3)=-Ltz1z;
Pz4(4,1)=Ltz1x;Pz4(4,2)=Ltz1y+Ltz3y;Pz4(4,3)=-Ltz1z;
Infz4(1,1)=nz1z;Infz4(1,2)=rz1z;
Infz4(2,1)=nz2x;Infz4(2,2)=rz2x;
Infz4(3,1)=nz3y;Infz4(3,2)=rz3y;
%Zone 5:Brick mesh
[nz5z, rz5z, Ltz5z, ~]=Maillage(Hm, Lz1zf, Lz5zf);

```

Matlab Code of the L-AMN Adaptive Meshing Scheme: 3D Finite Difference Modeling

```
Pz5(1,1)=0;Pz5(1,2)=0;Pz5(1,3)=-Ltz1z;
Pz5(2,1)=0;Pz5(2,2)=Ltz1y;Pz5(2,3)=-Ltz1z;
Pz5(3,1)=Ltz1x;Pz5(3,2)=0;Pz5(3,3)=-Ltz1z;
Pz5(4,1)=0;Pz5(4,2)=0;Pz5(4,3)=-Ltz1z-Ltz5z;
Infz5(1,1)=nz1y;Infz5(1,2)=rz1y;
Infz5(2,1)=nz1x;Infz5(2,2)=rz1x;
Infz5(3,1)=nz5z;Infz5(3,2)=rz5z;
%Zone 6:Brick mesh
Pz6(1,1)=Ltz1x;Pz6(1,2)=0;Pz6(1,3)=-Ltz1z;
Pz6(2,1)=Ltz1x;Pz6(2,2)=Ltz1y;Pz6(2,3)=-Ltz1z;
Pz6(3,1)=Ltz1x+Ltz2x;Pz6(3,2)=0;Pz6(3,3)=-Ltz1z;
Pz6(4,1)=Ltz1x;Pz6(4,2)=0;Pz6(4,3)=-Ltz1z-Ltz5z;
Infz6(1,1)=nz1y;Infz6(1,2)=rz1y;
Infz6(2,1)=nz2x;Infz6(2,2)=rz2x;
Infz6(3,1)=nz5z;Infz6(3,2)=rz5z;
%Zone 7:Brick mesh
Pz7(1,1)=0;Pz7(1,2)=Ltz1y;Pz7(1,3)=-Ltz1z;
Pz7(2,1)=0;Pz7(2,2)=Ltz1y+Ltz3y;Pz7(2,3)=-Ltz1z;
Pz7(3,1)=Ltz1x;Pz7(3,2)=Ltz1y;Pz7(3,3)=-Ltz1z;
Pz7(4,1)=0;Pz7(4,2)=Ltz1y;Pz7(4,3)=-Ltz1z-Ltz5z;
Infz7(1,1)=nz3y;Infz7(1,2)=rz3y;
Infz7(2,1)=nz1x;Infz7(2,2)=rz1x;
Infz7(3,1)=nz5z;Infz7(3,2)=rz5z;
%Zone 8:Brick mesh
Pz8(1,1)=Ltz1x;Pz8(1,2)=Ltz1y;Pz8(1,3)=-Ltz1z;
Pz8(2,1)=Ltz1x;Pz8(2,2)=Ltz1y+Ltz3y;Pz8(2,3)=-Ltz1z;
Pz8(3,1)=Ltz1x+Ltz2x;Pz8(3,2)=Ltz1y;Pz8(3,3)=-Ltz1z;
Pz8(4,1)=Ltz1x;Pz8(4,2)=Ltz1y;Pz8(4,3)=-Ltz1z-Ltz5z;
Infz8(1,1)=nz3y;Infz8(1,2)=rz3y;
Infz8(2,1)=nz2x;Infz8(2,2)=rz2x;
Infz8(3,1)=nz5z;Infz8(3,2)=rz5z;
%Zone 9:Brick mesh
[nz9y,rz9y,Ltz9y,~]=Maillage((lm-le1)/2,Lz3yf,Lz9yf);
Pz9(1,1)=0;Pz9(1,2)=Ltz1y+Ltz3y;Pz9(1,3)=-Ltz1z;
Pz9(2,1)=0;Pz9(2,2)=Ltz1y+Ltz3y+Ltz9y;Pz9(2,3)=-Ltz1z;
Pz9(3,1)=Ltz1x;Pz9(3,2)=Ltz1y+Ltz3y;Pz9(3,3)=-Ltz1z;
Pz9(4,1)=0;Pz9(4,2)=Ltz1y+Ltz3y;Pz9(4,3)=-Ltz1z-Ltz5z;
Infz9(1,1)=nz9y;Infz9(1,2)=rz9y;
Infz9(2,1)=nz1x;Infz9(2,2)=rz1x;
Infz9(3,1)=nz5z;Infz9(3,2)=rz5z;
%Zone 10:Brick mesh
Pz10(1,1)=Ltz1x;Pz10(1,2)=Ltz1y+Ltz3y;Pz10(1,3)=-Ltz1z;
Pz10(2,1)=Ltz1x;Pz10(2,2)=Ltz1y+Ltz3y+Ltz9y;Pz10(2,3)=-Ltz1z;
Pz10(3,1)=Ltz1x+Ltz2x;Pz10(3,2)=Ltz1y+Ltz3y;Pz10(3,3)=-Ltz1z;
Pz10(4,1)=Ltz1x;Pz10(4,2)=Ltz1y+Ltz3y;Pz10(4,3)=-Ltz1z-Ltz5z;
Infz10(1,1)=nz9y;Infz10(1,2)=rz9y;
Infz10(2,1)=nz2x;Infz10(2,2)=rz2x;
Infz10(3,1)=nz5z;Infz10(3,2)=rz5z;
%Output
for i=1:4
    for j=1:3
        Pz(i,j,1)=Pz1(i,j);Pz(i,j,2)=Pz2(i,j);Pz(i,j,3)=Pz3(i,j);
        Pz(i,j,4)=Pz4(i,j);Pz(i,j,5)=Pz5(i,j);Pz(i,j,6)=Pz6(i,j);
        Pz(i,j,7)=Pz7(i,j);Pz(i,j,8)=Pz8(i,j);Pz(i,j,9)=Pz9(i,j);
        Pz(i,j,10)=Pz10(i,j);
    end
end
```

```

end
for i=1:3
    for j=1:2

Infz (i, j, 1)=Infz1 (i, j); Infz (i, j, 2)=Infz2 (i, j); Infz (i, j, 3)=Infz3 (i, j)
;

Infz (i, j, 4)=Infz4 (i, j); Infz (i, j, 5)=Infz5 (i, j); Infz (i, j, 6)=Infz6 (i, j)
;

Infz (i, j, 7)=Infz7 (i, j); Infz (i, j, 8)=Infz8 (i, j); Infz (i, j, 9)=Infz9 (i, j)
;
        Infz (i, j, 10)=Infz10 (i, j);
    end
end
end

```

3. Function 2 : Codage

```

function [Fo_Cont, delxa, Nrp, Nch, Nfch]=Codage (Pch, fch, V, Nt, sx, sv, Pz,
Infz, hb, Lb, Lec, drp, Ltr, Est, Nes, Netc, Nete, K_RP, Esl, nsl, rosl, Asl, Iiysl
,
Iizsl, Iixsl, Er, nr, ror, Ar, Iiyr, Iizr, Iixr, Es, ns, ros, Eb, nb, rob, Esb, nsb,
rosb, Mro)
%Cette fonction permet d'initialiser les contraintes (sous
chargement
%statique) dans le modèle d'interaction TGV-Voie-Sol
ID0s = fopen('Sol.txt', 'w');
ID0r = fopen('Rail.txt', 'w');
ID1 = fopen('Model_Stat.txt', 'w');
%*****
*****
%Calcul des Contraintes Initiales dans le Sol+Embankment
%*****
*****
%Génération du Maillage
fprintf(ID0s, ';Generation du Maillage\r\n');
fprintf(ID0s, ';Zone1\r\n');
fprintf(ID0s, 'gen zone brick p0(%f,%f,%f) p1(%f,%f,%f) p2(%f,%f,%f)
p3(%f,%f,%f) &\r\n
', Pz (1, 1, 1), Pz (1, 2, 1), Pz (1, 3, 1), Pz (2, 1, 1), Pz (2, 2, 1), Pz (2, 3, 1), Pz (3, 1
, 1), Pz (3, 2, 1), Pz (3, 3, 1), Pz (4, 1, 1), Pz (4, 2, 1), Pz (4, 3, 1));
fprintf(ID0s, 'size %d %d %d rat %f %f
%f', Infz (1, 1, 1), Infz (2, 1, 1), Infz (3, 1, 1), Infz (1, 2, 1), Infz (2, 2, 1), Infz
(3, 2, 1));
fprintf(ID0s, '\r\n');
fprintf(ID0s, ';Zone2\r\n');
fprintf(ID0s, 'gen zone brick p0(%f,%f,%f) p1(%f,%f,%f) p2(%f,%f,%f)
p3(%f,%f,%f) &\r\n
', Pz (1, 1, 2), Pz (1, 2, 2), Pz (1, 3, 2), Pz (2, 1, 2), Pz (2, 2, 2), Pz (2, 3, 2), Pz (3, 1
, 2), Pz (3, 2, 2), Pz (3, 3, 2), Pz (4, 1, 2), Pz (4, 2, 2), Pz (4, 3, 2));
fprintf(ID0s, 'size %d %d %d rat %f %f
%f', Infz (1, 1, 2), Infz (2, 1, 2), Infz (3, 1, 2), Infz (1, 2, 2), Infz (2, 2, 2), Infz
(3, 2, 2));
fprintf(ID0s, '\r\n');
fprintf(ID0s, ';Zone3\r\n');

```

```

fprintf(ID0s, 'gen zone wedge p0(%f,%f,%f) p1(%f,%f,%f) p2(%f,%f,%f)
p3(%f,%f,%f) &\r\n
', Pz(1,1,3), Pz(1,2,3), Pz(1,3,3), Pz(2,1,3), Pz(2,2,3), Pz(2,3,3), Pz(3,1
,3), Pz(3,2,3), Pz(3,3,3), Pz(4,1,3), Pz(4,2,3), Pz(4,3,3));
fprintf(ID0s, 'size %d %d %d rat %f %f
%f', Infz(1,1,3), Infz(2,1,3), Infz(3,1,3), Infz(1,2,3), Infz(2,2,3), Infz
(3,2,3));
fprintf(ID0s, '\r\n');
fprintf(ID0s, ';Zone4\r\n');
fprintf(ID0s, 'gen zone wedge p0(%f,%f,%f) p1(%f,%f,%f) p2(%f,%f,%f)
p3(%f,%f,%f) &\r\n
', Pz(1,1,4), Pz(1,2,4), Pz(1,3,4), Pz(2,1,4), Pz(2,2,4), Pz(2,3,4), Pz(3,1
,4), Pz(3,2,4), Pz(3,3,4), Pz(4,1,4), Pz(4,2,4), Pz(4,3,4));
fprintf(ID0s, 'size %d %d %d rat %f %f
%f', Infz(1,1,4), Infz(2,1,4), Infz(3,1,4), Infz(1,2,4), Infz(2,2,4), Infz
(3,2,4));
fprintf(ID0s, '\r\n');
fprintf(ID0s, ';Zone5\r\n');
fprintf(ID0s, 'gen zone brick p0(%f,%f,%f) p1(%f,%f,%f) p2(%f,%f,%f)
p3(%f,%f,%f) &\r\n
', Pz(1,1,5), Pz(1,2,5), Pz(1,3,5), Pz(2,1,5), Pz(2,2,5), Pz(2,3,5), Pz(3,1
,5), Pz(3,2,5), Pz(3,3,5), Pz(4,1,5), Pz(4,2,5), Pz(4,3,5));
fprintf(ID0s, 'size %d %d %d rat %f %f
%f', Infz(1,1,5), Infz(2,1,5), Infz(3,1,5), Infz(1,2,5), Infz(2,2,5), Infz
(3,2,5));
fprintf(ID0s, '\r\n');
fprintf(ID0s, ';Zone6\r\n');
fprintf(ID0s, 'gen zone brick p0(%f,%f,%f) p1(%f,%f,%f) p2(%f,%f,%f)
p3(%f,%f,%f) &\r\n
', Pz(1,1,6), Pz(1,2,6), Pz(1,3,6), Pz(2,1,6), Pz(2,2,6), Pz(2,3,6), Pz(3,1
,6), Pz(3,2,6), Pz(3,3,6), Pz(4,1,6), Pz(4,2,6), Pz(4,3,6));
fprintf(ID0s, 'size %d %d %d rat %f %f
%f', Infz(1,1,6), Infz(2,1,6), Infz(3,1,6), Infz(1,2,6), Infz(2,2,6), Infz
(3,2,6));
fprintf(ID0s, '\r\n');
fprintf(ID0s, ';Zone7\r\n');
fprintf(ID0s, 'gen zone brick p0(%f,%f,%f) p1(%f,%f,%f) p2(%f,%f,%f)
p3(%f,%f,%f) &\r\n
', Pz(1,1,7), Pz(1,2,7), Pz(1,3,7), Pz(2,1,7), Pz(2,2,7), Pz(2,3,7), Pz(3,1
,7), Pz(3,2,7), Pz(3,3,7), Pz(4,1,7), Pz(4,2,7), Pz(4,3,7));
fprintf(ID0s, 'size %d %d %d rat %f %f
%f', Infz(1,1,7), Infz(2,1,7), Infz(3,1,7), Infz(1,2,7), Infz(2,2,7), Infz
(3,2,7));
fprintf(ID0s, '\r\n');
fprintf(ID0s, ';Zone8\r\n');
fprintf(ID0s, 'gen zone brick p0(%f,%f,%f) p1(%f,%f,%f) p2(%f,%f,%f)
p3(%f,%f,%f) &\r\n
', Pz(1,1,8), Pz(1,2,8), Pz(1,3,8), Pz(2,1,8), Pz(2,2,8), Pz(2,3,8), Pz(3,1
,8), Pz(3,2,8), Pz(3,3,8), Pz(4,1,8), Pz(4,2,8), Pz(4,3,8));
fprintf(ID0s, 'size %d %d %d rat %f %f
%f', Infz(1,1,8), Infz(2,1,8), Infz(3,1,8), Infz(1,2,8), Infz(2,2,8), Infz
(3,2,8));
fprintf(ID0s, '\r\n');
fprintf(ID0s, ';Zone9\r\n');
fprintf(ID0s, 'gen zone brick p0(%f,%f,%f) p1(%f,%f,%f) p2(%f,%f,%f)
p3(%f,%f,%f) &\r\n

```

Matlab Code of the L-AMN Adaptive Meshing Scheme: 3D Finite Difference Modeling

```

',Pz(1,1,9),Pz(1,2,9),Pz(1,3,9),Pz(2,1,9),Pz(2,2,9),Pz(2,3,9),Pz(3,1
,9),Pz(3,2,9),Pz(3,3,9),Pz(4,1,9),Pz(4,2,9),Pz(4,3,9));
fprintf(ID0s,'size %d %d %d rat %f %f
%f',Infz(1,1,9),Infz(2,1,9),Infz(3,1,9),Infz(1,2,9),Infz(2,2,9),Infz
(3,2,9));
fprintf(ID0s,'\r\n');
fprintf(ID0s,';Zone10\r\n');
fprintf(ID0s,'gen zone brick p0(%f,%f,%f) p1(%f,%f,%f) p2(%f,%f,%f)
p3(%f,%f,%f) &\r\n
',Pz(1,1,10),Pz(1,2,10),Pz(1,3,10),Pz(2,1,10),Pz(2,2,10),Pz(2,3,10),
Pz(3,1,10),Pz(3,2,10),Pz(3,3,10),Pz(4,1,10),Pz(4,2,10),Pz(4,3,10));
fprintf(ID0s,'size %d %d %d rat %f %f
%f',Infz(1,1,10),Infz(2,1,10),Infz(3,1,10),Infz(1,2,10),Infz(2,2,10)
,Infz(3,2,10));
fprintf(ID0s,'\r\n');
fprintf(ID0s,';Reflexion\r\n');
fprintf(ID0s,'gen zone reflect normal -1 0 0\r\n');
fprintf(ID0s,'group Ballast range z %f 0\r\n',-hb);
fprintf(ID0s,'group Subballast range z %f %f\r\n',Pz(4,3,1),-hb);
fprintf(ID0s,'group Sol range z %f %f\r\n',Pz(4,3,5),Pz(4,3,1));
fprintf(ID0s,'attach face range z %f 0\r\n',Pz(4,3,5));
fprintf(ID0s,';Propriétés mécaniques du Ballast,Sub-Ballast et du
Sol\r\n');
fprintf(ID0s,'model elas range group Ballast\r\n');
fprintf(ID0s,'prop bulk %f shear %f range group
Ballast\r\n',Eb/(3*(1-2*nb)),Eb/(2*(1+nb)));
fprintf(ID0s,'ini dens %f range group Ballast\r\n',rob);
fprintf(ID0s,'model elas range group Subballast\r\n');
fprintf(ID0s,'prop bulk %f shear %f range group
Subballast\r\n',Esb/(3*(1-2*nsb)),Esb/(2*(1+nsb)));
fprintf(ID0s,'ini dens %f range group Subballast\r\n',rosb);
fprintf(ID0s,'model elas range group Sol\r\n');
fprintf(ID0s,'prop bulk %f shear %f range group Sol\r\n',Es/(3*(1-
2*ns)),Es/(2*(1+ns)));
fprintf(ID0s,'ini dens %f range group Sol\r\n',ros);
%Conditions aux limites
fprintf(ID0s,';Les conditions aux limites\r\n');
fprintf(ID0s,'fix x y z range z=(%f,%f)\r\n',Pz(4,3,5)-
0.1,Pz(4,3,5)+0.1);
fprintf(ID0s,'fix x range x=(%f,%f)\r\n',Pz(3,1,2)-
0.1,Pz(3,1,2)+0.1);
fprintf(ID0s,'fix x range x=(%f,%f)\r\n',-Pz(3,1,2)-0.1,-
Pz(3,1,2)+0.1);
fprintf(ID0s,'fix y range y=(%f,%f)\r\n',Pz(2,2,9)-
0.1,Pz(2,2,9)+0.1);
fprintf(ID0s,'fix y range y=(-0.1,0.1)\r\n');
%Calcul0: Contraintes Initiales sous Poids Propre dans le sol
%*****
fprintf(ID0s,';Calcul des contraintes initiales dans le sol\r\n');
fprintf(ID0s,'set gravity=(0,0,-9.81)\r\n');
fprintf(ID0s,'set mech damp comb\r\n');
fprintf(ID0s,'solve rat %2.10f\r\n',Mro);
fprintf(ID0s,'save Sol_Cont0.sav\r\n');
fclose(ID0s);

```

Matlab Code of the L-AMN Adaptive Meshing Scheme: 3D Finite Difference Modeling

```

%*****
*****
%Génération de la Voie Ferrée
%*****
*****
iid=2;
fprintf(ID0r, ';La Voie Ferrée\r\n');
Nef=round(2*Pz(3,1,2)/(Est/Nes));%Nombre des EFs/rail
delx=(2*Pz(3,1,2)/Nef);%Taille des EFs/rail
delxa=round((2*Pz(3,1,2)/Nef)*10^6)*10^-6;%Taille arrondie des
EFs/rail
%Création des Parties Centrales des traverses (Eléments structuraux)
fprintf(ID0r, 'sel beam id=1 begin=(%f,%f,5) end=(%f,%f,5)
nseg=%d\r\n',-Pz(3,1,2),drp,-Pz(3,1,2),0,Netc);
for i=2:Nef+1%Boucle sur le nombre des noeuds
    if rem(i-1,Nes)==0
        fprintf(ID0r, 'sel beam id=1 begin=(%f,%f,5) end=(%f,%f,5)
nseg=%d\r\n',-Pz(3,1,2)+(i-1)*delx,drp,-Pz(3,1,2)+(i-
1)*delx,0,Netc);
        iid=iid+1;
    end
end
Ntra=iid-1;%Nombre total des traverses
%Création des rails (Eléments structuraux)
fprintf(ID0r, 'sel beam id=2 begin=(%f,%f,5) end=(%f,%f,5)
nseg=%d\r\n',-Pz(3,1,2),drp,Pz(3,1,2),drp,Nef);
%Création des Parties Extrêmes des traverses (Eléments structuraux)
fprintf(ID0r, 'sel beam id=1 begin=(%f,%f,5) end=(%f,%f,5)
nseg=%d\r\n',-Pz(3,1,2),(Ltr/2),-Pz(3,1,2),drp,Nete);
for i=2:Nef+1%Boucle sur le nombre des noeuds
    if rem(i-1,Nes)==0
        fprintf(ID0r, 'sel beam id=1 begin=(%f,%f,5) end=(%f,%f,5)
nseg=%d\r\n',-Pz(3,1,2)+(i-1)*delx,(Ltr/2),-Pz(3,1,2)+(i-
1)*delx,drp,Nete);
    end
end
fprintf(ID0r, 'sel link attach xd rigid\r\n');fprintf(ID0r, 'sel link
attach xr rigid\r\n');
fprintf(ID0r, 'sel link attach yd rigid\r\n');fprintf(ID0r, 'sel link
attach yr rigid\r\n');
fprintf(ID0r, 'sel link attach zd rigid\r\n');fprintf(ID0r, 'sel link
attach zr rigid\r\n');
%Numérotation/Coordonnée spatiale x des Noeuds des rails
Nrp=zeros(Nef+1,2);
%Noeud de départ rail+/rail-
Nrp(1,1)=Ntra*(Netc+1)+1;
%Noeud final rail+/rail-
Nrp(Nef+1,1)=Nrp(1,1)+1;
%Noeud 2 rail+/rail-
Nrp(2,1)=Nrp(Nef+1,1)+1;
for i=3:Nef
    Nrp(i,1)=Nrp(i-1,1)+1;
end
Nrp(1,2)=-Pz(3,1,2);
for i=2:Nef+1
    Nrp(i,2)=Nrp(i-1,2)+delx;

```

```

end
%Liaisons entre les noeuds à l'interface rail-traverse (Railpad)
NNLp=zeros(Ntra,2);
%Numéro des noeuds-Traverses
NNLp(1,1)=1;
for i=2:Ntra
    NNLp(i,1)=NNLp(i-1,1)+Netc+1;
end
%Numéro des noeuds-Rails
NNLp(1,2)=Ntra*(Netc+1)+1;%Noeud de départ rail+
NNLp(2,2)=Ntra*(Netc+1)+1+1+Nes;
for i=3:Ntra-1
    NNLp(i,2)=NNLp(i-1,2)+Nes;
end
if rem(Nef,Nes)==0
NNLp(Ntra,2)=Ntra*(Netc+1)+1+1;
else
    NNLp(Ntra,2)=NNLp(Ntra-1,2)+Nes;
end
%Noeuds IRT_Rp_Traverse
faNtp=fopen('IRT_Nt_p.his','w');
fprintf(faNtp,'Numero_Noeuds_tra_railp\r\n');
fprintf(faNtp,'%d\t%d\r\n',Ntra,1);
for i=1:Ntra
    fprintf(faNtp,'%d\r\n',NNLp(i,1));
end
fclose(faNtp);
fprintf(ID0r,'table 18 read IRT_Nt_p.his\r\n');
%Noeuds IRT_Rp_Rail
faNrp=fopen('IRT_Nr_p.his','w');
fprintf(faNrp,'Numero_Noeuds_rai_railp\r\n');
fprintf(faNrp,'%d\t%d\r\n',Ntra,1);
for i=1:Ntra
    fprintf(faNrp,'%d\r\n',NNLp(i,2));
end
fclose(faNrp);
fprintf(ID0r,'table 19 read IRT_Nr_p.his\r\n');
fprintf(ID0r,';Liaison Rail-Traverse\r\n');
fprintf(ID0r,'def Lai_IRT\r\n');
fprintf(ID0r,'loop ili (1,%d)\r\n',Ntra);
fprintf(ID0r,'idp=ili\r\n');
fprintf(ID0r,'Nsp=ytable(18,ili)\r\n');fprintf(ID0r,'Ntp=ytable(19,i
li)\r\n');
fprintf(ID0r,'command\r\n');
fprintf(ID0r,'sel link id=idp Nsp tar node tgt=Ntp\r\n');
fprintf(ID0r,'endcommand\r\n');
fprintf(ID0r,'end_loop\r\n');
fprintf(ID0r,'end\r\n');
fprintf(ID0r,'Lai_IRT\r\n');
fprintf(ID0r,'sel link attach zdirection lindeform\r\n');
fprintf(ID0r,'sel link constit lindeform 3 a=1 k=%f\r\n',K_RP);
fprintf(ID0r,';Propriétés méca des traverses\r\n');
fprintf(ID0r,'sel beam id=1 property d=%f e=%f n=%f xca=%2.8f
xcj=%2.8f xciy=%2.8f
xciz=%2.8f\r\n',rosl,Esl,nsl,Asl,Iixsl,Iiysl,Iizsl);
fprintf(ID0r,';Propriétés méca des rails\r\n');

```

Matlab Code of the L-AMN Adaptive Meshing Scheme: 3D Finite Difference Modeling

```
fprintf(ID0r,'sel beam id=2 property d=%f e=%f n=%f xca=%2.8f
xcj=%2.8f xcij=%2.8f xciz=%2.8f\r\n',ror,Er,nr,Ar,Iixr,IiyR,Iizr);
fclose(ID0r);
*****
%*****
*****
%Calcul1: Contraintes Initiales sous Poids Propre Sol-Voie
%*****
*****
fprintf(ID1,'N\r\n');
fprintf(ID1,'call Sol.txt\r\n');
fprintf(ID1,'call Rail.txt\r\n');
fprintf(ID1,'solve rat %2.10f\r\n',Mro/10);
fprintf(ID1,'save Sol_Voie_Cont0.sav\r\n');
fprintf(ID1,'plot block group lgra w br\r\n');
fprintf(ID1,'plot add sel geom red red id=off cid=off node=off
beam=on scale=0.05\r\n');
fprintf(ID1,'plot add axes\r\n');
fclose(ID1);
%*****
*****
%Application statique des charges à l'interface Roue-Rail
%*****
*****
ID2=fopen('App_Stat_Cha.txt','w');
fprintf(ID2,'sel node apply system global\r\n');
%Numéro des Noeuds Chargés
Lpa=(Nt/fch)*V;
dell=zeros(Nef+1,2);
%Noeuds chargés_Essieu 1
for i=1:Nef+1%Boucle sur le nombre des noeuds/rail
    dell(i,1)=abs(Nrp(i,2)-(-Lpa/2));%borne gauche
    dell(i,2)=abs(Nrp(i,2)-(Lpa/2));%borne droite
end
i1=find(dell(:,1)==min(dell(:,1)));d1=i1;
i2=find(dell(:,2)==min(dell(:,2)));d2=i2;
if length(d1)==1
    bg=d1;
else
    bg=d1(1,1);
end
if length(d2)==1
    bd=d2;
else
    bd=d2(1,1);
end
Nfch=bd-bg;%Nombre des noeuds chargés
Nch=zeros(Nfch,1,4);%Numéros des noeuds chargés rail+/rail-
for i=bg:bd-1
    Nch(i-bg+1,1,1)=Nrp(i,1);%Numéro des noeuds chargés/rail+
end
%Noeuds chargés_Essieu 2
for i=1:Nef+1%Boucle sur le nombre des noeuds/rail
    dell(i,1)=abs(Nrp(i,2)-(Nrp(bg,2)-Lb));%borne gauche
end
ile2=find(dell(:,1)==min(dell(:,1)));d1e2=ile2;
```

```

if length(d1e2)==1
    bg2=d1e2;
else
    bg2=d1e2(1,1);
end
for i=1:Nfch
    Nch(i,1,2)=Nrp(bg2-1+i,1);%Numéro des noeuds chargés/rail+
end
%Noeuds chargés_Essieu 3
for i=1:Nef+1%Boucle sur le nombre des noeuds/rail
    del1(i,1)=abs(Nrp(i,2)-(Nrp(bg2,2)-Lec));%borne gauche
end
ile3=find(del1(:,1)==min(del1(:,1)));d1e3=ile3;
if length(d1e3)==1
    bg3=d1e3;
else
    bg3=d1e3(1,1);
end
for i=1:Nfch
    Nch(i,1,3)=Nrp(bg3-1+i,1);%Numéro des noeuds chargés/rail+
end
%Noeuds chargés_Essieu 4
for i=1:Nef+1%Boucle sur le nombre des noeuds/rail
    del1(i,1)=abs(Nrp(i,2)-(Nrp(bg3,2)-Lb));%borne gauche
end
ile4=find(del1(:,1)==min(del1(:,1)));d1e4=ile4;
if length(d1e4)==1
    bg4=d1e4;
else
    bg4=d1e4(1,1);
end
for i=1:Nfch
    Nch(i,1,4)=Nrp(bg4-1+i,1);%Numéro des noeuds chargés/rail+
end
%Création du fichier de chargement
[Fo_Cont]=Fonc_Char(Pch,fch,V,sx,sv,Nfch,delxa);
%Application Statique des charges
fprintf(ID2,'sel node apply fo 0 0 %f ra id %d\r\n',-
Fo_Cont(1,2),Nch(1,1,1));
fprintf(ID2,'sel node apply fo 0 0 %f ra id %d\r\n',-
Fo_Cont(1,3),Nch(1,1,2));
fprintf(ID2,'sel node apply fo 0 0 %f ra id %d\r\n',-
Fo_Cont(1,4),Nch(1,1,3));
fprintf(ID2,'sel node apply fo 0 0 %f ra id %d\r\n',-
Fo_Cont(1,5),Nch(1,1,4));
%*****
*****
%Calcul2: Contraintes Initiales dans le Modèle d'Interaction
%*****
*****
fprintf(ID2,'solve rat %2.10f\r\n',Mro/10);
fprintf(ID2,'sel node apply remove force\r\n');
fprintf(ID2,'save Modele_Statique.sav\r\n');
fclose(ID2);
end

```

4. Function 3: Load_In

```

function []=Load_In(Fo_Cont,Pz,delxa,Nch,Nfch,V,Dr,Dsl,Db,Dsb,Es,ns,
ros,fch,Ds,sv,sx)
%Cette fonction sert à créer le code FLAC3D qui permet de modéliser
la
%réponse dynamique du modèle d'interaction sous charges mobiles
(TGV)
ID3=fopen('Model_Dyn.txt','w');
fprintf(ID3,'N\r\n');
fprintf(ID3,'restor Sol_Voie_Cont0.sav\r\n');
fprintf(ID3,'call App_Stat_Cha.txt\r\n');
fprintf(ID3,'conf dy\r\n');
fprintf(ID3,'set dyn=on\r\n');
fprintf(ID3,'ini stat 0\r\n');%Impossible d'avoir des zones
plastiques
fprintf(ID3,'ini xdisp=0 ydisp=0 zdisp=0\r\n');
fprintf(ID3,'ini xv=0 yv=0 zv=0\r\n');
fprintf(ID3,'sel node init xdisp=0 ydisp=0 zdisp=0\r\n');
fprintf(ID3,'sel node init xvel=0 yvel=0 zvel=0\r\n');
fprintf(ID3,'sel node apply system global\r\n');
Nb_d=length(Fo_Cont(:,1));%Longueur du fichier de chargement
Dst=Fo_Cont(2,1)-Fo_Cont(1,1);%Ecart entre 2 points de chargement
[m]
Tst=floor((delxa/V)*10^7)*10^-7;%Temps nécessaire pour traverser un
EF
fprintf(ID3,';Conditions aux Limites\r\n');
fprintf(ID3,'free x range x=(%f,%f)\r\n',Pz(3,1,2)-
0.1,Pz(3,1,2)+0.1);
fprintf(ID3,'free x range x=(%f,%f)\r\n',-Pz(3,1,2)-0.1,-
Pz(3,1,2)+0.1);
fprintf(ID3,'free y range y=(%f,%f)\r\n',Pz(2,2,9)-
0.1,Pz(2,2,9)+0.1);
fprintf(ID3,'fix y range y=(-0.1,0.1)\r\n');
fprintf(ID3,';Quiet Boundary\r\n');
fprintf(ID3,'apply nquiet squiet dquiet ran x %f %f z %f
%f\r\n',Pz(3,1,2)-0.1,Pz(3,1,2)+0.1,Pz(4,3,5),Pz(4,3,1));
fprintf(ID3,'apply nquiet squiet dquiet ran x %f %f z %f %f\r\n',-
Pz(3,1,2)-0.1,-Pz(3,1,2)+0.1,Pz(4,3,5),Pz(4,3,1));
fprintf(ID3,'apply nquiet squiet dquiet ran y %f %f z %f
%f\r\n',Pz(2,2,9)-0.1,Pz(2,2,9)+0.1,Pz(4,3,5),Pz(4,3,1));
%fprintf(ID3,'apply nquiet squiet dquiet ran y %f %f z %f
%f\r\n',-Pz(2,2,9)-0.1,-Pz(2,2,9)+0.1,Pz(4,3,5),Pz(4,3,1));
fprintf(ID3,';apply ff\r\n');
fprintf(ID3,';Amortissement des matériaux\r\n');
fprintf(ID3,'sel set damp=local %f ra selt beam id 1\r\n',Dsl*pi());
fprintf(ID3,'sel set damp=local %f ra selt beam id 2\r\n',Dr*pi());
fprintf(ID3,'ini damp=local %f rang group Ballast\r\n',Db*pi());
fprintf(ID3,'ini damp=local %f rang group Subballast\r\n',Dsb*pi());
[fr,psr]=Ray_Damp(Es,ns,ros,Pz(4,3,1)-Pz(4,3,5),fch,Ds);
fprintf(ID3,'ini damp=ray %f %f range group Sol\r\n',psr,fr);
%*****
*****
%Charges dynamiques à l'interface Roue-Rail
%*****
*****

```

```

fprintf(ID3, ';Application du chargement\r\n');
%Chargement essieu 1
FileName1=['Essieu' num2str(1) '.his'];
fid1=fopen(FileName1, 'w');
fprintf(fid1, 'time_forcel\r\n');
fprintf(fid1, '%d\t%2.10f\r\n', Nb_d, Dst/V);
for i=1:Nb_d
fprintf(fid1, '%f\r\n', -Fo_Cont(i,2));
end
fclose(fid1);
fprintf(ID3, 'table 1 read Essieu1.his\r\n');
%Chargement essieu 2
FileName2=['Essieu' num2str(2) '.his'];
fid2=fopen(FileName2, 'w');
fprintf(fid2, 'time_force2\r\n');
fprintf(fid2, '%d\t%2.10f\r\n', Nb_d, Dst/V);
for i=1:Nb_d
fprintf(fid2, '%f\r\n', -Fo_Cont(i,3));
end
fclose(fid2);
fprintf(ID3, 'table 2 read Essieu2.his\r\n');
%Chargement essieu 3
FileName3=['Essieu' num2str(3) '.his'];
fid3=fopen(FileName3, 'w');
fprintf(fid3, 'time_force3\r\n');
fprintf(fid3, '%d\t%2.10f\r\n', Nb_d, Dst/V);
for i=1:Nb_d
fprintf(fid3, '%f\r\n', -Fo_Cont(i,4));
end
fclose(fid3);
fprintf(ID3, 'table 3 read Essieu3.his\r\n');
%Chargement essieu 4
FileName4=['Essieu' num2str(4) '.his'];
fid4=fopen(FileName4, 'w');
fprintf(fid4, 'time_force4\r\n');
fprintf(fid4, '%d\t%2.10f\r\n', Nb_d, Dst/V);
for i=1:Nb_d
fprintf(fid4, '%f\r\n', -Fo_Cont(i,5));
end
fclose(fid4);
fprintf(ID3, 'table 4 read Essieu4.his\r\n');
%*****
%*****
%Numéro des noeuds chargés
%*****
%*****
%                               Essieu1
%Rail+
fid5=fopen('Num_NoEU_rp_es1.his', 'w');
fprintf(fid5, 'Num_NoEU_rp_es1\r\n');
fprintf(fid5, '%d\t%f\r\n', Nfch, 1);
for i=1:Nfch
    fprintf(fid5, '%d\r\n', Nch(i,1,1));
end
fclose(fid5);
fprintf(ID3, 'table 5 read Num_NoEU_rp_es1.his\r\n');

```

Matlab Code of the L-AMN Adaptive Meshing Scheme: 3D Finite Difference Modeling

```
% Essieu2
%Rail+
fid7=fopen('Num_Noeu_rp_es2.his','w');
fprintf(fid7,'Num_Noeu_rp_es2\r\n');
fprintf(fid7,'%d\t%f\r\n',Nfch,1);
for i=1:Nfch
    fprintf(fid7,'%d\r\n',Nch(i,1,2));
end
fclose(fid7);
fprintf(ID3,'table 6 read Num_Noeu_rp_es2.his\r\n');
% Essieu3
%Rail+
fid9=fopen('Num_Noeu_rp_es3.his','w');
fprintf(fid9,'Num_Noeu_rp_es3\r\n');
fprintf(fid9,'%d\t%f\r\n',Nfch,1);
for i=1:Nfch
    fprintf(fid9,'%d\r\n',Nch(i,1,3));
end
fclose(fid9);
fprintf(ID3,'table 7 read Num_Noeu_rp_es3.his\r\n');
% Essieu4
%Rail+
fid11=fopen('Num_Noeu_rp_es4.his','w');
fprintf(fid11,'Num_Noeu_rp_es4\r\n');
fprintf(fid11,'%d\t%f\r\n',Nfch,1);
for i=1:Nfch
    fprintf(fid11,'%d\r\n',Nch(i,1,4));
end
fclose(fid11);
fprintf(ID3,'table 8 read Num_Noeu_rp_es4.his\r\n');
%*****
%Fonctions d'application des charges
%*****
fprintf(ID3,'call Load_Apl.txt\r\n');
%*****
%Gestion des Résultats
%*****
fprintf(ID3,'set dyn=on\r\n');
fprintf(ID3,'set dyn time 0.0\r\n');
fprintf(ID3,'set sv %d\r\n',sv);
fprintf(ID3,'set sx %d\r\n',sx);
fprintf(ID3,'set Tst %2.8f\r\n',Tst);
fprintf(ID3,'set delxa %2.8f\r\n',delxa);
fprintf(ID3,'set mt %d\r\n',length(Nch(:,1,1)));
fprintf(ID3,'set dyn multi off\r\n');
fprintf(ID3,'Mov_Load\r\n');
fprintf(ID3,'call Gest_Res.txt\r\n');
fprintf(ID3,'table 9 name zdis_PM_Rp_1\r\n');
fprintf(ID3,'table 10 name zdis_PM_Rp_2\r\n');
fprintf(ID3,'table 11 name zdis_PM_Rp_3\r\n');
fprintf(ID3,'table 12 name zdis_PM_Rp_4\r\n');
fprintf(ID3,'save Reponse_Dynamique.sav\r\n');
```

```
fclose(ID3);
end
```

5. Function 4: Load_Apl

```
function []=Load_Apl(Er,nr,ror,Ar,Iixr,Iiy,Iizr,Dr)
ID4=fopen('Load_Apl.txt','w');
%-----
%Fonction1: Sert à supprimer un EF de CID=cid
fprintf(ID4,'def Ch_Nod\r\n');
fprintf(ID4,'sp=s_head\r\n');
fprintf(ID4,'loop while sp # null\r\n');
fprintf(ID4,'snext=s_next(sp)\r\n');
fprintf(ID4,'if s_cid(sp)=cid then\r\n');
fprintf(ID4,'ii=s_delete(sp)\r\n');
fprintf(ID4,'end_if\r\n');
fprintf(ID4,'sp=snext\r\n');
fprintf(ID4,'end_loop\r\n');
fprintf(ID4,'end\r\n');
%-----
%Fonction2: Sert à trouver le id du noeud repéré par (x,y,z)
fprintf(ID4,'def pr_id\r\n');
fprintf(ID4,'idn=nd_id(nd_near(xn,yn,0))\r\n');
fprintf(ID4,'end\r\n');
%-----
%Fonction3: Sert à trouver le cid du Sel où le point (x,y,z)
l'appartient
fprintf(ID4,'def pr_cid\r\n');
fprintf(ID4,'cid=s_cid(s_near(xc,yc,0))\r\n');
fprintf(ID4,'end\r\n');
%-----
%Fonction4: Fonction Recap de suppression
fprintf(ID4,'def Sup_Sel\r\n');
fprintf(ID4,'pr_cid\r\n');
fprintf(ID4,'Ch_Nod\r\n');
fprintf(ID4,'end\r\n');
%-----
%Fonction5: Sert à demander les historiques (calcul ke=0)
fprintf(ID4,'def Hist_Eti\r\n');
fprintf(ID4,'command\r\n');
fprintf(ID4,'History reset\r\n');
fprintf(ID4,'Hist n 20\r\n');
fprintf(ID4,'Hist dytime\r\n');%his #1
fprintf(ID4,'Hist sel node zdisp id Np1\r\n');%his #2
fprintf(ID4,'Hist sel node yrdisp id Np1\r\n');%his #3
fprintf(ID4,'Hist sel node zvel id Np1\r\n');%his #4
fprintf(ID4,'Hist sel node yrvel id Np1\r\n');%his #5
fprintf(ID4,'Hist sel node zdisp id Np2\r\n');%his #6
fprintf(ID4,'Hist sel node yrdisp id Np2\r\n');%his #7
fprintf(ID4,'Hist sel node zvel id Np2\r\n');%his #8
fprintf(ID4,'Hist sel node yrvel id Np2\r\n');%his #9
```

```

fprintf(ID4, 'Hist sel node zdisp id Np3\r\n');%his #10
fprintf(ID4, 'Hist sel node yrdisp id Np3\r\n');%his #11
fprintf(ID4, 'Hist sel node zvel id Np3\r\n');%his #12
fprintf(ID4, 'Hist sel node yrvel id Np3\r\n');%his #13
fprintf(ID4, 'Hist sel node zdisp id Np4\r\n');%his #14
fprintf(ID4, 'Hist sel node yrdisp id Np4\r\n');%his #15
fprintf(ID4, 'Hist sel node zvel id Np4\r\n');%his #16
fprintf(ID4, 'Hist sel node yrvel id Np4\r\n');%his #17
fprintf(ID4, 'Hist sel node zdisp id Nv1\r\n');%his #18
fprintf(ID4, 'Hist sel node yrdisp id Nv1\r\n');%his #19
fprintf(ID4, 'Hist sel node zvel id Nv1\r\n');%his #20
fprintf(ID4, 'Hist sel node yrvel id Nv1\r\n');%his #21
fprintf(ID4, 'Hist sel node zdisp id Nv2\r\n');%his #22
fprintf(ID4, 'Hist sel node yrdisp id Nv2\r\n');%his #23
fprintf(ID4, 'Hist sel node zvel id Nv2\r\n');%his #24
fprintf(ID4, 'Hist sel node yrvel id Nv2\r\n');%his #25
fprintf(ID4, 'Hist sel node zdisp id Nv3\r\n');%his #26
fprintf(ID4, 'Hist sel node yrdisp id Nv3\r\n');%his #27
fprintf(ID4, 'Hist sel node zvel id Nv3\r\n');%his #28
fprintf(ID4, 'Hist sel node yrvel id Nv3\r\n');%his #29
fprintf(ID4, 'Hist sel node zdisp id Nv4\r\n');%his #30
fprintf(ID4, 'Hist sel node yrdisp id Nv4\r\n');%his #31
fprintf(ID4, 'Hist sel node zvel id Nv4\r\n');%his #32
fprintf(ID4, 'Hist sel node yrvel id Nv4\r\n');%his #33
fprintf(ID4, 'endcommand\r\n');
fprintf(ID4, 'end\r\n');
%-----
-----
%Fonction6: Sert à demander les historiques (calcul intermédiaire)
fprintf(ID4, 'def Hist_Inte\r\n');
fprintf(ID4, 'command\r\n');
fprintf(ID4, 'History reset\r\n');
fprintf(ID4, 'Hist n 20\r\n');
fprintf(ID4, 'Hist dytime\r\n');%his #1
fprintf(ID4, 'Hist sel node zdisp id idp1\r\n');%his #2
fprintf(ID4, 'Hist sel node yrdisp id idp1\r\n');%his #3
fprintf(ID4, 'Hist sel node zvel id idp1\r\n');%his #4
fprintf(ID4, 'Hist sel node yrvel id idp1\r\n');%his #5
fprintf(ID4, 'Hist sel node zdisp id idp2\r\n');%his #6
fprintf(ID4, 'Hist sel node yrdisp id idp2\r\n');%his #7
fprintf(ID4, 'Hist sel node zvel id idp2\r\n');%his #8
fprintf(ID4, 'Hist sel node yrvel id idp2\r\n');%his #9
fprintf(ID4, 'Hist sel node zdisp id idp3\r\n');%his #10
fprintf(ID4, 'Hist sel node yrdisp id idp3\r\n');%his #11
fprintf(ID4, 'Hist sel node zvel id idp3\r\n');%his #12
fprintf(ID4, 'Hist sel node yrvel id idp3\r\n');%his #13
fprintf(ID4, 'Hist sel node zdisp id idp4\r\n');%his #14
fprintf(ID4, 'Hist sel node yrdisp id idp4\r\n');%his #15
fprintf(ID4, 'Hist sel node zvel id idp4\r\n');%his #16
fprintf(ID4, 'Hist sel node yrvel id idp4\r\n');%his #17
fprintf(ID4, 'Hist sel node zdisp id Nv1\r\n');%his #18
fprintf(ID4, 'Hist sel node yrdisp id Nv1\r\n');%his #19
fprintf(ID4, 'Hist sel node zvel id Nv1\r\n');%his #20
fprintf(ID4, 'Hist sel node yrvel id Nv1\r\n');%his #21
fprintf(ID4, 'Hist sel node zdisp id Nv2\r\n');%his #22
fprintf(ID4, 'Hist sel node yrdisp id Nv2\r\n');%his #23

```

```

fprintf(ID4, 'Hist sel node zvel id Nv2\r\n');%his #24
fprintf(ID4, 'Hist sel node yrvel id Nv2\r\n');%his #25
fprintf(ID4, 'Hist sel node zdisp id Nv3\r\n');%his #26
fprintf(ID4, 'Hist sel node yrdisp id Nv3\r\n');%his #27
fprintf(ID4, 'Hist sel node zvel id Nv3\r\n');%his #28
fprintf(ID4, 'Hist sel node yrvel id Nv3\r\n');%his #29
fprintf(ID4, 'Hist sel node zdisp id Nv4\r\n');%his #30
fprintf(ID4, 'Hist sel node yrdisp id Nv4\r\n');%his #31
fprintf(ID4, 'Hist sel node zvel id Nv4\r\n');%his #32
fprintf(ID4, 'Hist sel node yrvel id Nv4\r\n');%his #33
fprintf(ID4, 'endcommand\r\n');
fprintf(ID4, 'end\r\n');
%-----
-----
%Fonction7: Sert à calculer les fonctions de forme
fprintf(ID4, 'def Sha_Fun\r\n');
fprintf(ID4, 'Q1=(1/(Lt^3))*(2*(rp^3)-3*(rp^2)*(Lt)+(Lt^3))\r\n');
fprintf(ID4, 'Q2=(1/(Lt^3))*((rp^3)*(Lt)-
2*(rp^2)*(Lt^2)+(rp)*(Lt^3))\r\n');
fprintf(ID4, 'Q3=(1/(Lt^3))*(-2*(rp^3)+3*(rp^2)*(Lt))\r\n');
fprintf(ID4, 'Q4=(1/(Lt^3))*((rp^3)*(Lt)-(rp^2)*(Lt^2))\r\n');
fprintf(ID4, 'Q5=(1/(Lt^3))*(6*(rp^2)-6*rp*Lt)\r\n');
fprintf(ID4, 'Q6=(1/(Lt^3))*(3*(rp^2)*Lt-4*rp*(Lt^2)+(Lt^3))\r\n');
fprintf(ID4, 'Q7=(1/(Lt^3))*(-6*(rp^2)+6*rp*Lt)\r\n');
fprintf(ID4, 'Q8=(1/(Lt^3))*(3*(rp^2)*Lt-2*rp*(Lt^2))\r\n');
fprintf(ID4, 'end\r\n');
%-----
-----
%Fonction8: Sert à appliquer les charges aux noeuds mobiles à
l'instant t
fprintf(ID4, 'def Load_Apl\r\n');
%*****Numéros et positions des noeuds
principaux*****
fprintf(ID4, 'dpar=(m-1)\r\n');
fprintf(ID4, 'Tde=dpar*Tst\r\n');
fprintf(ID4, 'Np1=int(table(5,dpar))\r\n');fprintf(ID4, 'Np2=int(table
(6,dpar))\r\n');
fprintf(ID4, 'Np3=int(table(7,dpar))\r\n');fprintf(ID4, 'Np4=int(table
(8,dpar))\r\n');
%La position x des noeuds principaux
fprintf(ID4, 'xp1=nd_pos(nd_find(Np1),2,1)\r\n');
fprintf(ID4, 'xp2=nd_pos(nd_find(Np2),2,1)\r\n');
fprintf(ID4, 'xp3=nd_pos(nd_find(Np3),2,1)\r\n');
fprintf(ID4, 'xp4=nd_pos(nd_find(Np4),2,1)\r\n');
fprintf(ID4, 'yp1=nd_pos(nd_find(Np1),2,2)\r\n');
%La position x des noeuds voisins
fprintf(ID4, 'Nv1=Np1+1\r\n');fprintf(ID4, 'Nv2=Np2+1\r\n');fprintf(ID
4, 'Nv3=Np3+1\r\n');fprintf(ID4, 'Nv4=Np4+1\r\n');
fprintf(ID4, 'xv1=nd_pos(nd_find(Nv1),2,1)\r\n');
fprintf(ID4, 'xv2=nd_pos(nd_find(Nv2),2,1)\r\n');
fprintf(ID4, 'xv3=nd_pos(nd_find(Nv3),2,1)\r\n');
fprintf(ID4, 'xv4=nd_pos(nd_find(Nv4),2,1)\r\n');
%////////////////////////////////////Calcul0\\\\\\\\\\\\\\\\\\\\\\\\\\\\\\\\\\\\\\\\
\\\\\\\\\\\\
%*****Condition initial du premier
calcul*****

```

```

%Initialisation des déplacements:Interpolation d'Hermite
fprintf(ID4, 'ahj1=ytable(17,1)\r\n');fprintf(ID4, 'ahj2=ytable(17,2)\r\n');
fprintf(ID4, 'ahj3=ytable(17,3)\r\n');fprintf(ID4, 'ahj4=ytable(17,4)\r\n');
fprintf(ID4, 'ahj5=ytable(17,5)\r\n');fprintf(ID4, 'ahj6=ytable(17,6)\r\n');
fprintf(ID4, 'ahj7=ytable(17,7)\r\n');fprintf(ID4, 'ahj8=ytable(17,8)\r\n');
fprintf(ID4, 'ahj9=ytable(17,9)\r\n');fprintf(ID4, 'ahj10=ytable(17,10)\r\n');
fprintf(ID4, 'ahj11=ytable(17,11)\r\n');fprintf(ID4, 'ahj12=ytable(17,12)\r\n');
fprintf(ID4, 'ahj13=ytable(17,13)\r\n');fprintf(ID4, 'ahj14=ytable(17,14)\r\n');
fprintf(ID4, 'ahj15=ytable(17,15)\r\n');fprintf(ID4, 'ahj16=ytable(17,16)\r\n');
fprintf(ID4, 'command\r\n');
fprintf(ID4, 'sel node init zdisp=ahj1 yrdisp=ahj2 zvel=ahj3 yrvel=ahj4 range id=Np1\r\n');
fprintf(ID4, 'sel node init zdisp=ahj5 yrdisp=ahj6 zvel=ahj7 yrvel=ahj8 range id=Np2\r\n');
fprintf(ID4, 'sel node init zdisp=ahj9 yrdisp=ahj10 zvel=ahj11 yrvel=ahj12 range id=Np3\r\n');
fprintf(ID4, 'sel node init zdisp=ahj13 yrdisp=ahj14 zvel=ahj15 yrvel=ahj16 range id=Np4\r\n');
fprintf(ID4, 'table 17 erase\r\n');
fprintf(ID4, 'endcommand\r\n');
%*****Demander les Historiques*****
fprintf(ID4, 'Hist_Eti\r\n');
%*****Variabilité dans le temps*****
fprintf(ID4, 'loop ij (1,sv)\r\n');
fprintf(ID4, 'xx=Tde+(ij-1)*det\r\n');
fprintf(ID4, 'Fo_No1=table(1,xx)\r\n');fprintf(ID4, 'Fo_No2=table(2,xx)\r\n');
fprintf(ID4, 'Fo_No3=table(3,xx)\r\n');fprintf(ID4, 'Fo_No4=table(4,xx)\r\n');
fprintf(ID4, 'Tt=Tde+ij*det\r\n');
%Calcul des fonctions de forme:Interpolation d'Hermite
fprintf(ID4, 'delet=(ij-1)*(delxa/(sx*sv))\r\n');
fprintf(ID4, 'command\r\n');
fprintf(ID4, 'set Lt delxa\r\n');
fprintf(ID4, 'set rp delet\r\n');
fprintf(ID4, 'Sha_Fun\r\n');
fprintf(ID4, 'endcommand\r\n');
%Calcul des forces nodales équivalentes
fprintf(ID4, 'f11=Q1*Fo_No1\r\n');fprintf(ID4, 'm11=Q2*Fo_No1\r\n');fprintf(ID4, 'f12=Q3*Fo_No1\r\n');
fprintf(ID4, 'm12=Q4*Fo_No1\r\n');fprintf(ID4, 'f21=Q1*Fo_No2\r\n');fprintf(ID4, 'm21=Q2*Fo_No2\r\n');
fprintf(ID4, 'f22=Q3*Fo_No2\r\n');fprintf(ID4, 'm22=Q4*Fo_No2\r\n');fprintf(ID4, 'f31=Q1*Fo_No3\r\n');
fprintf(ID4, 'm31=Q2*Fo_No3\r\n');fprintf(ID4, 'f32=Q3*Fo_No3\r\n');fprintf(ID4, 'm32=Q4*Fo_No3\r\n');
fprintf(ID4, 'f41=Q1*Fo_No4\r\n');fprintf(ID4, 'm41=Q2*Fo_No4\r\n');fprintf(ID4, 'f42=Q3*Fo_No4\r\n');
fprintf(ID4, 'm42=Q4*Fo_No4\r\n');
%Application des forces nodales équivalentes
fprintf(ID4, 'command\r\n');
%N#1

```

```

fprintf(ID4, 'sel node apply fo 0 0 f11 ra id
Np1\r\n'); fprintf(ID4, 'sel node apply mo 0 m11 0 ra id=Np1\r\n');
fprintf(ID4, 'sel node apply fo 0 0 f12 ra id
Nv1\r\n'); fprintf(ID4, 'sel node apply mo 0 m12 0 ra id=Nv1\r\n');
%N#2
fprintf(ID4, 'sel node apply fo 0 0 f21 ra id
Np2\r\n'); fprintf(ID4, 'sel node apply mo 0 m21 0 ra id=Np2\r\n');
fprintf(ID4, 'sel node apply fo 0 0 f22 ra id
Nv2\r\n'); fprintf(ID4, 'sel node apply mo 0 m22 0 ra id=Nv2\r\n');
%N#3
fprintf(ID4, 'sel node apply fo 0 0 f31 ra id
Np3\r\n'); fprintf(ID4, 'sel node apply mo 0 m31 0 ra id=Np3\r\n');
fprintf(ID4, 'sel node apply fo 0 0 f32 ra id
Nv3\r\n'); fprintf(ID4, 'sel node apply mo 0 m32 0 ra id=Nv3\r\n');
%N#4
fprintf(ID4, 'sel node apply fo 0 0 f41 ra id
Np4\r\n'); fprintf(ID4, 'sel node apply mo 0 m41 0 ra id=Np4\r\n');
fprintf(ID4, 'sel node apply fo 0 0 f42 ra id
Nv4\r\n'); fprintf(ID4, 'sel node apply mo 0 m42 0 ra id=Nv4\r\n');
fprintf(ID4, 'endcommand\r\n');
fprintf(ID4, 'pav=(m-1)*sv*sx+ij\r\n');
fprintf(ID4, 'command\r\n');
fprintf(ID4, 'print(pav)\r\n'); fprintf(ID4, 'print(ptar)\r\n');
fprintf(ID4, 'solve age Tt\r\n');
fprintf(ID4, 'sel node apply remove force\r\n');
fprintf(ID4, 'endcommand\r\n');
fprintf(ID4, 'end_loop\r\n');
%*****Ecriture des
résultats*****
fprintf(ID4, 'command\r\n');
fprintf(ID4, 'his write 2 vs 1 table 9\r\n'); %Zdisp_Np1
fprintf(ID4, 'his write 6 vs 1 table 10\r\n'); %Zdisp_Np2
fprintf(ID4, 'his write 10 vs 1 table 11\r\n'); %Zdisp_Np3
fprintf(ID4, 'his write 14 vs 1 table 12\r\n'); %Zdisp_Np4
fprintf(ID4, 'endcommand\r\n');
%*****Aspect
adaptatif*****
%Calcul des fonctions de forme:Interpolation d'Hermite
fprintf(ID4, 'delel=delxa/sx\r\n');
fprintf(ID4, 'command\r\n');
fprintf(ID4, 'set Lt delxa\r\n');
fprintf(ID4, 'set rp delel\r\n');
fprintf(ID4, 'Sha_Fun\r\n');
fprintf(ID4, 'endcommand\r\n');
fprintf(ID4, 'loop ihi (1,4)\r\n');
%Déplacements linéaire et angulaire
fprintf(ID4, 'Nhi1=4*ihi-2\r\n'); fprintf(ID4, 'Nhi2=4*ihi-1\r\n');
fprintf(ID4, 'Nhi3=4*ihi+14\r\n'); fprintf(ID4, 'Nhi4=4*ihi+15\r\n');
fprintf(ID4, 'command\r\n');
fprintf(ID4, 'his write Nhi1 vs 1 table 13\r\n'); %Zdisp Npi
fprintf(ID4, 'his write Nhi2 vs 1 table 14\r\n'); %yrdisp Npi
fprintf(ID4, 'his write Nhi3 vs 1 table 15\r\n'); %Zdisp Nvi
fprintf(ID4, 'his write Nhi4 vs 1 table 16\r\n'); %yrdisp Nvi
fprintf(ID4, 'endcommand\r\n');
fprintf(ID4, 'tas=table_size(13)\r\n');
fprintf(ID4, 'xtable(17,4*ihi-3)=4*ihi-3\r\n');

```



```

fprintf(ID4, 'xip3=xp3+(ke*delxa)/sx\r\n');
fprintf(ID4, 'xip4=xp4+(ke*delxa)/sx\r\n');
%Suppression des EF/rail+
fprintf(ID4, 'command\r\n');
fprintf(ID4, 'set yc yp1\r\n');
fprintf(ID4, 'set xc xip1\r\n');fprintf(ID4, 'Sup_Sel\r\n');
fprintf(ID4, 'set xc xip2\r\n');fprintf(ID4, 'Sup_Sel\r\n');
fprintf(ID4, 'set xc xip3\r\n');fprintf(ID4, 'Sup_Sel\r\n');
fprintf(ID4, 'set xc xip4\r\n');fprintf(ID4, 'Sup_Sel\r\n');
fprintf(ID4, 'endcommand\r\n');
fprintf(ID4, 'command\r\n');
%*****Création des
noeuds/Rail+*****
fprintf(ID4, 'sel beam id=2 begin=(xp1,yp1,0) end=(xip1,yp1,0)
nseg=1\r\n');
fprintf(ID4, 'sel beam id=2 begin=(xip1,yp1,0) end=(xv1,yp1,0)
nseg=1\r\n');
fprintf(ID4, 'sel beam id=2 begin=(xp2,yp1,0) end=(xip2,yp1,0)
nseg=1\r\n');
fprintf(ID4, 'sel beam id=2 begin=(xip2,yp1,0) end=(xv2,yp1,0)
nseg=1\r\n');
fprintf(ID4, 'sel beam id=2 begin=(xp3,yp1,0) end=(xip3,yp1,0)
nseg=1\r\n');
fprintf(ID4, 'sel beam id=2 begin=(xip3,yp1,0) end=(xv3,yp1,0)
nseg=1\r\n');
fprintf(ID4, 'sel beam id=2 begin=(xp4,yp1,0) end=(xip4,yp1,0)
nseg=1\r\n');
fprintf(ID4, 'sel beam id=2 begin=(xip4,yp1,0) end=(xv4,yp1,0)
nseg=1\r\n');
%*****Caractéristiques mécaniques et
dynamiques*****
fprintf(ID4, 'sel beam id=2 property d=%f e=%f n=%f xca=%2.8f
xcj=%2.8f xcij=%2.8f xciz=%2.8f\r\n',ror,Er,nr,Ar,Iixr,IiyR,Iizr);
fprintf(ID4, 'sel set damp=local %f ra selt beam id 2\r\n',Dr*pi());
fprintf(ID4, 'endcommand\r\n');
%*****Détermination de ID des noeuds
chargés*****
fprintf(ID4, 'command\r\n');
fprintf(ID4, 'set yn yp1\r\n');
fprintf(ID4, 'set xn
xip1\r\n');fprintf(ID4, 'pr_id\r\n');fprintf(ID4, 'endcommand\r\n');
fprintf(ID4, 'idp1=idn\r\n');
fprintf(ID4, 'command\r\n');
fprintf(ID4, 'set yn yp1\r\n');
fprintf(ID4, 'set xn
xip2\r\n');fprintf(ID4, 'pr_id\r\n');fprintf(ID4, 'endcommand\r\n');
fprintf(ID4, 'idp2=idn\r\n');
fprintf(ID4, 'command\r\n');
fprintf(ID4, 'set yn yp1\r\n');
fprintf(ID4, 'set xn
xip3\r\n');fprintf(ID4, 'pr_id\r\n');fprintf(ID4, 'endcommand\r\n');
fprintf(ID4, 'idp3=idn\r\n');
fprintf(ID4, 'command\r\n');
fprintf(ID4, 'set yn yp1\r\n');
fprintf(ID4, 'set xn
xip4\r\n');fprintf(ID4, 'pr_id\r\n');fprintf(ID4, 'endcommand\r\n');

```

```

fprintf(ID4, 'idp4=idn\r\n');
%*****Condition initial du calcul
ke*****
%Initialisation des déplacements:Interpolation d'Hermite
fprintf(ID4, 'ahj1=ytable(17,1)\r\n');fprintf(ID4, 'ahj2=ytable(17,2)\r\n');
fprintf(ID4, 'ahj3=ytable(17,3)\r\n');fprintf(ID4, 'ahj4=ytable(17,4)\r\n');
fprintf(ID4, 'ahj5=ytable(17,5)\r\n');fprintf(ID4, 'ahj6=ytable(17,6)\r\n');
fprintf(ID4, 'ahj7=ytable(17,7)\r\n');fprintf(ID4, 'ahj8=ytable(17,8)\r\n');
fprintf(ID4, 'ahj9=ytable(17,9)\r\n');fprintf(ID4, 'ahj10=ytable(17,10)\r\n');
fprintf(ID4, 'ahj11=ytable(17,11)\r\n');fprintf(ID4, 'ahj12=ytable(17,12)\r\n');
fprintf(ID4, 'ahj13=ytable(17,13)\r\n');fprintf(ID4, 'ahj14=ytable(17,14)\r\n');
fprintf(ID4, 'ahj15=ytable(17,15)\r\n');fprintf(ID4, 'ahj16=ytable(17,16)\r\n');
fprintf(ID4, 'command\r\n');
fprintf(ID4, 'sel node init zdisp=ahj1 yrdisp=ahj2 zvel=ahj3 yrvel=ahj4 range id=idp1\r\n');
fprintf(ID4, 'sel node init zdisp=ahj5 yrdisp=ahj6 zvel=ahj7 yrvel=ahj8 range id=idp2\r\n');
fprintf(ID4, 'sel node init zdisp=ahj9 yrdisp=ahj10 zvel=ahj11 yrvel=ahj12 range id=idp3\r\n');
fprintf(ID4, 'sel node init zdisp=ahj13 yrdisp=ahj14 zvel=ahj15 yrvel=ahj16 range id=idp4\r\n');
fprintf(ID4, 'table 17 erase\r\n');
fprintf(ID4, 'endcommand\r\n');
%*****Demander les Historiques*****
fprintf(ID4, 'Hist_Inte\r\n');
%*****Variabilité dans le temps*****
fprintf(ID4, 'loop ij (1,sv)\r\n');
fprintf(ID4, 'xx=Tde+ke*(Tst/sx)+(ij-1)*det\r\n');
fprintf(ID4, 'Fo_No1=table(1,xx)\r\n');fprintf(ID4, 'Fo_No2=table(2,xx)\r\n');
fprintf(ID4, 'Fo_No3=table(3,xx)\r\n');fprintf(ID4, 'Fo_No4=table(4,xx)\r\n');
fprintf(ID4, 'Tt=Tde+ke*(Tst/sx)+ij*det\r\n');
%Calcul des fonctions de forme:Interpolation d'Hermite
fprintf(ID4, 'delet=(ij-1)*(delxa/(sx*sv))\r\n');
fprintf(ID4, 'command\r\n');
fprintf(ID4, 'set Lt delxa\r\n');
fprintf(ID4, 'set rp delet\r\n');
fprintf(ID4, 'Sha_Fun\r\n');
fprintf(ID4, 'endcommand\r\n');
%Calcul des forces nodales équivalentes
fprintf(ID4, 'f11=Q1*Fo_No1\r\n');fprintf(ID4, 'm11=Q2*Fo_No1\r\n');fprintf(ID4, 'f12=Q3*Fo_No1\r\n');
fprintf(ID4, 'm12=Q4*Fo_No1\r\n');fprintf(ID4, 'f21=Q1*Fo_No2\r\n');fprintf(ID4, 'm21=Q2*Fo_No2\r\n');
fprintf(ID4, 'f22=Q3*Fo_No2\r\n');fprintf(ID4, 'm22=Q4*Fo_No2\r\n');fprintf(ID4, 'f31=Q1*Fo_No3\r\n');
fprintf(ID4, 'm31=Q2*Fo_No3\r\n');fprintf(ID4, 'f32=Q3*Fo_No3\r\n');fprintf(ID4, 'm32=Q4*Fo_No3\r\n');
fprintf(ID4, 'f41=Q1*Fo_No4\r\n');fprintf(ID4, 'm41=Q2*Fo_No4\r\n');fprintf(ID4, 'f42=Q3*Fo_No4\r\n');
fprintf(ID4, 'm42=Q4*Fo_No4\r\n');
%Application des forces nodales équivalentes

```

```

fprintf(ID4, 'command\r\n');
%N#1
fprintf(ID4, 'sel node apply fo 0 0 f11 ra id
idp1\r\n'); fprintf(ID4, 'sel node apply mo 0 m11 0 ra id=idp1\r\n');
fprintf(ID4, 'sel node apply fo 0 0 f12 ra id
Nv1\r\n'); fprintf(ID4, 'sel node apply mo 0 m12 0 ra id=Nv1\r\n');
%N#2
fprintf(ID4, 'sel node apply fo 0 0 f21 ra id
idp2\r\n'); fprintf(ID4, 'sel node apply mo 0 m21 0 ra id=idp2\r\n');
fprintf(ID4, 'sel node apply fo 0 0 f22 ra id
Nv2\r\n'); fprintf(ID4, 'sel node apply mo 0 m22 0 ra id=Nv2\r\n');
%N#3
fprintf(ID4, 'sel node apply fo 0 0 f31 ra id
idp3\r\n'); fprintf(ID4, 'sel node apply mo 0 m31 0 ra id=idp3\r\n');
fprintf(ID4, 'sel node apply fo 0 0 f32 ra id
Nv3\r\n'); fprintf(ID4, 'sel node apply mo 0 m32 0 ra id=Nv3\r\n');
%N#4
fprintf(ID4, 'sel node apply fo 0 0 f41 ra id
idp4\r\n'); fprintf(ID4, 'sel node apply mo 0 m41 0 ra id=idp4\r\n');
fprintf(ID4, 'sel node apply fo 0 0 f42 ra id
Nv4\r\n'); fprintf(ID4, 'sel node apply mo 0 m42 0 ra id=Nv4\r\n');
fprintf(ID4, 'endcommand\r\n');
fprintf(ID4, 'pav=(m-1)*sv*sx+ke*sv+ij\r\n');
fprintf(ID4, 'command\r\n');
fprintf(ID4, 'print(pav)\r\n'); fprintf(ID4, 'print(ptar)\r\n');
fprintf(ID4, 'solve age Tt\r\n');
fprintf(ID4, 'sel node apply remove force\r\n');
fprintf(ID4, 'endcommand\r\n');
fprintf(ID4, 'end_loop\r\n');
%*****Ecriture des
résultats*****
fprintf(ID4, 'command\r\n');
fprintf(ID4, 'his write 2 vs 1 table 9\r\n'); %Zdisp_pt1
fprintf(ID4, 'his write 6 vs 1 table 10\r\n'); %Zdisp_pt2
fprintf(ID4, 'his write 10 vs 1 table 11\r\n'); %Zdisp_pt3
fprintf(ID4, 'his write 14 vs 1 table 12\r\n'); %Zdisp_pt4
fprintf(ID4, 'endcommand\r\n');
%*****Aspect
adaptatif*****
%Calcul des fonctions de forme:Interpolation d'Hermite
fprintf(ID4, 'delel=delxa/sx\r\n');
fprintf(ID4, 'dere=delxa-(ke*delxa/sx)\r\n');
fprintf(ID4, 'command\r\n');
fprintf(ID4, 'set Lt dere\r\n');
fprintf(ID4, 'set rp delel\r\n');
fprintf(ID4, 'Sha_Fun\r\n');
fprintf(ID4, 'endcommand\r\n');
fprintf(ID4, 'loop ihi (1,4)\r\n');
%Déplacements linéaire et angulaire
fprintf(ID4, 'Nhi1=4*ihi-2\r\n'); fprintf(ID4, 'Nhi2=4*ihi-1\r\n');
fprintf(ID4, 'Nhi3=4*ihi+14\r\n'); fprintf(ID4, 'Nhi4=4*ihi+15\r\n');
fprintf(ID4, 'command\r\n');
fprintf(ID4, 'his write Nhi1 vs 1 table 13\r\n'); %Zdisp_pti
fprintf(ID4, 'his write Nhi2 vs 1 table 14\r\n'); %yrdisp_pti
fprintf(ID4, 'his write Nhi3 vs 1 table 15\r\n'); %Zdisp Nvi
fprintf(ID4, 'his write Nhi4 vs 1 table 16\r\n'); %yrdisp Nvi

```

```

fprintf(ID4, 'endcommand\r\n');
fprintf(ID4, 'tas0=table_size(13)\r\n');
fprintf(ID4, 'xtable(17,4*ihi-3)=4*ihi-3\r\n');
fprintf(ID4, 'ytable(17,4*ihi-3)=Q1*ytable(13,tas0)+Q2*ytable(14,tas0)+Q3*ytable(15,tas0)+Q4*ytable(16,tas0)\r\n');;%deplacement
fprintf(ID4, 'xtable(17,4*ihi-2)=4*ihi-2\r\n');
fprintf(ID4, 'ytable(17,4*ihi-2)=Q5*ytable(13,tas0)+Q6*ytable(14,tas0)+Q7*ytable(15,tas0)+Q8*ytable(16,tas0)\r\n');;%rotation
fprintf(ID4, 'command\r\n');
fprintf(ID4, 'table 13 erase\r\n');fprintf(ID4, 'table 14 erase\r\n');
fprintf(ID4, 'table 15 erase\r\n');fprintf(ID4, 'table 16 erase\r\n');
fprintf(ID4, 'endcommand\r\n');
%Vitesse linéaire et angulaire
fprintf(ID4, 'Nhi1=4*ihi\r\n');fprintf(ID4, 'Nhi2=4*ihi+1\r\n');
fprintf(ID4, 'Nhi3=4*ihi+16\r\n');fprintf(ID4, 'Nhi4=4*ihi+17\r\n');
fprintf(ID4, 'command\r\n');
fprintf(ID4, 'his write Nhi1 vs 1 table 13\r\n');;%Zvel Npi
fprintf(ID4, 'his write Nhi2 vs 1 table 14\r\n');;%yrvel Npi
fprintf(ID4, 'his write Nhi3 vs 1 table 15\r\n');;%Zvel Nvi
fprintf(ID4, 'his write Nhi4 vs 1 table 16\r\n');;%yrvel Nvi
fprintf(ID4, 'endcommand\r\n');
fprintf(ID4, 'tas0=table_size(13)\r\n');
fprintf(ID4, 'xtable(17,4*ihi-1)=4*ihi-1\r\n');
fprintf(ID4, 'ytable(17,4*ihi-1)=Q1*ytable(13,tas0)+Q2*ytable(14,tas0)+Q3*ytable(15,tas0)+Q4*ytable(16,tas0)\r\n');;%Vitesse linéaire
fprintf(ID4, 'xtable(17,4*ihi)=4*ihi\r\n');
fprintf(ID4, 'ytable(17,4*ihi)=Q5*ytable(13,tas0)+Q6*ytable(14,tas0)+Q7*ytable(15,tas0)+Q8*ytable(16,tas0)\r\n');;%Vitesse angulaire
fprintf(ID4, 'command\r\n');
fprintf(ID4, 'table 13 erase\r\n');fprintf(ID4, 'table 14 erase\r\n');
fprintf(ID4, 'table 15 erase\r\n');fprintf(ID4, 'table 16 erase\r\n');
fprintf(ID4, 'endcommand\r\n');
fprintf(ID4, 'end_loop\r\n');
fprintf(ID4, 'end_loop\r\n');
%*****Réparation de l'EF chargé*****
%Suppression des EF gauche
fprintf(ID4, 'xrgp1=xp1+((sx-1)*delxa)/(2*sx)\r\n');
fprintf(ID4, 'xrgp2=xp2+((sx-1)*delxa)/(2*sx)\r\n');
fprintf(ID4, 'xrgp3=xp3+((sx-1)*delxa)/(2*sx)\r\n');
fprintf(ID4, 'xrgp4=xp4+((sx-1)*delxa)/(2*sx)\r\n');
%Suppression des EF/rail+
fprintf(ID4, 'command\r\n');
fprintf(ID4, 'set yc yp1\r\n');
fprintf(ID4, 'set xc xrgp1\r\n');fprintf(ID4, 'Sup_Sel\r\n');fprintf(ID4, 'set xc xrgp2\r\n');fprintf(ID4, 'Sup_Sel\r\n');
fprintf(ID4, 'set xc xrgp3\r\n');fprintf(ID4, 'Sup_Sel\r\n');fprintf(ID4, 'set xc xrgp4\r\n');fprintf(ID4, 'Sup_Sel\r\n');
fprintf(ID4, 'endcommand\r\n');
%Suppression des EF droite

```

```

fprintf(ID4, 'xrdp1=xp1+((sx-
1)*delxa)/(sx)+(delxa)/(2*sx)\r\n'); fprintf(ID4, 'xrdp2=xp2+((sx-
1)*delxa)/(sx)+(delxa)/(2*sx)\r\n');
fprintf(ID4, 'xrdp3=xp3+((sx-
1)*delxa)/(sx)+(delxa)/(2*sx)\r\n'); fprintf(ID4, 'xrdp4=xp4+((sx-
1)*delxa)/(sx)+(delxa)/(2*sx)\r\n');
%Suppression des EF/Rail+
fprintf(ID4, 'command\r\n');
fprintf(ID4, 'set yc yp1\r\n');
fprintf(ID4, 'set xc
xrdp1\r\n'); fprintf(ID4, 'Sup_Sel\r\n'); fprintf(ID4, 'set xc
xrdp2\r\n'); fprintf(ID4, 'Sup_Sel\r\n');
fprintf(ID4, 'set xc
xrdp3\r\n'); fprintf(ID4, 'Sup_Sel\r\n'); fprintf(ID4, 'set xc
xrdp4\r\n'); fprintf(ID4, 'Sup_Sel\r\n');
fprintf(ID4, 'endcommand\r\n');
%*****Création des
EF*****
%Création des EF/Rail+
fprintf(ID4, 'command\r\n');
fprintf(ID4, 'sel beam id=2 begin=(xp1,yp1,0) end=(xv1,yp1,0)
nseg=1\r\n');
fprintf(ID4, 'sel beam id=2 begin=(xp2,yp1,0) end=(xv2,yp1,0)
nseg=1\r\n');
fprintf(ID4, 'sel beam id=2 begin=(xp3,yp1,0) end=(xv3,yp1,0)
nseg=1\r\n');
fprintf(ID4, 'sel beam id=2 begin=(xp4,yp1,0) end=(xv4,yp1,0)
nseg=1\r\n');
%*****Caractéristiques mécaniques et
dynamiques*****
fprintf(ID4, 'sel beam id=2 property d=%f e=%f n=%f xca=%2.8f
xcj=%2.8f xcij=%2.8f xciz=%2.8f\r\n',ror,Er,nr,Ar,Iixr,IiyR,Iizr);
fprintf(ID4, 'sel set damp=local %f ra selt beam id 2\r\n',Dr*pi());
fprintf(ID4, 'endcommand\r\n');
%%%%%%%%%%%%%%%%%%%%%%%%%%%%%%%%%%%%%%%%%%%%%%%%%%%%%%%%%%%%%%%%%%%%%%%%
fprintf(ID4, 'end\r\n');
%Fonction9: Sert à faire bouger les charges
%*****
fprintf(ID4, 'def Mov_Load\r\n');
fprintf(ID4, 'det=Tst/(sv*sx)\r\n');
fprintf(ID4, 'ptar=mt*sx*sv\r\n');
fprintf(ID4, 'loop ihi (1,4)\r\n');
fprintf(ID4, 'xtable(17,4*ihi-3)=4*ihi-
3\r\n'); fprintf(ID4, 'ytable(17,4*ihi-3)=0\r\n');
fprintf(ID4, 'xtable(17,4*ihi-2)=4*ihi-
2\r\n'); fprintf(ID4, 'ytable(17,4*ihi-2)=0\r\n');
fprintf(ID4, 'xtable(17,4*ihi-1)=4*ihi-
1\r\n'); fprintf(ID4, 'ytable(17,4*ihi-1)=0\r\n');
fprintf(ID4, 'xtable(17,4*ihi)=4*ihi\r\n'); fprintf(ID4, 'ytable(17,4*i
hi)=0\r\n');
fprintf(ID4, 'end_loop\r\n');
fprintf(ID4, 'loop m (1,mt)\r\n');
fprintf(ID4, 'Load_Apl\r\n');
fprintf(ID4, 'end_loop\r\n');
fprintf(ID4, 'end\r\n');
fclose(ID4);

```

end

6. Function 5: Fonc_Pass

```
function []=Fonc_Pass()
%Fonction sert à transformer les éléments des tableaux de réponse du
%"Float" en "string"
ID5=fopen('Gest_Res.txt','w');
fprintf(ID5,'def dimf\r\n');
fprintf(ID5,'xsi=table_size(9)\r\n');
fprintf(ID5,'end\r\n');
fprintf(ID5,'dimf\r\n');
fprintf(ID5,'def Lec_Tab\r\n');
fprintf(ID5,'array ady(xsi)\r\n');
fprintf(ID5,'array alp(xsi) a2p(xsi) a3p(xsi) a4p(xsi)\r\n');
fprintf(ID5,'loop ii (1,xsi)\r\n');
fprintf(ID5,'ady(ii)=string(xtable(9,ii))\r\n');
fprintf(ID5,'alp(ii)=string(ytable(9,ii))\r\n');
fprintf(ID5,'a2p(ii)=string(ytable(10,ii))\r\n');
fprintf(ID5,'a3p(ii)=string(ytable(11,ii))\r\n');
fprintf(ID5,'a4p(ii)=string(ytable(12,ii))\r\n');
fprintf(ID5,'end_loop\r\n');
fprintf(ID5,'oo=open('Dyn_time.txt',1,1)\r\n');
fprintf(ID5,'oo=write(ady,xsi)\r\n');
fprintf(ID5,'oo=close\r\n');
fprintf(ID5,'oo=open('Rep_PM_Rp_1.txt',1,1)\r\n');
fprintf(ID5,'oo=write(alp,xsi)\r\n');
fprintf(ID5,'oo=close\r\n');
fprintf(ID5,'oo=open('Rep_PM_Rp_2.txt',1,1)\r\n');
fprintf(ID5,'oo=write(a2p,xsi)\r\n');
fprintf(ID5,'oo=close\r\n');
fprintf(ID5,'oo=open('Rep_PM_Rp_3.txt',1,1)\r\n');
fprintf(ID5,'oo=write(a3p,xsi)\r\n');
fprintf(ID5,'oo=close\r\n');
fprintf(ID5,'oo=open('Rep_PM_Rp_4.txt',1,1)\r\n');
fprintf(ID5,'oo=write(a4p,xsi)\r\n');
fprintf(ID5,'oo=close\r\n');
fprintf(ID5,'end\r\n');
fprintf(ID5,'Lec_Tab\r\n');
fclose(ID5);
end
```

7. Function 6 : Fonc_Char

```
%Cette fonction sert à créer la fonction de chargement
function [Fo_Cont]=Fonc_Char(Pch,fch,V,sx,sv,Nfch,delxa)
Ndis=sx*sv;
dto=Nfch*delxa;
dd=(delxa/Ndis);
lse=floor(dto/dd)+1;
Fo_Cont=zeros(lse+1,5);
for i=1:lse+1
    Fo_Cont(i,1)=(i-1)*dd;
    Fo_Cont(i,2)=Pch*sin(2*pi()*fch*((i-1)*dd/V));
end
end
```